K

NATIONAL AERONAUTICS AND SPACE ADMINISTRATION

APOLLO 12 MISSION REPORT

GUIDANCE, NAVIGATION AND CONTROL SYSTEMS

PERFORMANCE ANALYSIS

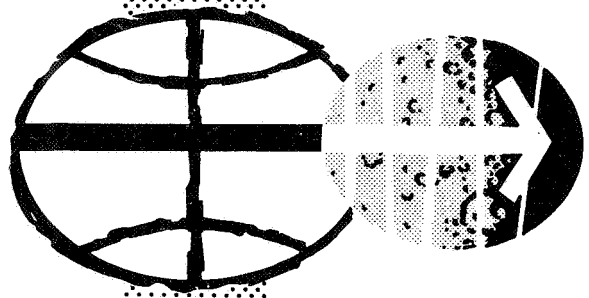### DISTRIBUTION AND REFERENCING

MANNED SPACECRAFT CENTER
HOUSTON, TEXAS
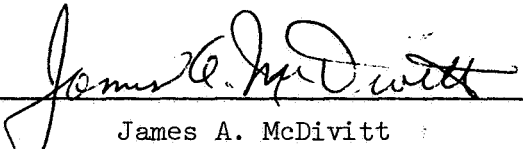### August 1970

APOLLO 12 MISSION REPORT

SUPPLEMENT 2

GUIDANCE, NAVIGATION AND CONTROL SYSTEMS PERFORMANCE ANALYSIS

PREPARED BY

TRW Systems

APPROVED BY

James A. McDivitt
Manager, Apollo Spacecraft Program

NATIONAL AERONAUTICS AND SPACE ADMINISTRATION

MANNED SPACECRAFT CENTER

HOUSTON, TEXAS

August 1970

PROJECT TECHNICAL REPORT

TASK E - 38 C
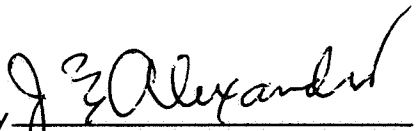
APOLLO XII GUIDANCE, NAVIGATION AND CONTROL
SYSTEMS PERFORMANCE ANALYSIS REPORT

NAS 9-8166   8 APRIL 1970

Prepared for
NATIONAL AERONAUTICS AND SPACE ADMINISTRATION
MANNED SPACECRAFT CENTER
HOUSTON, TEXAS

Prepared by
Guidance and Control Systems Department

Approved by _____
J. E. Alexander, Manager
Guidance & Control Systems
Department

TRW
SYSTEMS GROUP

PREFACE

This report has been prepared as supplement 2 to the Apollo 12 Mission Report (MSC-01855).

CONTENTS

CONTENTS (Continued)

TABLES

ILLUSTRATIONS

ILLUSTRATIONS (Continued)

NOMENCLATURE

AGS	Abort Guidance System
AOS	Offset Acceleration
APS	Ascent Propulsion System
ASA	Abort Sensor Assembly
BET	Best Estimate Trajectory
BMAG	Body Mounted Attitude Gyro
CDH	Concentric Delta Height
CDU	Coupling Data Unit
CES	Control Electronics Section
cg	Center of gravity
CM	Command Module
CMC	Command Module Computer
CSI	Concentric Sequence Initiation
CSM	Command & Service Module
DAP	Digital Autopilot
DOI	Descent Orbit Insertion
DPS	Descent Propulsion System
FCI	Flight Control Integration
FDAI	Flight Director Attitude Indicator
GDA	Gimbal Drive Actuator
GET	Ground Elapsed Time (from liftoff)
GN&C	Guidance, Navigation & Control
HOPE	Houston Operations Predictor Estimator
IMU	Inertial Measurement Unit
ISS	Inertial Subsystem
IU	Instrumentation Unit (Saturn S-IVB)
LGC	Lunar Module Guidance Computer
LM	Lunar Module
LOI 1	Lunar Orbit Insertion #1
LOI 2	Lunar Orbit Insertion #2 (circularization)

Omega P error	Rate error about P axis
Omega U' error	Rate error about U' axis
Omega V' error	Rate error about V' axis
P error	Yaw axis error
U error	Computed errors - refer to Figure 6-1
U' error	Computed errors - refer to Figure 6-1
V error	Computed errors - refer to Figure 6-1
V' error	Computed errors - refer to Figure 6-1
a_x	Measured gravity vector in IMU coordinates (X)
a_y	Measured gravity vector in IMU coordinates (Y)
a_z	Measured gravity vector in IMU coordinates (Z)

1.0 INTRODUCTION

1.1 GENERAL

This report presents the conclusions of the analyses of the inflight performance of the Apollo 12 mission Guidance, Navigation and Control equipment onboard the CSM-108 and LM-6 spacecraft. The analyses will supplement that presented in the Apollo 12 Mission Report (Reference 1). This document was prepared and submitted under MSC/TRW Task E-38C, "G&C Test Analysis."

2.0   SUMMARY

CSM IMU performance was good during the mission. Error separation studies conducted for the TLI burn indicated 31 of the 34 error sources evaluated were within one sigma of the preflight expected error. The other three were easily within three sigma of the preflight expected error value.

The CSM DAP exhibited no anomalous behavior during the Apollo 12 mission. Five of the six SPS burns were typical of TVC DAP performance on previous missions; the other burn exhibited an unexpected 60% over-shoot in the initial attitude transient. The transients were quickly damped and the rest of the burn was nominal. The large transient was caused by an undesirable combination of mistrim error and attitude error. A disturbance to the PTC limit-cycle during LM docked lunar orbit coast was investigated. Detailed analysis indicated the cause was most probably a CDU transient which generated a short term unrealistic atti-tude error.

Performance of the LM DAP during powered descent was quite similar to the Apollo 11 mission results with the exception of two new functions. A landing site redesignation of 4200 feet downrange was implemented in P63 via the ΔRLS procedure with no adverse guidance/control interaction. The attitude error deadband was decreased to 0.3 degree in P64 which re-sulted in reduced attitude errors during the Visibility Phase. Slosh oscillations of 0.55 to 0.60 H_Z were apparent in the P63 phase but were attenuated in amplitude in the P64 phase by the deadband change. The spacecraft response and RCS propellant consumption during the P63 and P64 phases agreed closely with results from the MSC bit-by-bit simulator. The LM DAP performed well in damping the fire-in-the-hole transients at lunar liftoff and performed the pitchover maneuver smoothly. The steady-state response duplicated the Apollo 11 powered ascent response. The three RCS burns in the rendezvous sequence were nominal. A new mission

phase required a LM deorbit burn to impact the empty ascent stage on the moon. The deorbit burn was essentially a long four-jet ullage maneuver. Biased limit-cycle responses during the burn resulted from the torques caused by the cg offset from the geometric center of the RCS quads. This response was verified to be nominal.

Star-horizon (P23) data were processed. Reasonable and consistent values for earth-horizon bias were obtained and the trunnion noise was within specification for the sextant. The average value for horizon bias was 51,300 ft (15.6 km) and the one sigma trunnion error was 0.003 degree.

LM IMU performance was satisfactory. Correcting of sensed IMU data during descent and ascent burns to meet best estimate terminal conditions (lunar touchdown location and insertion state vectors) yielded sets of errors which will account for most of the differences between IMU data and the reference data. None of the determined error sources were greater than two sigma. The PIPA bias shift which occurred across the IMU shutdown period accounted for a majority of the ascent insertion error.

The lunar surface IMU alignment (P57) star sighting data were processed in the iterated weighted least squares program for the purpose of determining IMU misalignments. Results indicate the platform was aligned prior to PDI and prior to LM liftoff within the one sigma AOT accuracy (0.06 degree).

AGS performance as a mission monitor was excellent and in general AGS accuracy was in agreement with current capability estimates. All of the estimated sensor errors for the descent and ascent burns were within the AGS error budget limits. The sensor errors were also compared to a set of expected values based on preflight testing of the ASA flown on Apollo 12. During descent all of the estimated errors were within the predicted 3σ range. During ascent, only one error, X accelerometer dynamic bias, exceeded the predicted 3σ range.

3.0 CSM IMU PERFORMANCE

Performance of CSM IMU #46 was based exclusively on the translunar insertion (TLI) phase. The electrical anomaly which occurred at approximately t+30 seconds after liftoff rendered the GN&C system non-usable for the remainder of the boost phase. For reference purposes only, an abbreviated error analysis was performed for the first 30 seconds of flight and no severe errors were present. However, derivation of a set of errors which fits both this small time segment and the TLI phase is not practical or meaningful. IMU performance was satisfactory during the TLI phase of flight.

3.1 TLI VELOCITY COMPARISONS

For previous missions, analysis of the CSM IMU system accuracy was based upon a common set of errors which, when used to correct the Apollo data, resulted in small residual velocities between Saturn IU data and Apollo data for both the boost to orbit phase and the TLI phase. This was not possible for Apollo 12 because of the occurrence of the electrical discharge shortly after liftoff. Therefore, for Apollo 12, IMU accuracy was based on velocity comparisons between Saturn IU data and Apollo data for the TLI phase only. Uncompensated velocity comparisons for TLI are presented in Figures 3-1 through 3-3.

Several constraints were placed on the selected error sources. Accelerometer biases and constant gyro drift biases were forced to be in close agreement with inflight measurements. Other error sources were chosen which agreed with preflight calibration data. Actual acceleration sensitive parameter shifts between boost and TLI could not be considered because of the references anomaly. Based upon engineering judgement, the approach implemented was to determine a set of error sources which resulted in small velocity residuals and minimum deviation from their corresponding a priori values. The error terms derived from the analysis are presented in Table 3.1. Using these values,

the corrected G&N TLI trajectory fits the corresponding external measurement trajectory. The compensated velocity comparison plots are presented as Figures 3-4 through 3-6.

3.2 ISS ERRORS

Of the 34 derived error sources, only 3 deviated by more than 1 sigma from their corresponding a priori values. These error sources were well within the 3 sigma range. Each of three errors are discussed in detail below.

a) <u>X Gyro Drift Due to Acceleration Along Input Axis (ADIAX)</u>

The a priori value for this error source was -7.53 meru/g. This was established using the available six samples of data (preflight data mean) and subtracting the CSM compensation load value (i.e., preflight data mean minus preflight load). Using -7.53 meru/g as an a priori value, the derived value (5.66 meru/g) represents a deviation of 1.65 sigma (1 sigma = 8 meru/g) from the a priori. Realizing that the preflight data mean was established using only six samples of data, a second a priori value was established by using zero as an initial input value instead of -7.53 meru/g. A corresponding error value of 11.11 meru/g resulted showing that the error source was seeking a comparatively large positive value. For consistency purposes, the first value derived for ADIAX using the preflight data mean minus mission load as an a priori, will be reflected in Table 3.1.

The Apollo 12 ADIAX preflight calibration data evidenced a pronounced shift from a small value to a large positive value ($\approx$15 meru/g) for the last two KSC calibrations. Since the compensation load was 13 meru/g a possible explanation for the 5.66 meru/g error is that the value continued to shift more positive.

b) <u>Z Gyro Drift Due to Acceleration Along Input Axis (ADIAZ)</u>

The derived ADIAZ error source deviated by 2.2 sigma from the initial ADIAZ a priori value established (i.e., preflight data mean minus compensation load). In a manner equivalent to the ADIAX error source development, the preflight data mean for ADIAZ was established from six

samples of data. As a consequence, an investigation was conducted which was identical to that described for the ADIAX error source. Using the a priori established value of 0.484 meru/g, the derived ADIAZ value was -17.3 meru/g. Using zero as an initial value, a second ADIAZ error of -15.92 meru/g was established, again confirming that the value was seeking a comparatively large negative value.

Investigation of the available preflight data for ADIAZ revealed no erratic trends during the April to September 1969 KSC test period. The maximum preflight data mean excursions during this time interval were from -4.2 meru/g to 1.8 meru/g. Consequently, it is difficult to arrive at a conclusion as to the cause of the ADIAZ error source deviation of approximately 17 meru/g from its a priori value.

c)   Y Accelerometer Scale Factor (SFEY)

The derived value for SFEY was -18 ppm or 0.155 sigma in an absolute sense (1 sigma = 116 ppm). However, a comparison of this derived value of -18 ppm with the a priori value of 119 ppm (using preflight data mean minus compensation load) shows a deviation of 1.18 sigma.

Preflight SFEY data shows a pronounced negative data trend during the November 1968 to September 1969 KSC test period with data trending from +126 ppm to -319 ppm. Since the data was trending negatively the a priori value was expectedly high and a negative error of the size obtained is reasonable.

Error Source	Preflight Data Mean	Flight Load	Expected Error*	Standard Deviation	Preflight Expected 1σ Bounds Maximum	Minimum	Ascent Output Error Value	TLI Output Error Value	|TLI Output Error Value|/σ	Comments
VOX (ft/sec)	NA	NA	NA	NA	NA	NA	****	2.353	NA	
VOY (ft/sec)	NA	NA	NA	NA	NA	NA	****	-0.125	NA	
VOZ (ft/sec)	NA	NA	NA	NA	NA	NA	****	-3.653	NA	
DT (sec)	NA	NA	NA	NA	NA	NA	****	0.017	NA	
ACBX (cm/sec²)	0.003	-0.090	0.093	0.20	0.293	-0.107	****	0.090	NA	Output error values
ACBY (cm/sec²)	-0.137	-0.090	-0.047	0.20	0.153	-0.247	****	-0.059	NA	established from inflight
ACBZ (cm/sec²)	-0.186	-0.160	-0.026	0.20	0.174	-0.226	****	0.010	NA	measurements
SFEX (ppm)	-168	-220	52	116	168	-64	****	14	0.121σ	
SFEY (ppm)	-231	-350	119	116	235	3	****	-18	0.155σ	
SFEZ (ppm)	-292	-370	78	116	194	-38	****	121	1.043σ	
MUAZ (arc sec)	NA	NA	NA	20	20	- 20	****	2.5	0.125σ	
MUAY (arc sec)	NA	NA	NA	20	20	- 20	****	-11.7	0.585σ	
MUAZ (arc sec)	NA	NA	NA	20	20	- 20	****	-1.8	0.090σ	
MUAX (arc sec)	NA	NA	NA	20	20	- 20	****	-14	0.70σ	
MUAY (arc sec)	NA	NA	NA	20	20	- 20	****	5.3	0.265σ	
MUAX (arc sec)	NA	NA	NA	20	20	- 20	****	3.1	0.155σ	
NBDX (meru)	-1.525	-0.100	-1.425	2	0.58	-3.43	****	0.83	NA	Output error values
NBDY (meru)	-0.812	-0.100	-0.712	2	1.29	-2.71	****	1.65	NA	established from inflight
NBDZ (meru)	-2.666	0.100	-2.766	2	-0.77	-4.77	****	1.06	NA	measurements
ADIAX (meru/g)	5.466	13.000	-7.534	8	0.47	-15.5	****	5.66	0.708σ	
ADIAY (meru/g)	0.666	0	0.666	8	8.67	-7.33	****	2.42	0.303σ	
ADIAZ (meru/g)	-0.516	-1.000	0.484	8	8.48	-7.52	****	-17.3	.16σ	Insensitive in TLI
ADSRAX (meru/g)	-1.150	-4.000	2.850	5.0	7.85	-2.15	****	1.19	0.240σ	
ADSRAY (meru/g)	-3.383	-4.000	0.617	5.0	5.62	-4.38	****	4.29	0.858σ	
ADSRAZ (meru/g)	-3.066	-6.000	2.934	5.0	7.93	-2.07	****	4.70	0.94σ	
ADOAX (meru/g)	0.933	NA	0.933	2-5**	5.93	-4.07	****	-4.85	0.97σ	
ADOAY (meru/g)	-1.133	NA	-1.133	2-5**	3.87	-6.13	****	1.18	0.236σ	
ADOAZ (meru/g)	0.633	NA	0.633	2-5**	5.63	-4.37	****	-3.75	0.75σ	
MLMX (arc sec)	NA	NA	NA	50***	50***	- 50***	****	-186	NA	values based on platform
MLMY (arc sec)	NA	NA	NA	50***	50***	- 50***	****	-22	NA	misalignments and 2.5 hours
MLMZ (arc sec)	NA	NA	NA	50***	50***	- 50***	****	160	NA	drift before TLI.

* Data mean minus flight load.

** Recent measurements by MIT

*** Boost Phase only.

NA = Not applicable

**** Indicates - that it was not possible to derive meaningful ascent output error values because of the electrical anomaly occuring during ascent.

Table 3.1   CSM IMU SYSTEM ERRORS

3-5

Apollo Mnemonic	Accelerometer Errors	Apollo Mnemonic	Gyro Errors
ACBX ACBY ACBZ	Bias	ADIAX ADIAY ADIAZ	Drift rate sensitivity to acceleration along input axis.
SFEX SFEY SFEZ	Scale Factor	ADSRAX ADSRAY ADSRAZ	Drift rate sensitivity to acceleration along spin axis.
NCXX NCYY NCZZ	SF sensitivity to input acceleration squared	ADOAX ADOAY ADOAZ	Drift rate sensitivity to acceleration along output axis.
	IKMSL is the misalignment of accelerometer "I" toward the "K" the platform axis.	ADSXX ADSYY ADSZZ	Drift rate sensitivity to acceleration squared along the spin reference axis.
(not modeled)	SF sensitivity to coupling of acceleration along input and output axes (ppm/g)	NBDX NBDY NBDZ	Constant drift rate

Platform Errors

Platform misalignment

Timing Error

Velocity Offset

Table 3.2   IMU ERROR SOURCES
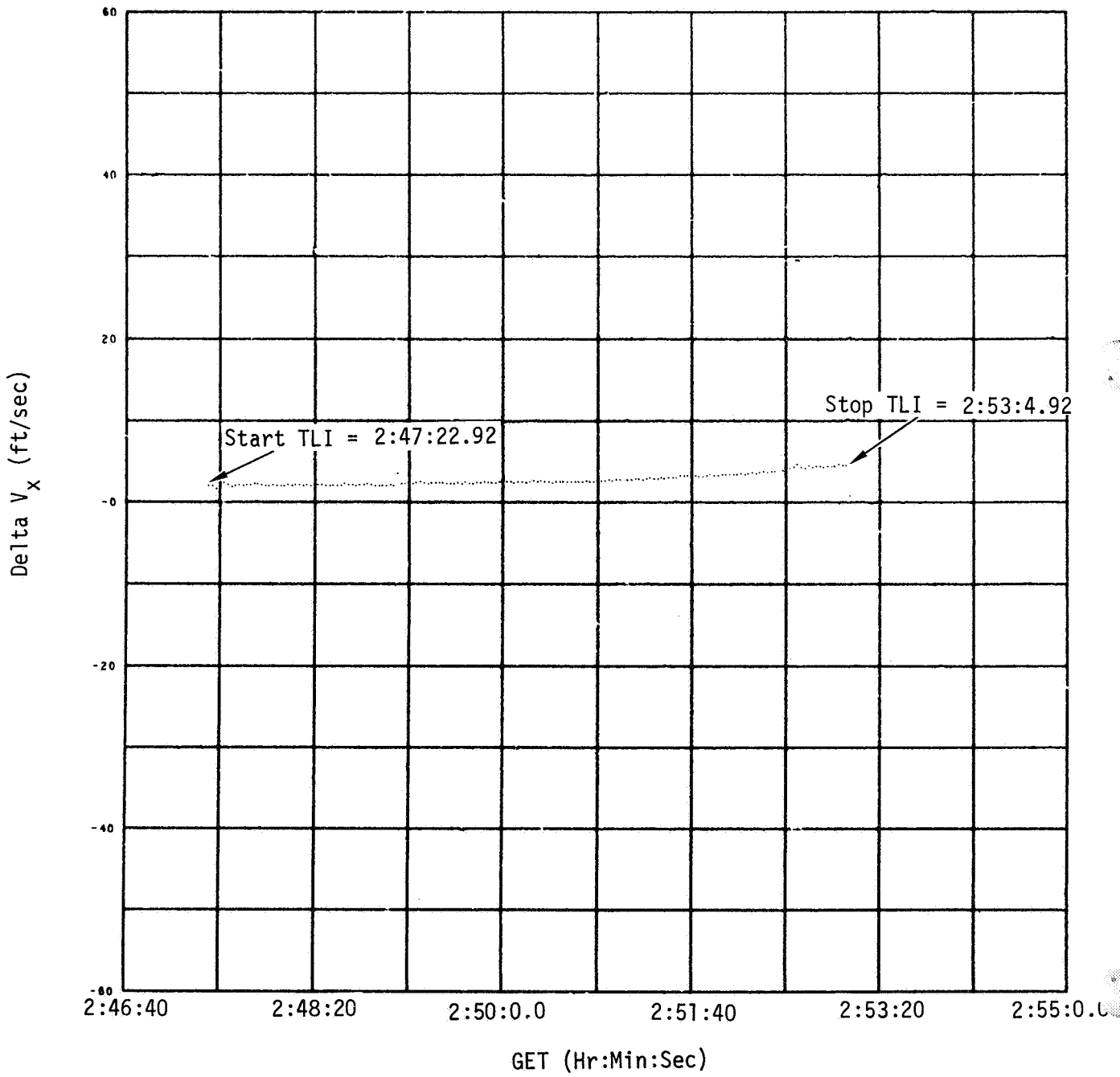
Figure 3-1   UNCOMPENSATED TLI VELOCITY COMPARISON (G&N MINUS S-IVB)

3-8
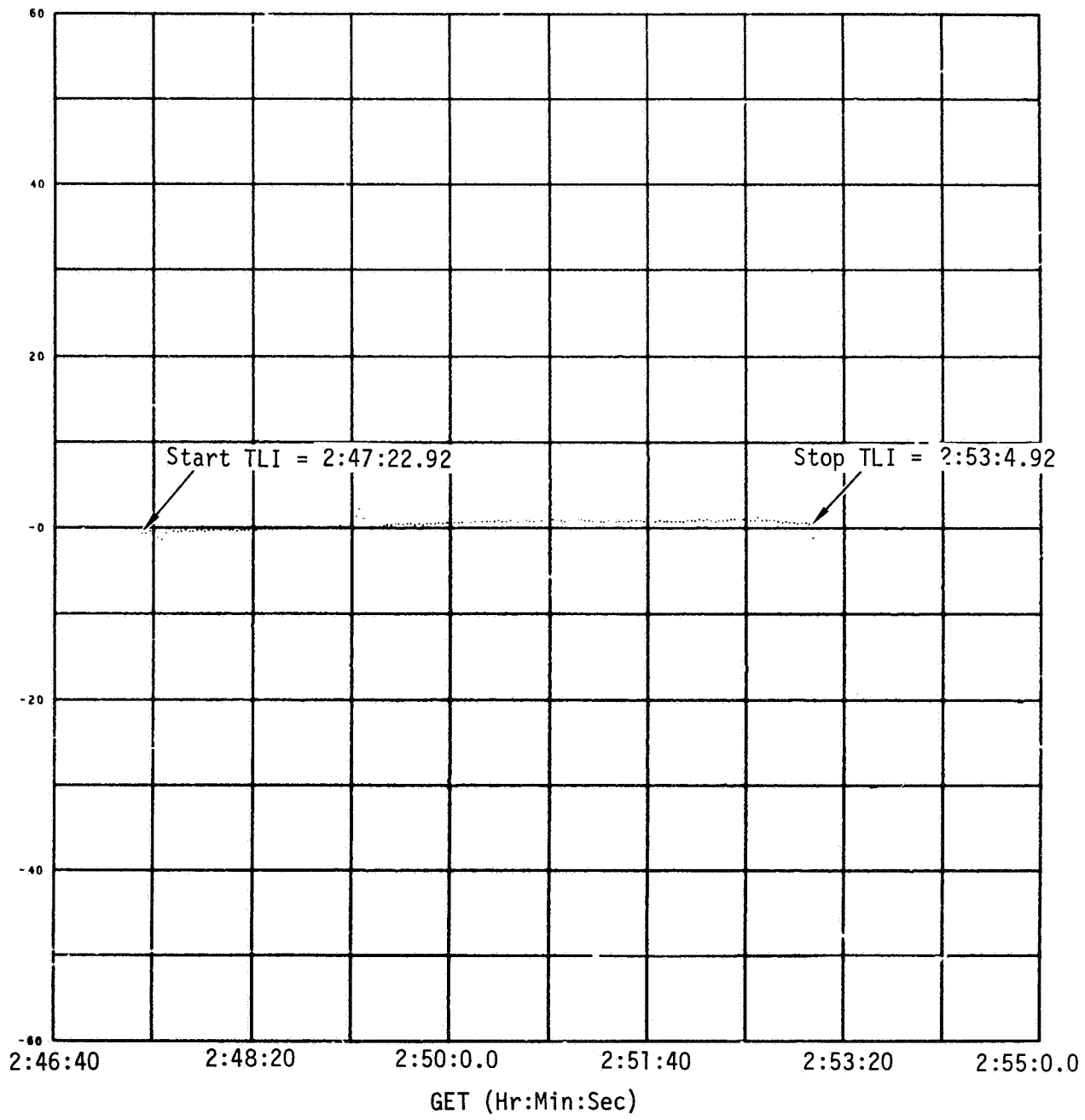
Figure 3-2 UNCOMPENSATED TLI VELOCITY COMPARISON (G&N MINUS S-IVB)
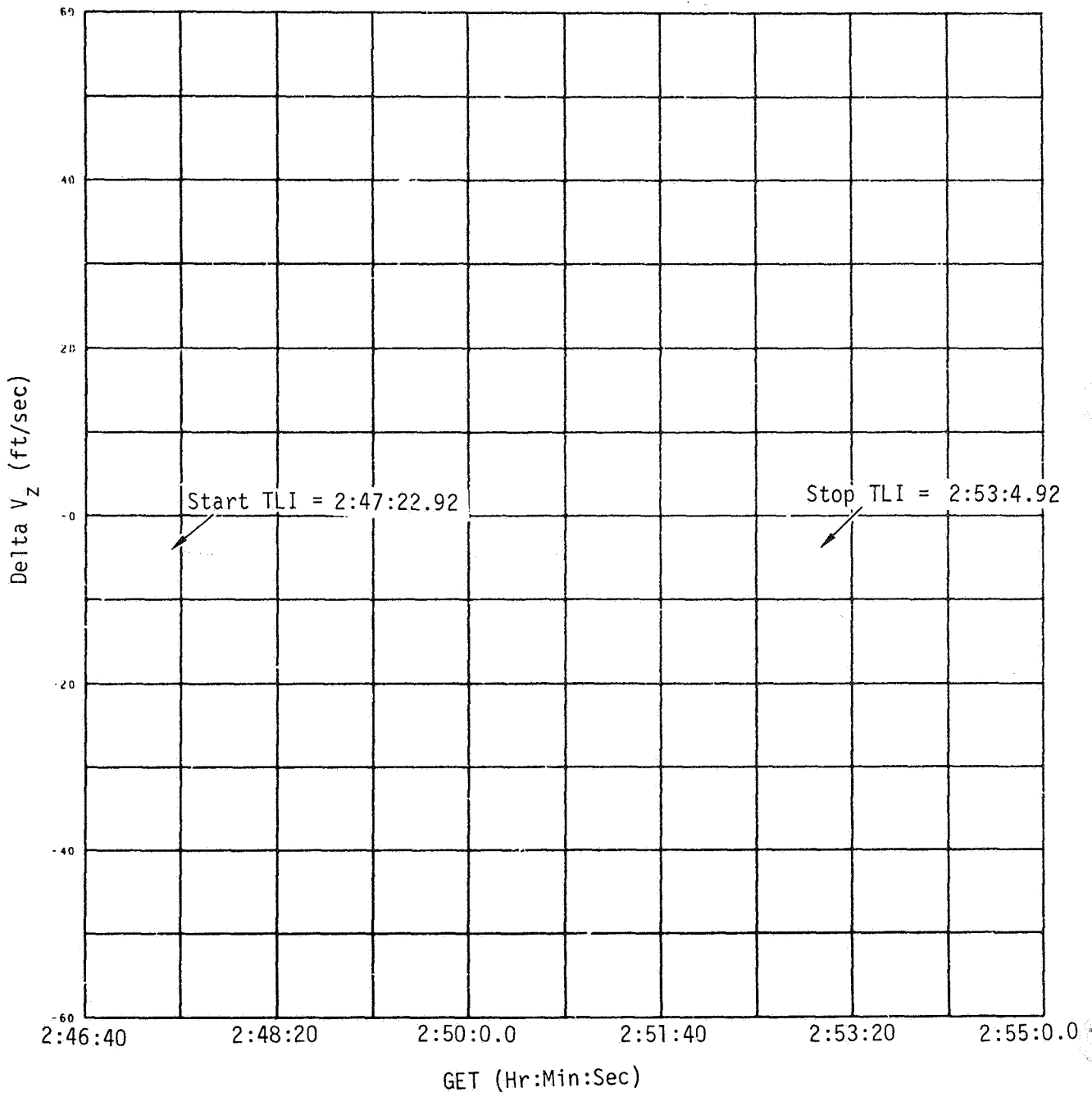
Figure 3-3   UNCOMPENSATED TLI VELOCITY COMPARISON (G&N MINUS S-IVB)
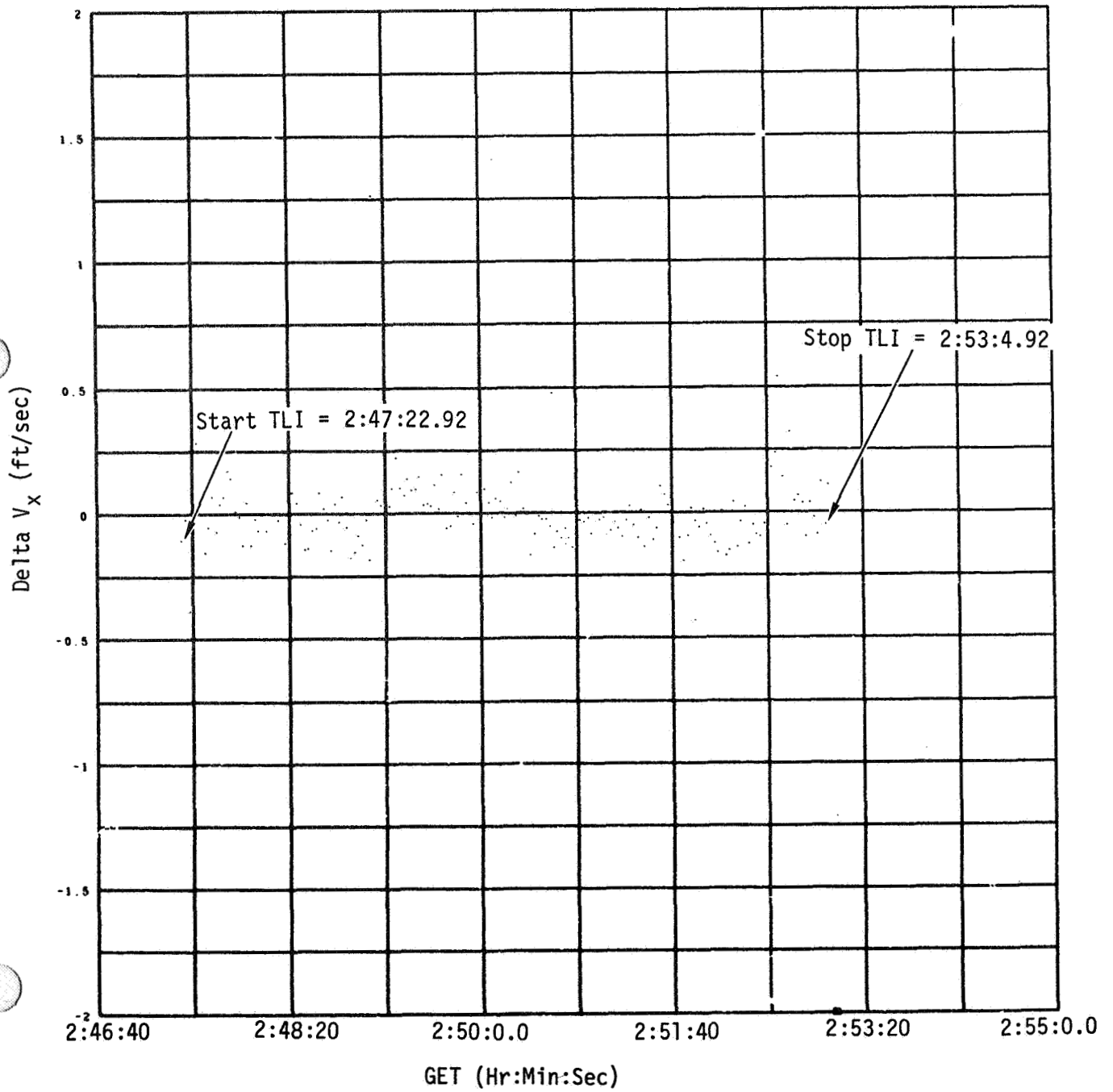
Figure 3-4   COMPENSATED TLI VELOCITY COMPARISON (G&N MINUS S-IVB)
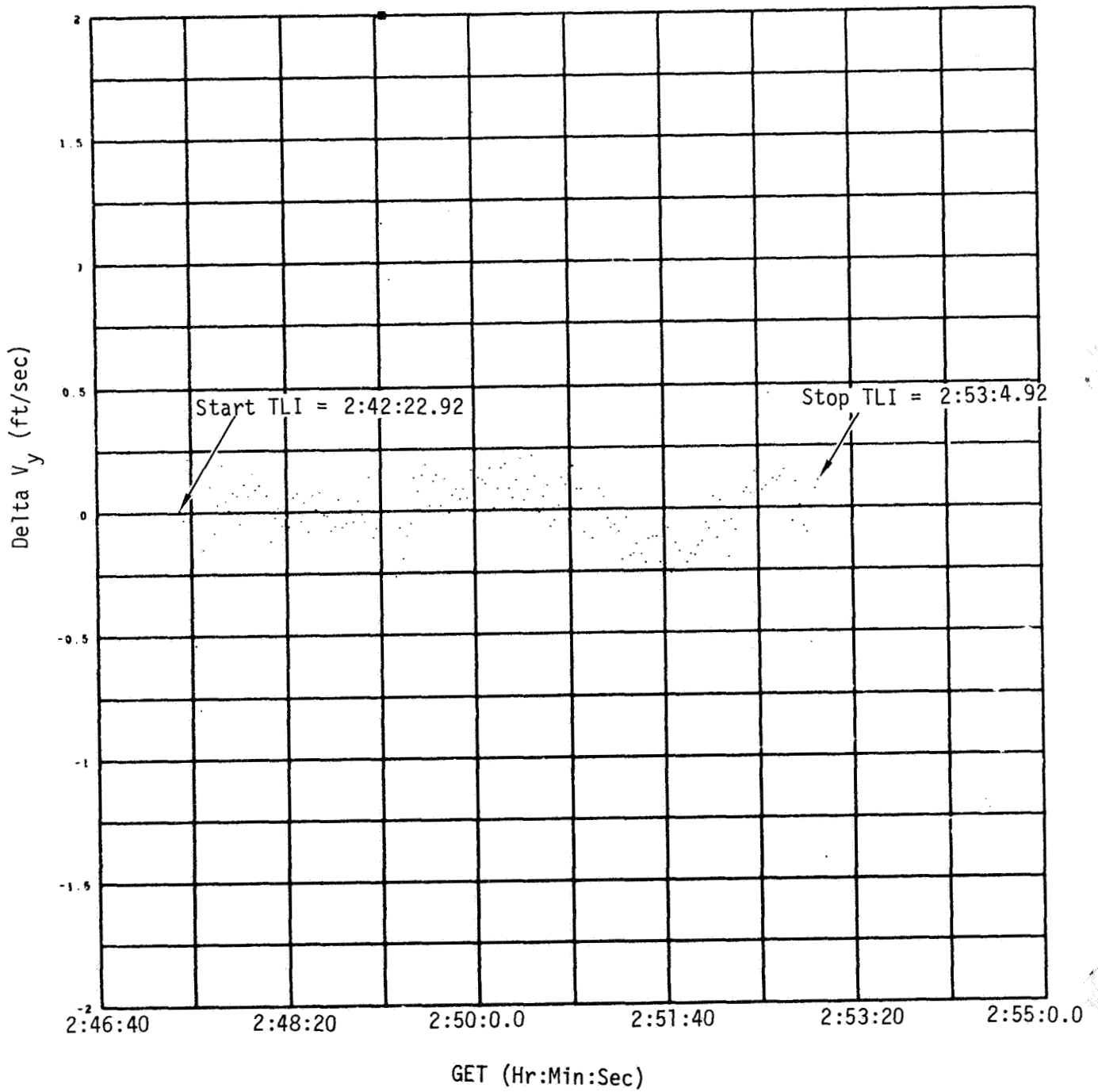
Figure 3-5   COMPENSATED TLI VELOCITY COMPARISON (G&N MINUS S-IVB)
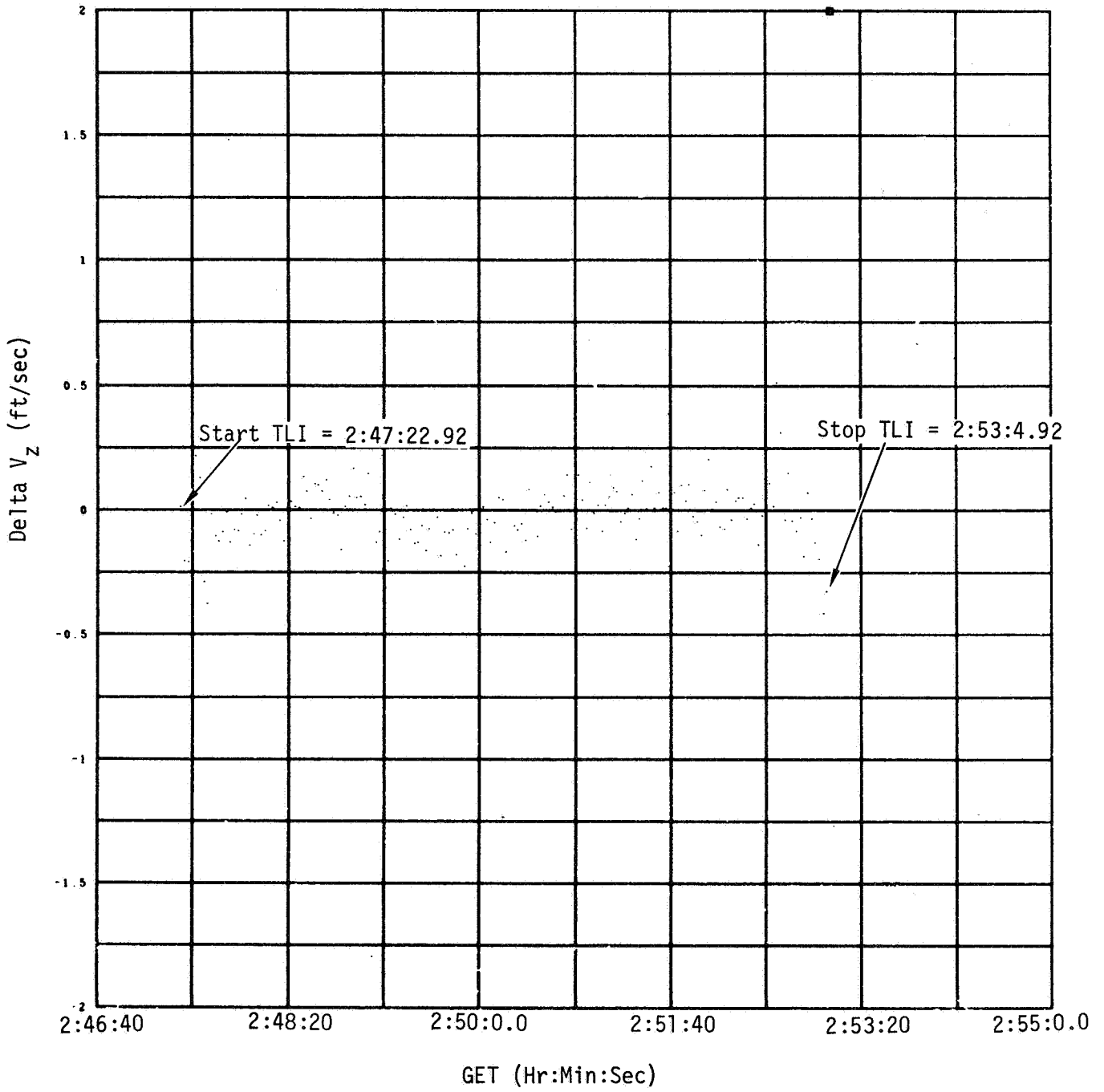
Figure 3-6   COMPENSATED TLI VELOCITY COMPARISON (G&N MINUS S-IVB)

4.0   CSM DIGITAL AUTOPILOT

The COLOSSUS 2C Digital Autopilot (DAP) was implemented for the Apollo 12 (CSM 108) mission. No major CSM DAP modifications were implemented for this mission. This postflight analysis is oriented toward the performance of the CSM Thrust Vector Control (TVC) DAP with the only coasting flight DAP analysis directed toward areas of questionable performance determined from real time monitoring. In particular, a disturbance to the PTC limit-cycle occurred in lunar orbit prior to LM separation and lunar descent. Detailed analysis indicated the initial cause was most probably a CDU transient which generated a short term unrealistic attitude error. No serious problem resulted since the DAP reinstated the vehicle into the nominal limit-cycle. However, in the process extra propellant was expended. CDU transients are a known deficiency in the CDU design but have negligible effect upon DAP performance.

The TVC DAP performance was nominal throughout the mission. Performance of the CSM TVC DAP during five of the six SPS burns were similar to SPS burns on previous missions; the second plane change burn exhibited a 60% overshoot in the initial attitude transient and will be the only burn discussed. The spacecraft dynamics during the burns are shown in Figures 4-1 through 4-6. Velocity-to-be-gained plots during MCC-2, LOI-1, LOI-2 and TEI are shown in Figures 4-7 through 4-10.

4.1   PLANE CHANGE 2 MANEUVER

The initial transient during the second CSM plane change were more complex than for the other undocked burns on Apollo 12. The pitch rate reached 1.6 deg/sec and caused a 60% overshoot in the initial attitude correction. The momentum of the slosh caused the attitude error to persist for about three seconds before the DAP could null the pitch attitude error. The large initial transient was caused by a worst-case combination of the small mistrim and a large initial attitude error. The yaw mistrim opposed the initial yaw error and prevented the DAP from nulling the initial error for about the same length of time. The transients

lasted about six seconds in both pitch and yaw; the rest of the burn was routine. No adverse effect on slosh control was evident from either combination of initial errors.

During an Apollo 12 debriefing, the pilot referred to a yaw/roll sensation during the second CSM plane change maneuver. A roll oscillation of over one deg/sec at the slosh frequency was combined with both pitch and yaw transients. The roll oscillations was most likely due to control activity in the pitch and yaw TVC channels and was not unusual in amplitude. The sensation was due to the phasing between the roll and yaw acceleration which were equivalent to a "yaw left, bank right" maneuver in an airplane. The peak roll rate was 1.5 deg/sec which compares well with the 0.7 deg/sec peak rate during the first plane change maneuver.

4.2 EXCESSIVE PTC JET FIRINGS

A pair of abnormally long RCS jet firings occurred during the last sleep cycle before LM undocking for descent to the lunar surface. The docked spacecraft was in attitude hold with a ten degree deadband used for Passive Thermal Control (PTC) by the CSM DAP. Due to gravity-gradient torques, the DAP was expected to maintain control near one deadband using minimum-impulse firings. The operation of the CSM DAP appeared normal until 100:27:12.4 GET when pitch and yaw jets began firing simultaneously and continued to fire 0.440 seconds in pitch and 0.755 seconds in yaw. The firing times are consistent with the DAP attitude errors, but are not consistent with the spacecraft dynamics, CDU angles or the BMAG rates.

The incorrect DAP attitude error was most probably generated by a CDUY transient which was subsequently resolved into DAP pitch and yaw errors by the k-matrix. A transient error of 0.38 degree in CDUY would have caused DAP attitude errors sufficient to cause the 0.440 and 0.755 second pitch and yaw jet firings. The duration of the transient was certainly less than 1 second because it did not appear on the one sample per second telemetry data. It may have only lasted for one DAP cycle (20 ms) since the DAP logic is such that an "engine on" time once calculated and set is not reset, even if on the next DAP cycle the attitude error is back within the deadband.

The philosophy of the analog-to-digital loop of the LM Coupling Data Unit (CDU) is depicted in Figure 4-11.

The CDU receives analog signals from the IMU gimbal angle 1X and 16X resolvers. The magnitude of these signals varies with the angular displacement of the resolver; the phase is indicative of the direction of angular displacement.

These signals, after appropriate phase shifts, attenuation, and mixing are input to an error detection circuit. If the magnitude of the 800 cps error signal exceeds a deadband, a train of digital pulses, each equivalent to 20 sec of gimbal displacement, are generated. The pulse rate is dependent on the amplitude of the error signal; the phase of the error signal determines whether the digital signal increments or decrements the counter. The digital pulse train is input to a binary read counter consisting of 16 binary bits or stages.

The read counter provides incremental ψ angles to be used in the coarse-fine mixing and switching logic which mechanizes the trigonometric identify sin ($\theta_G - \psi$). When the read counter has accumulated ψ equal (within a small deadband) to θ_G the error signal is nulled and the read counter will not receive additional pulses until a change in gimbal angle occurs.

The most significant bits in the read counter control switches in the "coarse" error network and are mixed with the 1X resolver signals. The least significant bits control switches in the "fine" error network and are mixed with the 16X resolver signals.

Transient switching in the coarse and fine error system have been observed in laboratory testing. The transients cause a short term error in the CDU counter which represents an error in the CMC's knowledge of the IMU gimbal positions. Coarse error switching transients observed in the laboratory only occur at 0 degree and plus or minus integer multiples of 45 degrees, which was not the case at the time of this problem. Fine error transients, which was probably the cause of the problem on Apollo 12, have been observed in the laboratory when the CDU is first

turned on and when the CDU sets at the same value for a relatively long period of time. The transients result from a design deficiency in the transistor switches of the read counter. Since the problem normally causes only short term effects (less than a second) hardware changes have not been implemented.
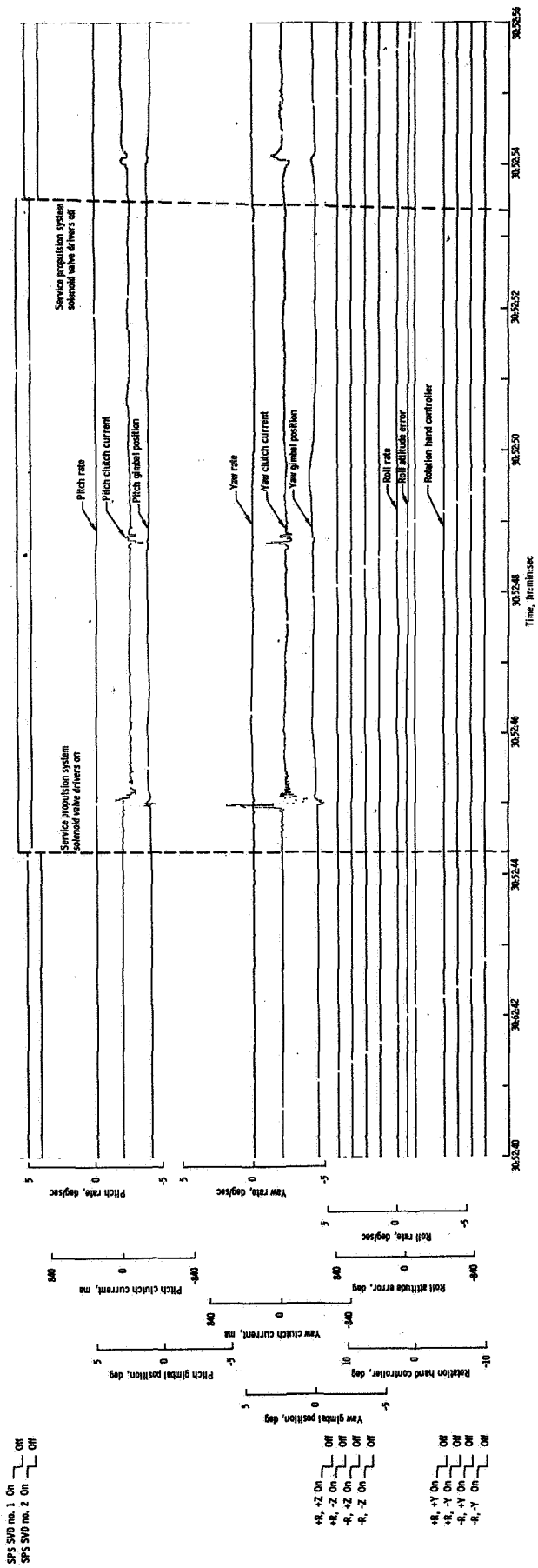
Figure 4-1 SPACECRAFT DYNAMICS DURING MCC₂

4-5
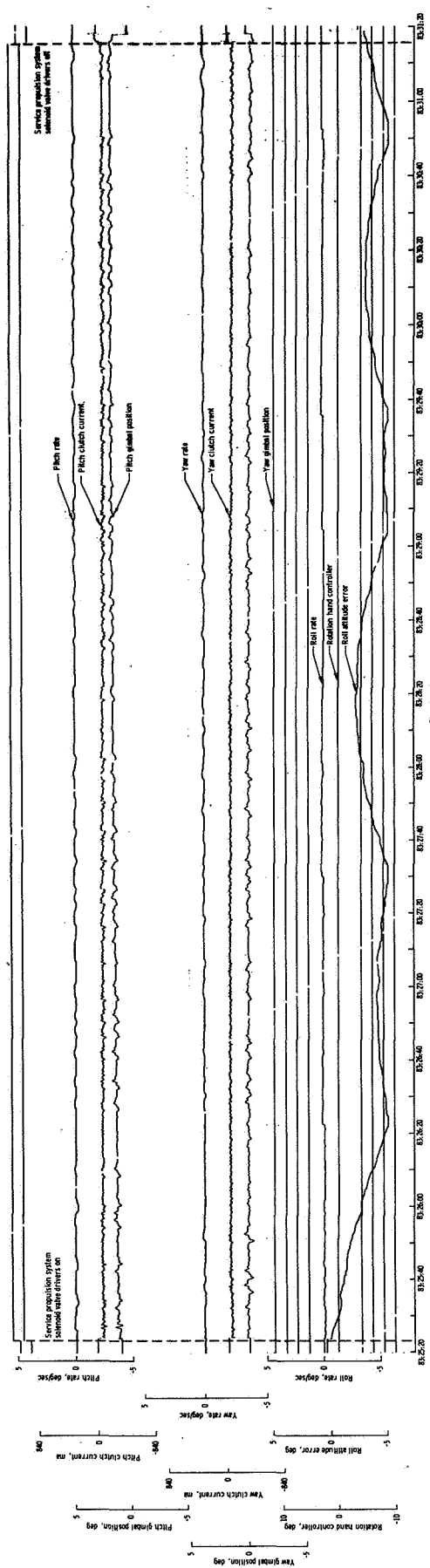
Figure 4-2 SPACECRAFT DYNAMICS DURING LOI₁

4-7
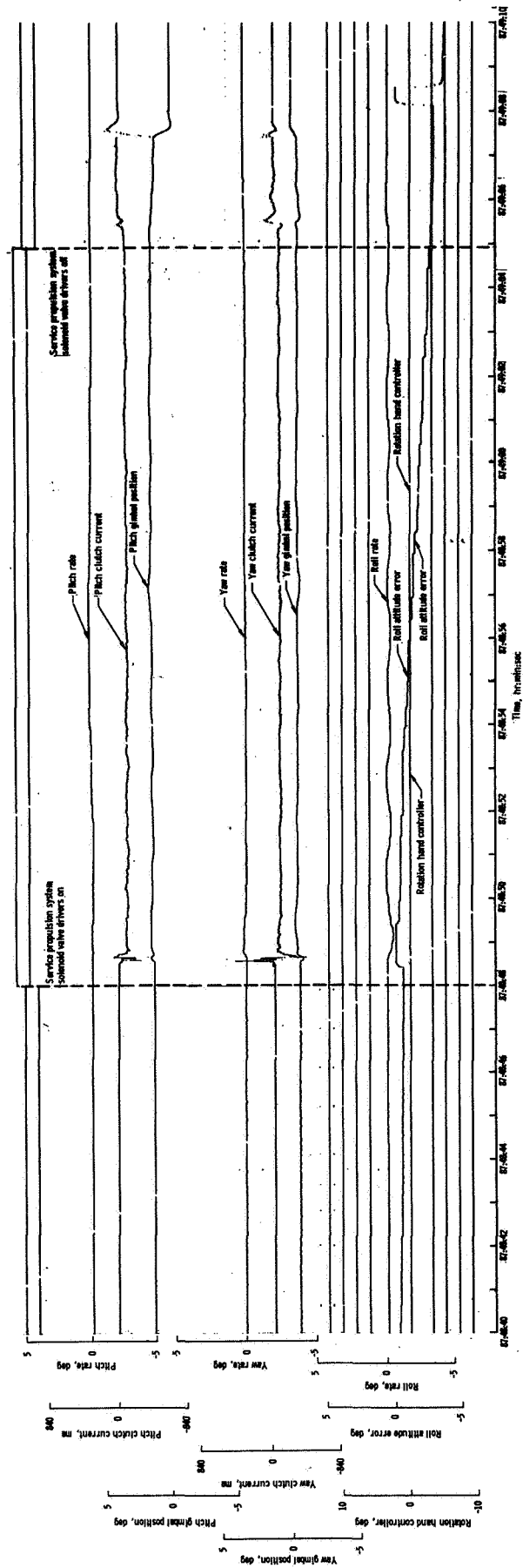
Figure 4-3   SPACECRAFT DYNAMICS DURING LOI$_2$

4-9
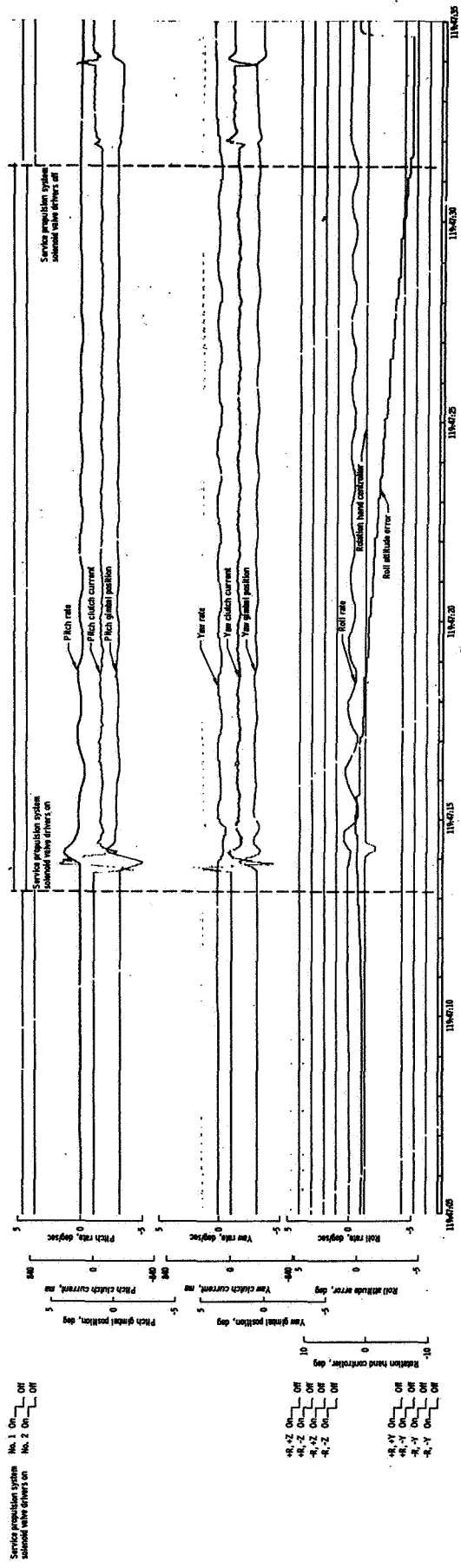
Figure 4-4 SPACECRAFT DYNAMICS DURING
PLANE CHANGE ONE

4-11
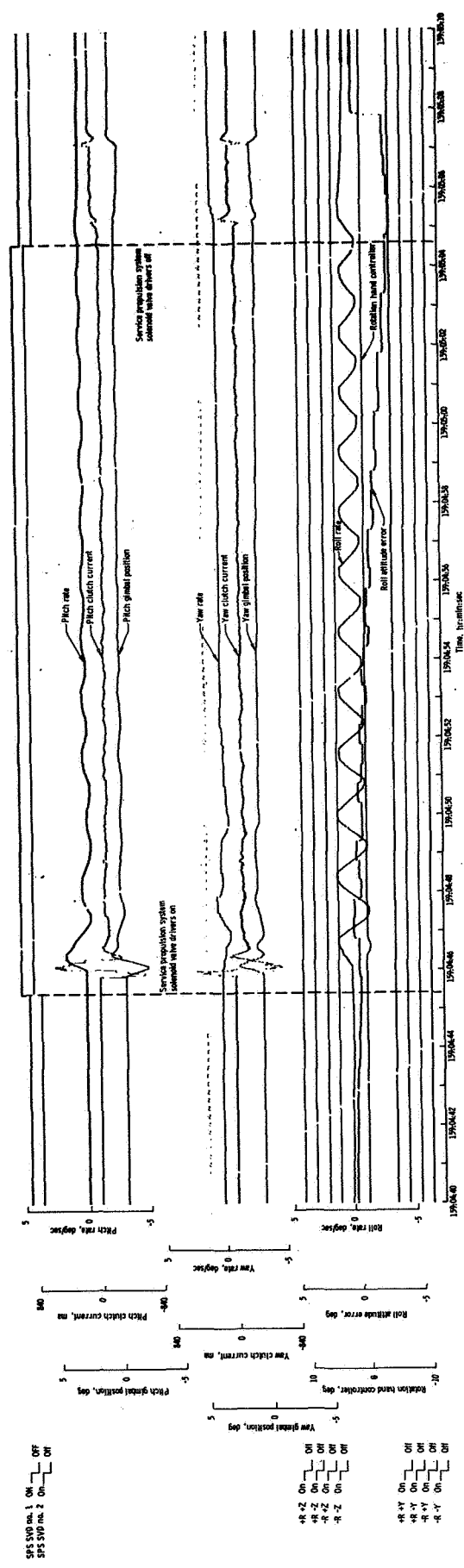
Figure 4-5 SPACECRAFT DYNAMICS DURING PLANE CHANGE TWO

4-13
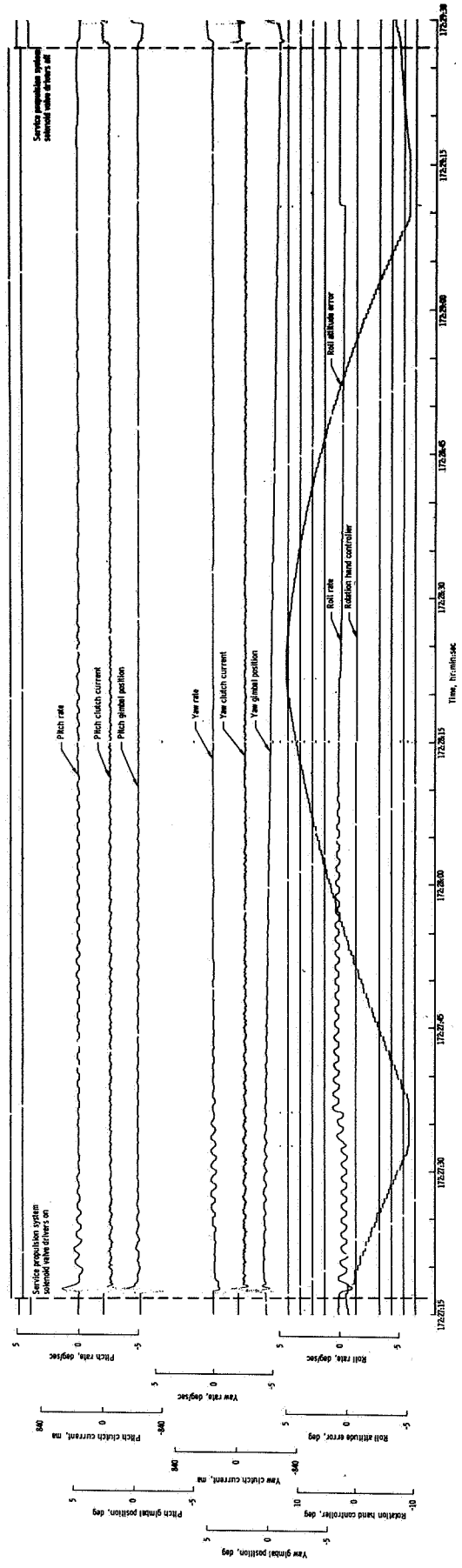
Figure 4-6 SPACECRAFT DYNAMICS DURING TRANSEARTH INJECTION

4-15
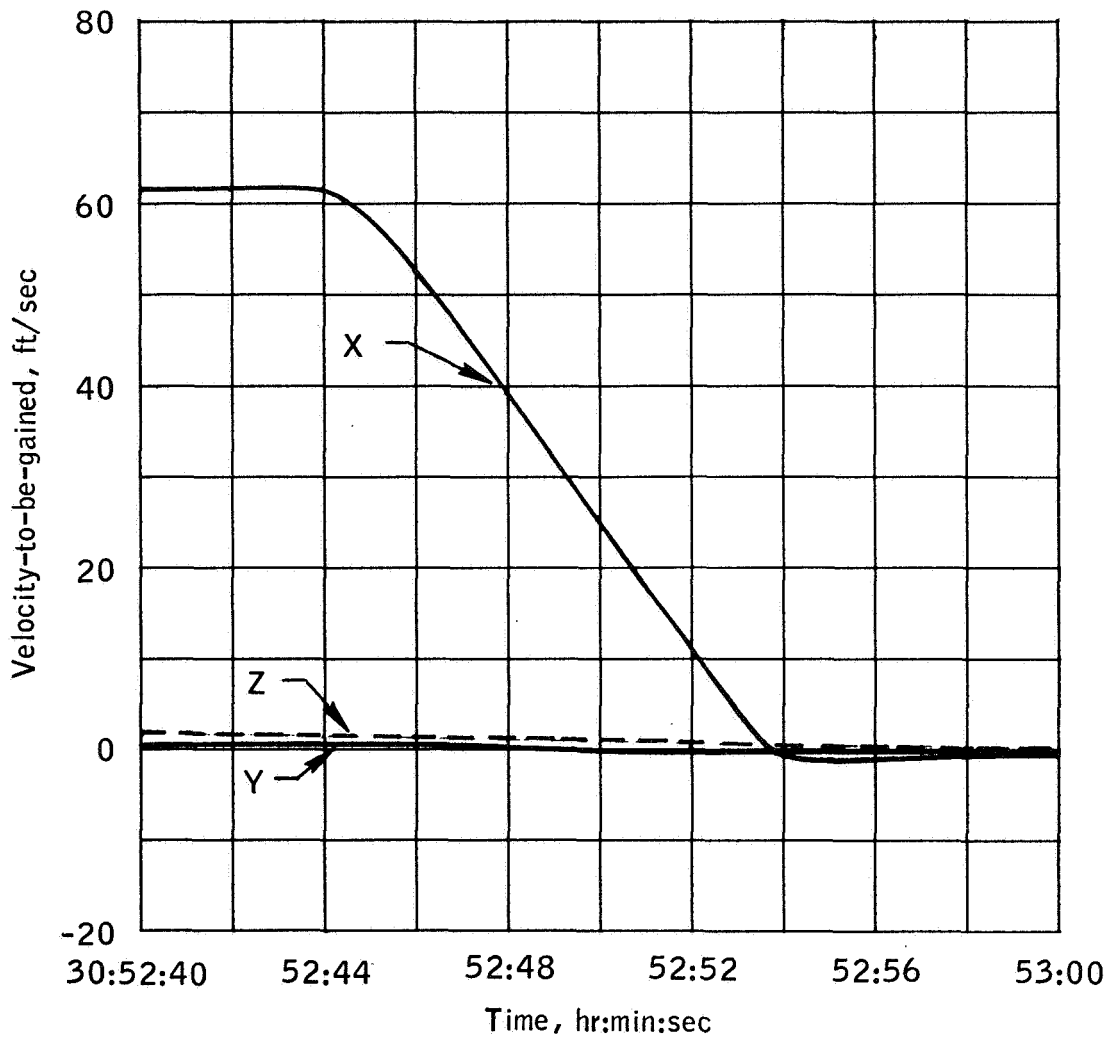
Figure 4-7   MCC-2 VELOCITY-TO-BE-GAINED
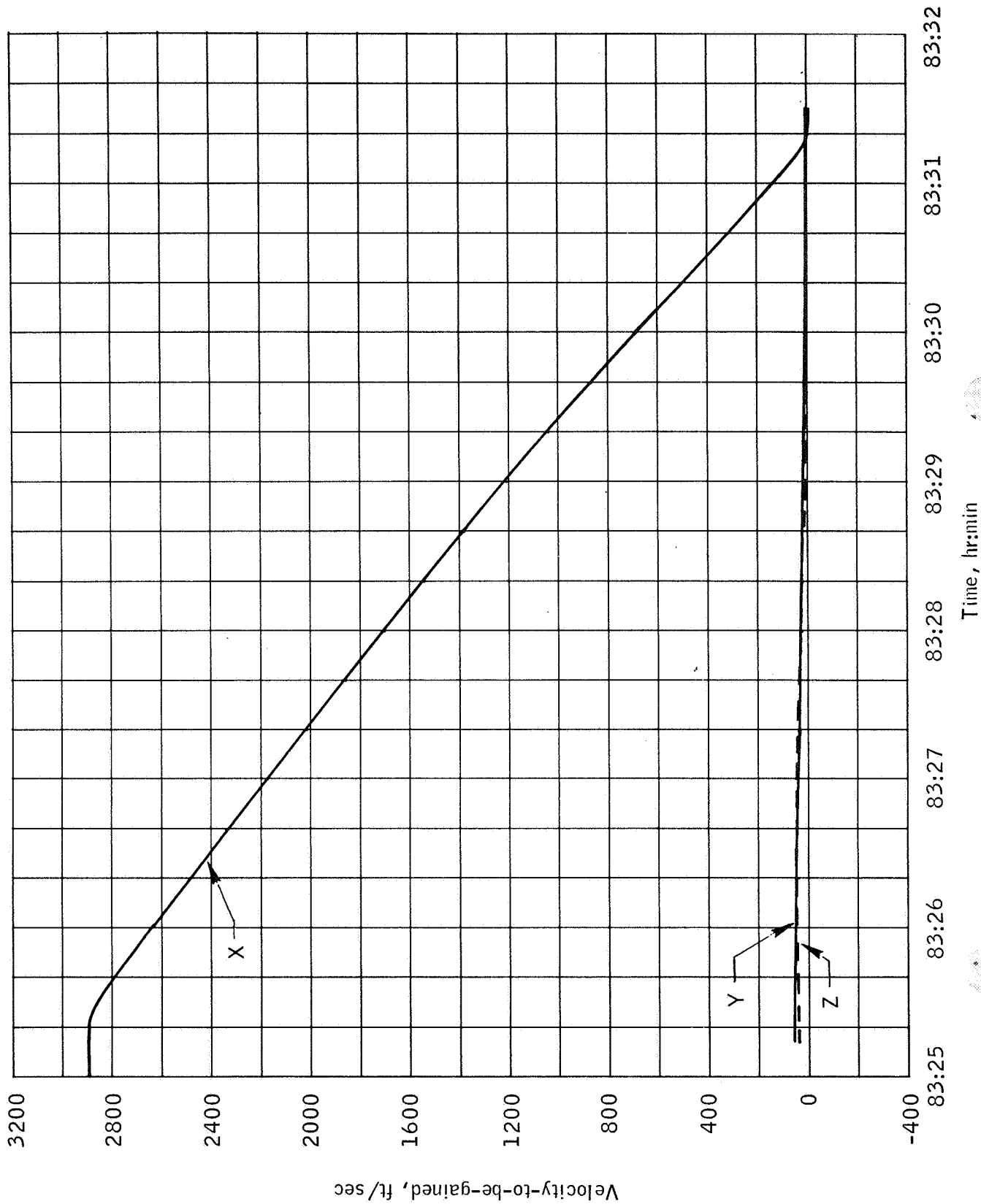
Figure 4-8   LOI-1 VELOCITY-TO-BE-GAINED
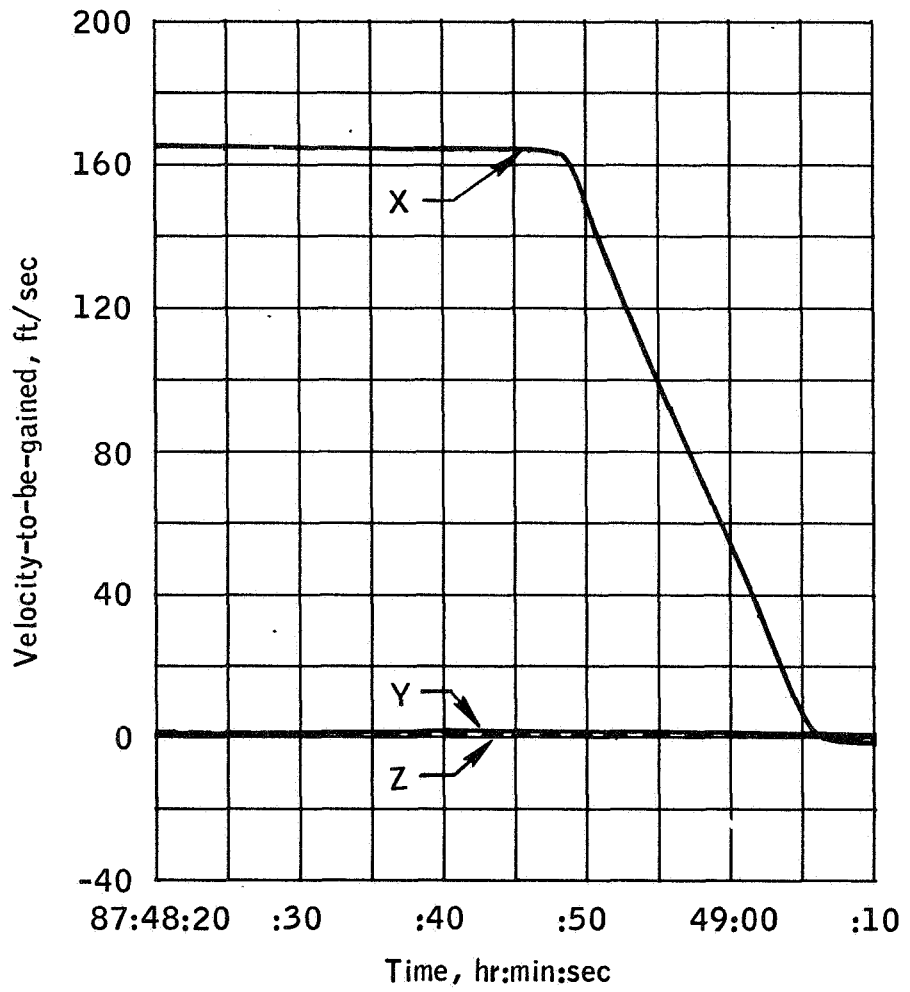
Figure 4-9   LOI-2 VELOCITY-TO-BE-GAINED

4-19
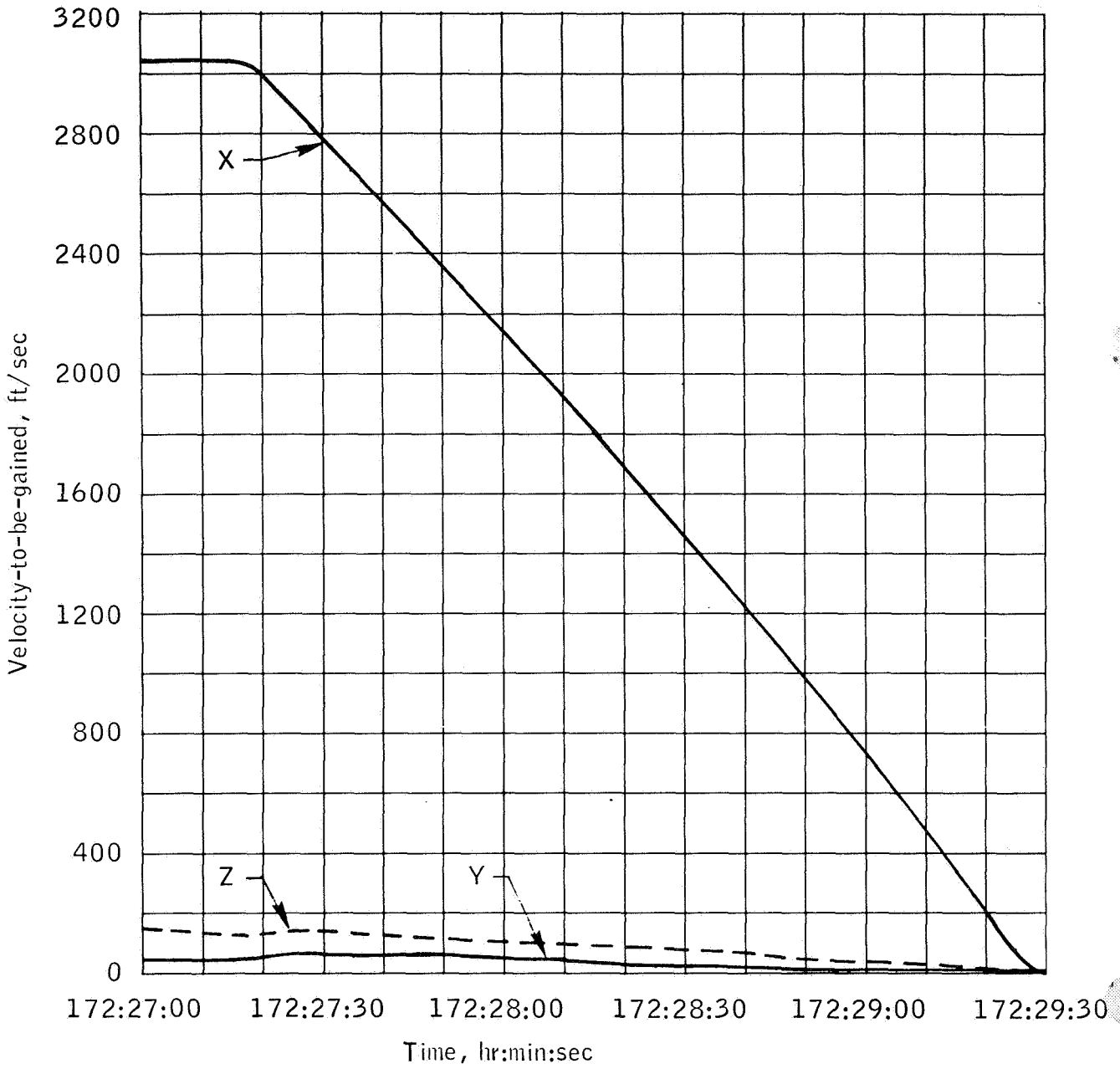
Figure 4-10   TEI VELOCITY-TO-BE-GAINED
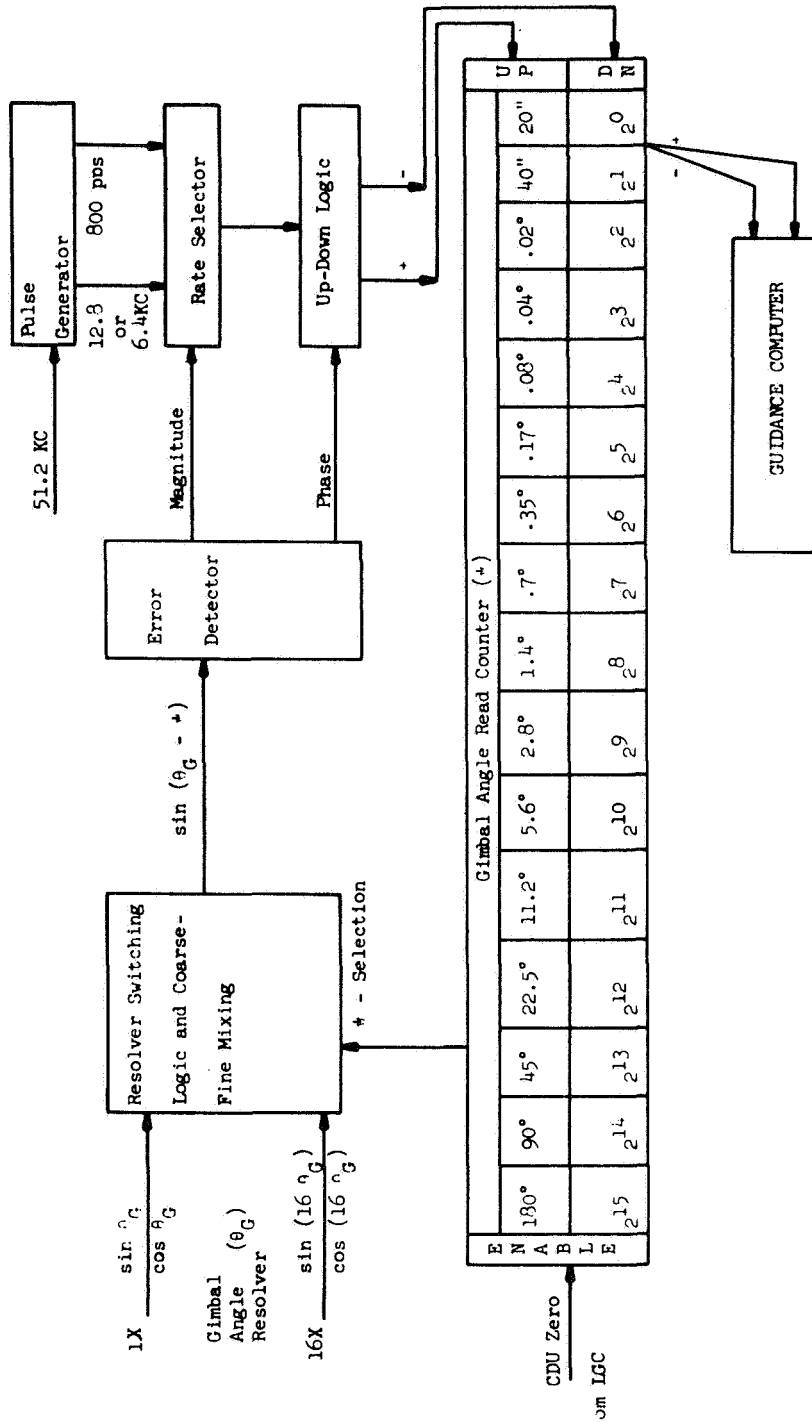
Figure 4-11   CDU MECHANIZATION

5.0 LM DIGITAL AUTOPILOT

The LUMINARY 1B Digital Autopilot was implemented in the LM Guidance Computer (LGC) for the Apollo 12 (LM-6) mission. Emphasis for the postflight analysis was placed on DAP changes incorporated into LUMINARY 1B and on changes in DAP requirements due to the steeper trajectory used for the Apollo 12 mission. No significant modifications in the control logic for coasting flight were implemented for this mission.

5.1 LM DAP PERFORMANCE DURING EARLY PHASES OF POWERED DESCENT

Powered descent initiation began using LGC program P63. RCS jets 6 and 14 were used for a two-jet 8.0 second ullage. Jet 6 toggled during ullage to maintain attitude control. DPS ignition occurred approximately 0.236 second before ullage termination. The conditions existing at DPS ignition as observed on the DSKY were:

LM inertial velocity magnitude:	5562.4 fps
Altitude rate:	- 3.3 fps
Altitude:	48,656 ft

The delta-V monitor performed satisfactorily through the burn. The ΔV threshold limit of 36 cm/sec was exceeded at the second sampling of the PIPA counts (approximately 4 seconds after ignition) and the accumulated ΔV over two-second intervals remained well above the delta-V monitor threshold limit for the duration of the burn.

After throttle up a DSKY entry was used to change the landing site downrange via the ΔRLS method. The flight controllers supplied a value of 4200 feet as the desired downrange landing site change. The landing site correction was displayed in Register 1 on the DSKY at 110:22:16.808 GET. After it was verified that the proper value had been loaded into the DSKY the data was incorporated into the LGC by striking the ENTER key at approximately 110:22:26.808 GET. Since the ΔRLS method was used after throttle up, the landing site was changed immediately. Figure 5-1 shows

a change of 4200 feet in the downrange position of the landing site in stable member coordinates. The ΔRLS method for changing the landing site worked properly, verifying this LUMINARY 1B modification.

Throttle down in P63 began at 6 minutes and 22.995 seconds after DPS ignition. This actual throttle-down time agrees closely with the value of 6 minutes and 23 seconds supplied by the ground prior to the burn.

Table 5.1 shows the maximum values during P63 for the estimated body rates, body rate gyro signals, control axes attitude errors, and control axes rate errors.

The P-axis attitude error exhibited a tendency to "hang" on the -P deadband showing the effect of an X-axis torque. Similar behavior of the P-axis attitude error was observed during Apollo 11 postflight analyses (Reference 2). The data from the Apollo 12 powered descent burn were compared with the preflight simulations and the maximum estimated rates showed good agreement with the simulation results. The attitude errors about the control axes obtained during the Apollo 12 powered descent burn (P63) were slightly higher than predicted by the simulation results and the Apollo 12 rate error data showed slightly lower values than the simulation predicted. In general, the preflight simulation results show good correlation with the actual flight results.

The downlink computer words monitoring accumulated commanded torques about the control axes (POSTORK, NEGTORK) were used to obtain information concerning the RCS jet on-time and RCS propellant required to maintain attitude control during P63. This information relates only to the RCS jet firings which produce torques about the P, U', or V' axes and does not include ullage or any other translations produced by appropriate RCS jets. Table 5.2 compares the RCS propellant required for Powered Descent with preflight simulations. The total RCS propellant required to maintain attitude control during P63 was 15.69 pounds. This core-elates well with the predicted value of 15.16 pounds.

Table 5.3 compares the durations of the LGC programs for the actual flight and the simulation. No manual control of the LM was exercised during P63 for the Apollo 12 mission.

Body rate gyro data were examined during the P63 phase to determine the general trends. Oscillations in the pitch rate were observed approximately 200 seconds after ignition. The frequency of these oscillations which were apparently due to slosh was approximately 0.55 to 0.60 Hz. Oscillations in the roll rate were observed approximately 300 seconds after ignition. These oscillations occurred at a frequency of approximately 0.60 Hz. No significant changes in the magnitudes on frequencies of the oscillations in the pitch and roll axes were observed during the initial stages of throttle down. The oscillations observed were expected and the amount of RCS activity was nominal.

5.2 LM DAP PERFORMANCE DURING POWERED DESCENT APPROACH PHASE

Upon entering P64, the phase-plane deadband was changed from 1.0 degree to 0.3 degree. The conditions at the initiation of P64 as observed on the DSKY displays were:

LM Inertial Velocity Magnitude: 477.5 fps
Altitude Rate: - 169.8 fps
Altitude: 7328.0 ft

Approximately 0.7 seconds after entering P64, the automatic pitchover maneuver was initiated. Figure 5-2 shows the actual and desired inner gimbal angle (CDUY) during pitchover. The total pitchover maneuver was -32.8161 deg. The maximum recorded estimated pitch rate during pitchover was -12.1542 deg/sec. These values were in good agreement with the simulation results. The maximum inner gimbal angle overshoot during pitchover was approximately 2 degrees. Table 5.1 shows the maximum estimated rates, rate gyro signals, attitude errors, and rate errors during the pitchover phase of P64, the overshoot during pitchover, and P64 exclusive of the pitchover maneuver. During pitchover the attitude errors were approximately twice the predicted values and the rate errors

were slightly less than twice the values predicted by the preflight simulations. During P64 (exclusive of pitchover) the attitude errors, rate errors, and actual rates were slightly larger than the corresponding, maximum values predicted by the simulation results.

Table 5.2 shows the RCS propellant required to maintain attitude control during P64. The total RCS propellant required for attitude control during P64 was 16.35 pounds. This compares extremely well with the predicted value of 16.88 pounds. More RCS jet firings were required in P64 than in P63. This results was expected based on preflight simulations and was partly due to the reduced phase-plane deadband used during P64.

The redesignations during P64 were identified and no problems were encountered even though some coupling was observed between the cross-range and downrange redesignations. Redesignations are performed by deflecting the rotational hand controller in the direction of the desired displacement of the landing site. Figures 5-3 and 5-4 show the changes in the downrange and crossrange positions of the landing site in stable member coordinates during the time of expected redesignations. These figures indicate the following sequence of input redesignations:

a)   One redesignate right (110:29:43.308) with coupling observed in the downrange position of the landing site.

b)   Two redesignates downrange (110:30:01.328).

c)   One redesignate right (110:30:11.308).

d)   Two redesignates uprange (110:30:29.328) with coupling observed in the crossrange position of the landing site.

e)   One redesignate right (110:30:41.308).

The total effect of the redesignations observed from Figures 5-3 and 5-4 was to change the position of the landing site by approximately 360 feet downrange (long) and 750 feet to the right (crossrange).

The mode control switch was changed from AUTO to ATT HOLD at 110:30:45.688 GET. This was 3.14 seconds prior to entering P66. During this time interval of P64 in the ATT HOLD mode, no RHC input commands were observed in the LGC input register (Channel 31) monitored on telemetry. The only manual control exerted during P64 would be short commands which would not be seen on Channel 31 due to the two second data read cycle and the use of the hand controller for redesignation.

Nominal behavior was observed during the P64 phase of Apollo 12 powered descent. The change in the phase-plane deadband from 1.0 degree to 0.3 degree appears to reduce the magnitude of the slosh oscillations with an increase in RCS jet firings being obtained. The P64 redesignation capability was exercised extensively and appears to have performed well.

5.3 LM DAP PERFORMANCE DURING POWERED DESCENT LANDING PHASE

The LM DAP performance during P66 cannot be compared to preflight testing since the MSC bit-by-bit simulation does not easily lend itself to testing manual control modes. Indeed, any simulation of P66 will not accurately predict flight conditions due to the profusion of RCS activity obtained in achieving lunar touchdown.

The conditions observed on the DSKY at the entrance to P66 were:

Horizontal velocity:	78.7 fps
Altitude rate:	- 8.8 fps
Altitude:	368.0 ft (P66 entered at higher altitude on Apollo 11)

Table 5.1 shows the maximum estimated rates, rate gyro signals, attitude errors, and rate errors during P66 (excluding the region near touchdown) and near lunar touchdown.

Approximately 3.6% of the usable DPS propellant was still available after the DPS engine was cutoff. Table 5.2 shows the RCS propellant required to maintain attitude control during P66 (Apollo 12) and P65 (preflight simulation).

The total RCS propellant required to maintain attitude control during P66 was 60.2550 pounds. The total RCS propellant required to maintain attitude control during Powered Descent (P63, P64, and P66) was 92.2966 pounds. No RCS jet firings were observed after 110:32:37.04 GET which is approximately 0.24 seconds after touchdown occurred. Approximately 9.21 pounds more RCS propellant was used during P66 for Apollo 12 than for Apollo 11.

5.4 POWERED ASCENT

The Ascent Propulsion System (APS) was utilized from lunar liftoff to lunar orbit insertion. The LM DAP utilized the powered ascent program (P12) during this phase. Review of the flight data indicated body accelerations at fire-in-the-hole were close to those experienced on Apollo 11. For both Apollo 11 and 12 data indicated the dynamics had higher pitch effects and lower roll effects than were modeled in preflight simulators. Control dynamics during the steady state periods of the burn were in close agreement with preflight predictions. A 32.5 ft/sec overburn was experienced at orbit insertion as the result of a procedure error. The additional ΔV was quickly detected by the LM crew and the RCS thrusters were used to remove the extra ΔV.

5.4.1 Lunar Liftoff

The ignition signal to the APS engine occurred at 142:03:47.75 GET. From Figure 5-5, a short period (0.5 seconds) of low amplitude transients in the spacecraft angular rates can be detected after the "on" signal. Later significant rate changes are evident indicating the liftoff from the descent stage. To correlate the small, initial transient period with the APS thrust buildup, the theoretical engine-start thrust profile (Figure 5-6) indicates that after receipt of the engine-start signal the thrust sufficient for liftoff could have occurred as long as 0.520 seconds later. The telemetry sample rate of 0.1 seconds caused an uncertainty, so the liftoff could have occurred 0.1 seconds earlier than shown on Figure 5-5. The time at which large angular accelerations were first detected was 0.5 seconds after the engine-start signal. Hence,

a good correlation existed between the theoretical thrust buildup and the occurrence of the large angular motion which is concluded to be start of liftoff. The small, initial transients prior to liftoff were caused by a lifting force exerted by 1000 PSIA oxygen entrapped in an ECS line running from the descent to the ascent stage. The ECS line has a telescope type interface connection that is held in the retracted position by the separation bolts. When the bolts are blown the tele-scoped line expands and acts as a pneumatic shock absorber, thus the initial low amplitude "rocking" of the vehicle.

The maximum angular rates experienced at liftoff were -1.09, 4.25 and 3.06 deg/sec about the yaw, pitch and roll, axis, respectively. The values obtained from preflight simulations were -0.3, 3.5 and 10.9 deg/sec. The actual dynamics had higher pitch effects and lower roll effects than were modeled. This rate response was essentially the same as that ob-served from Apollo 11 data. Estimates of the angular accelerations at liftoff were obtained by determining the slopes of the rate data pre-sented in Figure 5.9. The maximum indicated accelerations were 4.0, 38, and 18 deg/sec^2 about the yaw, pitch, and roll axes, respectively. The correponding accelerations observed from the flight of Apollo 11 were -6.0, 25, and 12 deg/sec^2. The staging or fire-in-the-hole (FITH) forces modeled in the simulator are defined in Reference 2. The yaw and roll accelerations are less than the values obtained from the MSC bit-by-bit simulator. The pitch acceleration is over twice the value expected from the preflight simulations. Indeed, the model of FITH moments predicts roll accelerations an order of magnitude greater than the pitch accelerations. However, the converse was true from the flight data of both Apollo 11 and 12.

5.4.2 Pitchover Maneuver

The pitchover maneuver was initiated at 142:03:57.06 GET. The dynamic response of the LM during the pitchover is shown in Figure 5-7. The graph of CDUY (actual) less CDUY (desired) is the approximate body attitude error with respect to the X-axis steering vector. One may

observe from the figures that the pitchover was accomplished smoothly within 5 seconds with no significant overshoot. The CDUY output rate was 16.1 deg/sec and the maximum angular acceleration was 11.05 deg/sec^2. The low frequency oscillation apparent on the pitch rate data in Figure 5-16 was the limit cycle frequency caused by the eccentric thrust vector. The magnitude and frequency of the pitch rate limit-cycle during the pitchover maneuver were the same as experience on Apollo 11 and as predicted by the preflight simulations.

5.4.3 Manual X-Axis Maneuver

At 142:04:48.0 GET the astronaut yawed the LM 20 degrees to the right to improve communications. The rate and attitude responses for this maneuver are shown in Figure 5-8 . The maximum rate experienced in the maneuver was 4.7 deg/sec. There was no significant attitude or rate overshoot when the astronaut commanded the rate to zero. The predominate oscillations apparent in the yaw rate trace are the result of a cross-couple with the pitch-roll limit-cycle. This cross-couple oscillation in yaw is apparent throughout the burn; however, it never reached a magnitude large enough to cause a control jet to fire.

5.4.4 Steady State Operation

During the course of the ascent burn the pitch and yaw rates exhibited limit-cycle response caused by the eccentric thrust vector. Averaging over several oscillation cycles at various times in the burn gave a frequency range of 0.34 to 0.37 Hz for the limit-cycle frequency, which agrees with the preflight simulation estimates of 0.32 to 0.36 Hz. Following the pitchover maneuver, the maximum peak-to-peak amplitudes of the pitch and roll limit-cycle rates were 5.3 deg/sec and 3.3 deg/sec, respectively. These rates were approximately half the magnitude of those experienced on Apollo 11 and as predicted by the preflight simulation estimates. As predicted, a low frequency modulation of the pitch and roll rates may be seen in the data. As the burn progressed, the cg moved into close alignment with the thrust vector so that at cutoff the limit-cycle magnitudes had been reduced essentially to zero. This behavior was also as predicted by the preflight simula-

tions. Following the pitchover, the maximum attitude errors resulting from the limit-cycle oscillations were ± 3 degrees in both pitch and roll, with an approximate average deviation throughout the burn of ±1.5 degrees. Spacecraft dynamics during ascent are shown in Figures 5-9a and 5-9b.

5.5 LM DEORBIT

To provide a lunar surface disturbance of known magnitude and location, the LM ascent stage was deorbited by an RCS burn and subsequently impacted on the lunar surface. The burn was quite similar to the RCS rendezvous burns in that two of the four RCS jets toggled during the burn to provide control torques for attitude control. The phase-plane plots for the burn indicated that the attitude errors were small in amplitude and were biased at the expected 1.8 degrees. Also, the limit-cycles exhibited a rate offset. Since the APS engine was never utilized, the rate estimator did not incorporate any estimates of offset accelerations in its computations of rate. Hence, the torques resulting from the offset of the cg from the geometric center of the RCS quads created "unmodeled accelerations" causing the rate offset. The LM DAP performed nominally throughout the LM deorbit burn.

5.5.1 Burn Implementation

The RCS burn was implemented by ground command. The APS (Ascent Propulsion System) external ΔV program P42 was requested on the DSKY and normal program sequencing was maintained through ullage. At this point in P42, the LGC awaits depression of the PROCEED key to permit APS ignition and subsequent continuation through the program. If this input is not received, the ullage is continued and existing displays are maintained. Also if the PROCEED command has not been received, the LGC further interrogates the DSKY to determine if it is desired to complete the burn via the RCS. Depression of the ENTER key indicates to the LGC that the burn has been satisfactorily completed via the RCS. This was the procedure followed for the deorbit. The downlink RCS bi-level data indicates shutting off of the translational jets with the telemetered depression of the ENTER key. To compensate for the communication time lag associated with the remote control of the burn,

5-9

the command to depress the ENTER key was issued when the total ∆V accumulated was approximately 169.7 ft/sec (86 sec) compared to a desired ∆V of 191.0 ft/sec. This produced an effective two second lead in the cutoff signal. Also, with the depression of the ENTER key, the attitude errors were zeroed by setting the desired CDU's equal to the present actual CDU's. With the completion of the burn, the LGC idle program P00 was entered. Entrance to P00 places the LGC in an idle mode with the DAP attitude hold about the last set of desired CDU's defined.

The actual ∆V achieved, as observed on the DSKY at termination of the burn, was 196.2 ft/sec. The overburn is most reasonably attributed to inaccuracies in the lag compensation required for remote termination of the burn.

5.5.2 DAP Performance

The DAP configuration for this type of burn utilizes a composite of powered and coasting flight parameters. Even though the LGC was in powered flight program P42, the DAP was configured for coasting flight and no offset accelerations were expected (DRIFTBIT discrete of DAPBOOLS set to one). The flow through P42 had, however, proceeded sufficiently far to reset the RCS deadband to 1 degree (the nominal powered flight attitude error deadband). The deorbit RCS burn was performed on the drifting flight phase plane with a 1 degree deadband.

As shown in Figures 5-10 and 5-11, the maximum rates observed during the ignition transients period were 1.9 deg/sec and -1.54 deg/sec in pitch and roll, respectively. The maximum control axes attitude errors during this period were 2.17 deg in U' and 2.05 deg in V'. The ignition transients were damped quickly by toggling of the translational jets. Substantial jet toggling was present throughout the burn. This jet toggling was necessary for attitude control of the vehicle under the influence of disturbance torques due to cg offset. The resulting limit-cycle was centered in the vicinity of 1.8 degrees, the expected deadband when rates are low. Also due to steady-state rate errors generated by the

state estimator, the limit-cycle was displaced above (or below) the attitude error axis. The phase planes for a portion of the deorbit burns are presented in Figures 5-12 and 5-13. As shown, the RCS limit-cycles are based around the deadbands and also displaced vertically due to steady-state errors. The steady-state indicated by the data are approximately +.44 deg/sec and -0.30 deg/sec in U' and V', respectively. The switching line defined for this configuration intercepts the attitude error axes at ± 1.8 degrees. The limit-cycle is biased around the deadband since a constant disturbance is present due to the cg offset relative to the geometric center of the four translational jets being fired. Since the APS engine was never utilized, the rate estimator did not incorporate any estimates of offset accelerations in its rate computations. Hence, the torques resulting from the offset of the cg from the geometric center of the RCS quads created "unmodeled accelerations." An estimation of these "unmodeled accelerations" was made and the effect of these accelerations on the rate estimator correlated well with the steady-state rate error evidenced in the phase plane plots. This phenomenon has been observed during RCS burns on previous flights and is not considered a serious problem.

As shown in Figure 5-10 and 5-11, the vehicle steady-state response was quiescent and well bounded. Rate amplitudes as defined by data from the body mounted gyros were ± 0.5 deg/sec in both pitch and roll. Attitude errors, while biased around the deadbands oscillated with very small amplitudes.

The onboard estimate of vehicle mass at ignition was 5335 lbs and just prior to impact the vehicle mass was 5254 lbs. As these values indicate, the LM-deorbit burn represents flight of the lightest ascent vehicle ever flown in a RCS translational burn.

As mentioned earlier, a slight overburn resulted from remote termination of the burn. The residuals as displayed on the DSKY via NOUN 85 were:

$$VG(X) = -5.1 \text{ ft/sec}$$
$$VG(Y) = +1.0 \text{ ft/sec}$$
$$VG(Z) = -8.2 \text{ ft/sec}$$

At approximately 149:53:0.0 GET, the DSKY defined attitude maneuver routine, R62, was entered via VERB 49. An attitude maneuver to return the vehicle to burn attitude was performed. This was a three axis maneuver and involved only a few degrees change in attitude. At the time, the vehicle was in drifting flight attitude hold with a 5 degree deadband with small overshooting. The CDUD's at this time were those existing when the "Enter" was uplinked to command RCS cutoff. Thus, the DAP was maintaining attitude about a desired attitude slightly different than that defined at the beginning of the burn. The attitude maneuver in effect returned the DAP to attitude hold about the original burn attitude which was only slightly different from the present desired attitude. Overall, the downlink data shows nominal attitude control for the entire deorbit event.

Table 5.1 MAXIMUM ESTIMATED RATES, RATE GYRO SIGNALS, ATTITUDE ERRORS, AND RATE ERRORS DURING VARIOUS PHASES OF POWERED DESCENT

Powered Descent Phase	DAP Estimated Body Rates (deg/sec)			Body Rate Gyro Signals (deg/sec)		
	OMEGAP	OMEGAQ	OMEGAR	Yaw Rate	Pitch Rate	Roll Rate
P63	.420	-2.351	-1.527	.494	+2.273	+1.680
Pitchover Phase of P64	-----	-----	-----	-----	-----	-----
Overshoot During Pitchover	-----	-----	-----	-----	-----	-----
P64 (exclusive of pitchover)	-2.304	-1.445	1.772	-2.273	2.075	1.878
P66 (excluding region near touchdown)	-6.334	7.641	-4.592	-7.213	8.794	-6.621
Near touchdown	-2.332	17.229	-4.112	-4.279	19.466	-7.806

5-13

Table 5.1 MAXIMUM ESTIMATED RATES, RATE GYRO SIGNALS, ATTITUDE ERRORS, AND RATE ERRORS DURING VARIOUS PHASES OF POWERED DESCENT (cont'd)

Powered Descent Phase	Attitude Errors (deg)				Rate Errors (deg/sec)	
	PERROR	U'ERROR	V'ERROR	OMEGAP ERROR	OMEGAU'ERROR	OMEGAV'ERROR
P63	-1.82	-1.62	1.75	3.1	1.98	1.41
Pitchover Phase of P64	-1.62	6.78	-7.09	1.12	-4.57	4.34
Overshoot During Pitchover		-1.50	1.19	-	1.89	-.91
P64 (exclusive of pitchover)	-.90	-.67	-.79	.69	.88	1.51
P66 (excluding region near touchdown)	.92	-3.56	3.80	-6.33	4.70	-5.15
Near touchdown	-.35	-1.01	-.94	-2.33	7.95	-14.22

TABLE 5.2 RCS PROPELLANT REQUIRED TO MAINTAIN ATTITUDE
CONTROL DURING VARIOUS PHASES OF POWERED DESCENT

Powered Descent Phase	Preflight Simulation RCS Propellant Consumption (pounds)	Apollo 12 RCS Propellant Consumption (pounds)						
		+U' Control	-U' Control	+V' Control	-V' Control	+P Control	-P Control	TOTAL
P63	15.16 pounds + 5.03 pounds for "windows-up" maneuver	5.825	2.929	3.534	2.135	1.253	.016	15.69
P64	16.88	3.751	3.266	3.077	2.755	1.851	1.649	16.348
P65	1.28			N/A				N/A
P66	N/A	13.111	12.110	11.200	11.201	6.651	5.982	60.255

5-15

Table 5.3   TIME DURATION OF DESCENT PROGRAMS

Program	Preflight Simulation	Apollo 12
DPS Ignition to End of P63	504.515 seconds	512.364 seconds
P64	144.217 seconds	98.00 seconds
P65 to Touchdown	30.065 seconds	N/A
P66 to Touchdown	N/A	107.972 seconds
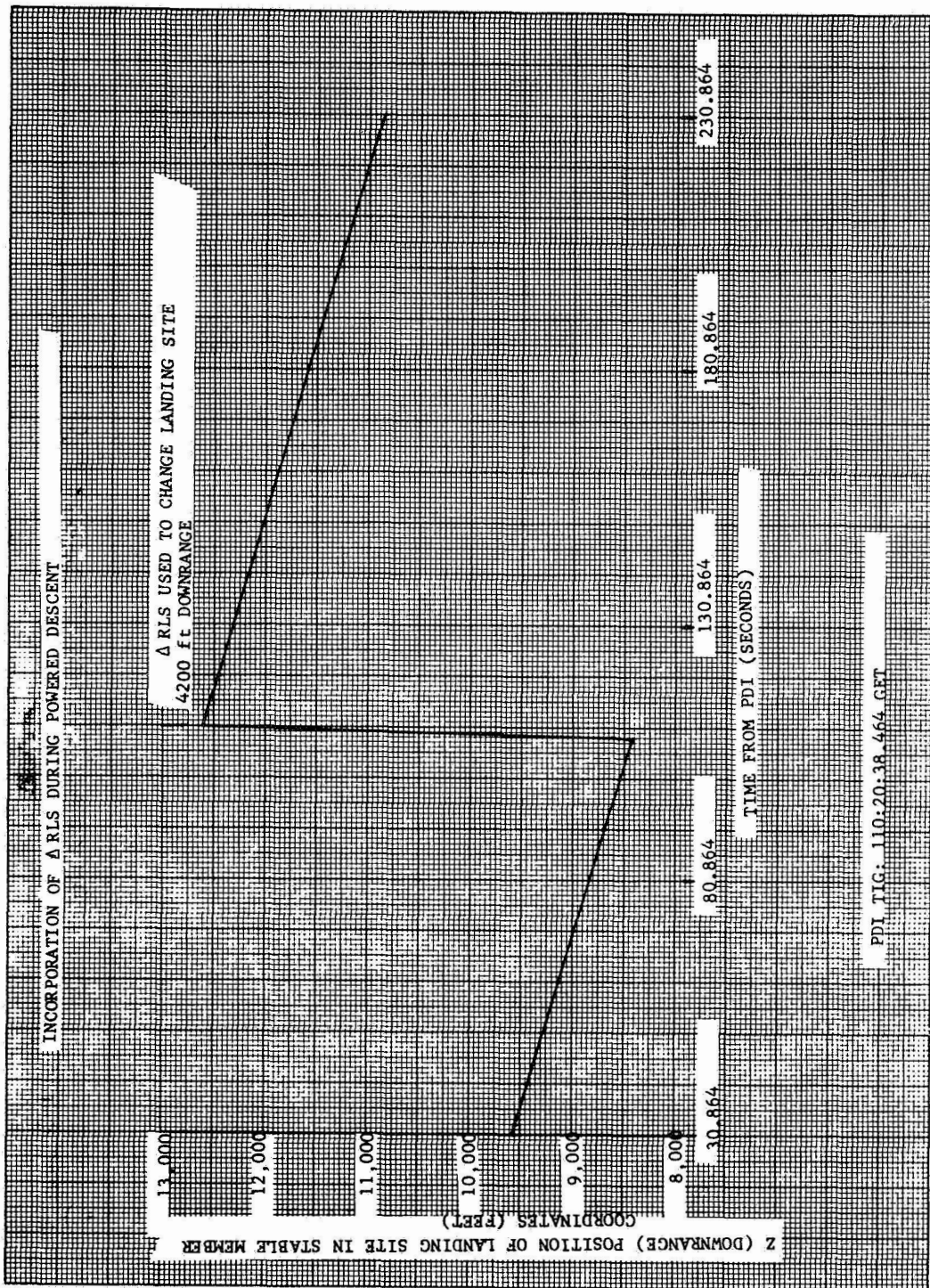
Figure 5-1   INCORPORATIONS OF ΔRLS DURING POWERED DESCENT
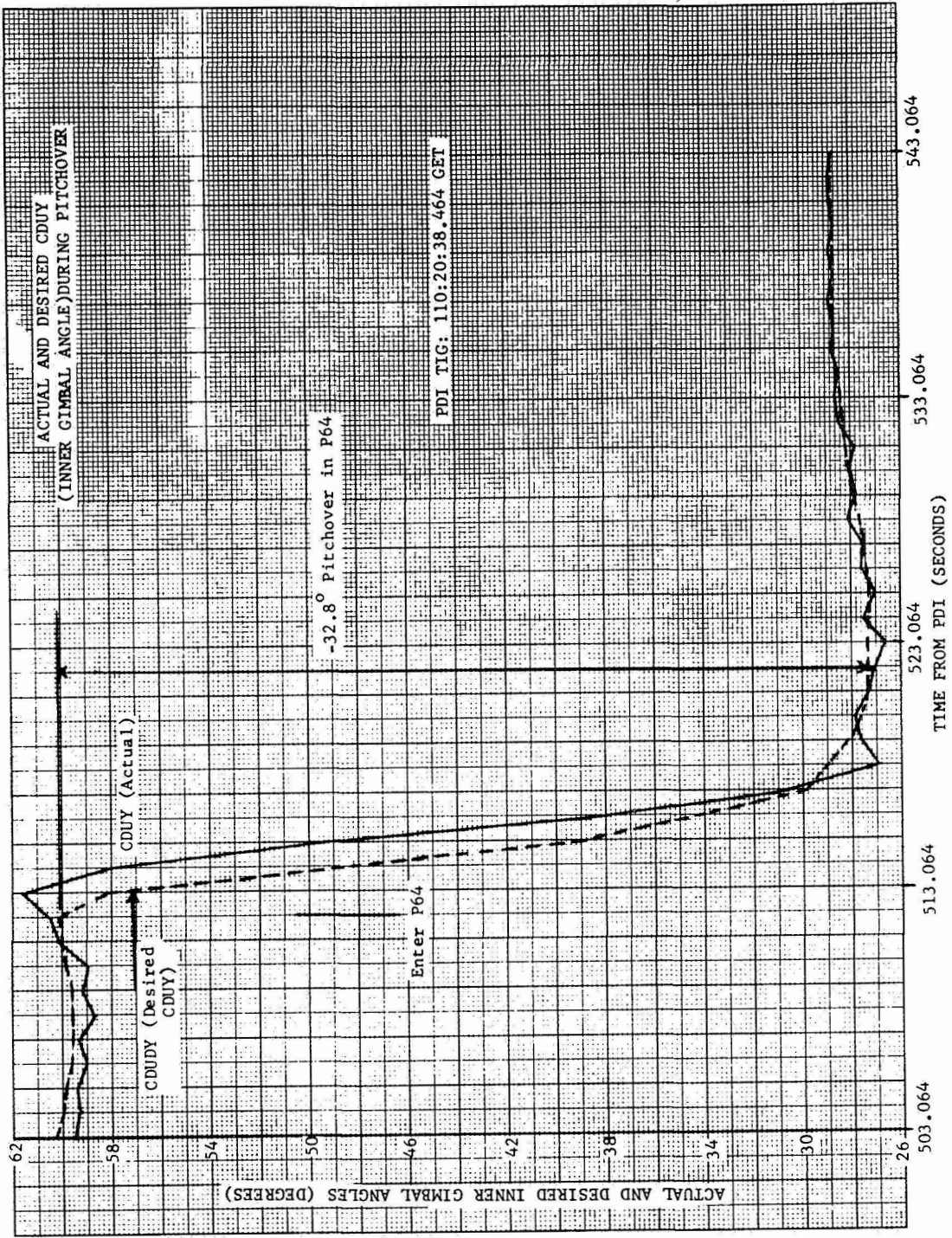
Figure 5-2   ACTUAL & DESIRED CDUY DURING PITCHOVER
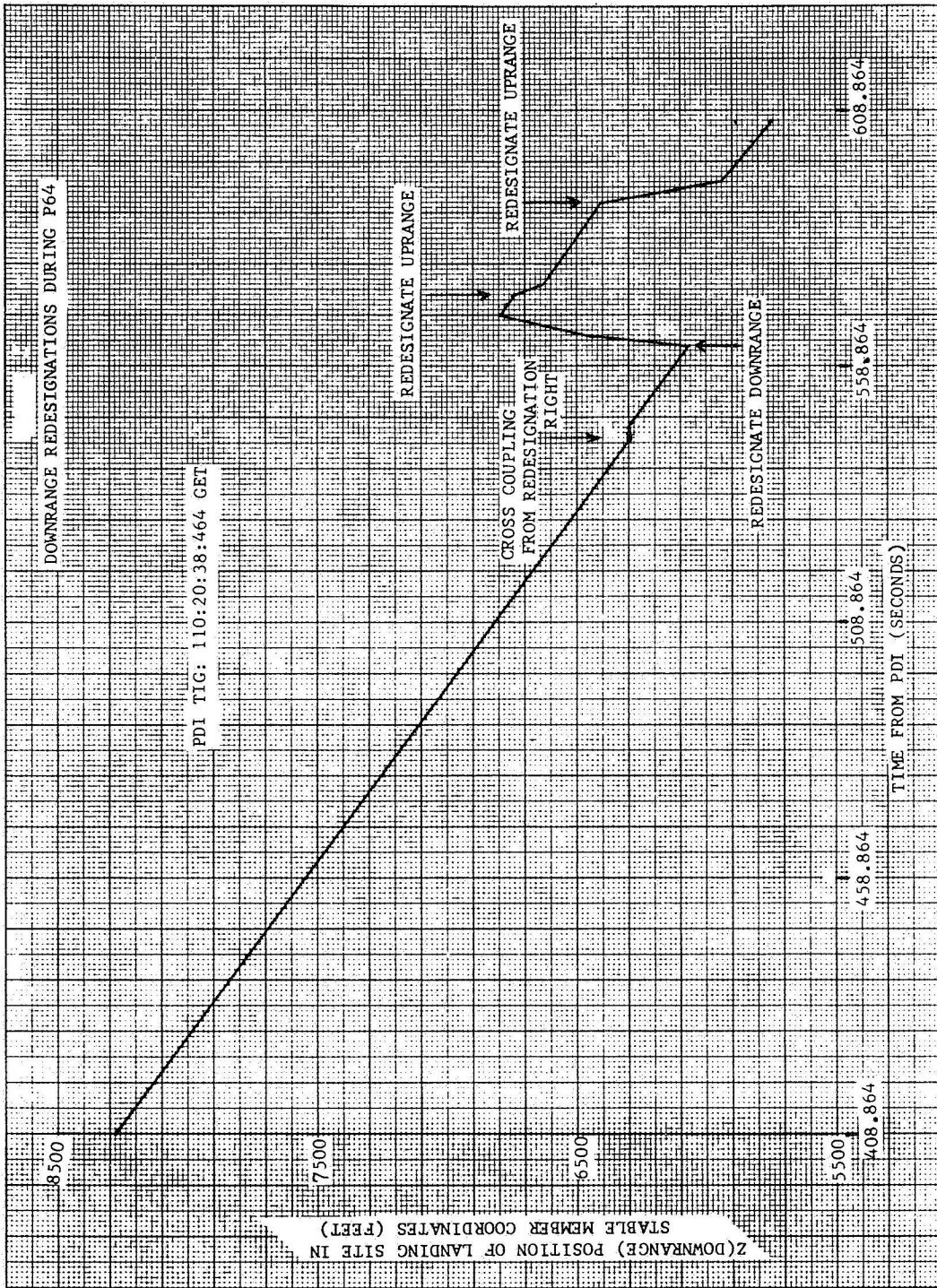
Figure 5-3   DOWNRANGE REDESIGNATIONS DURING P64
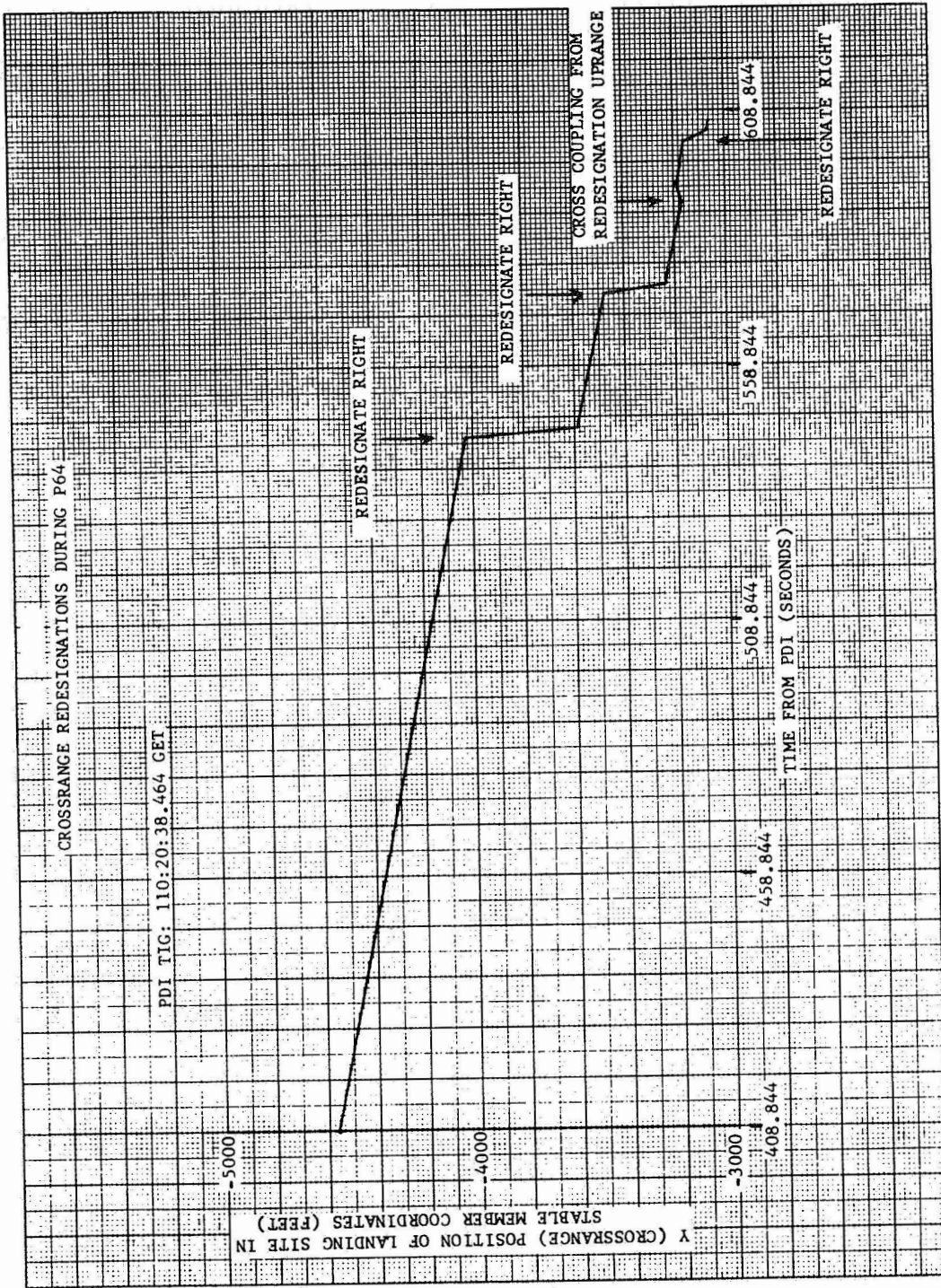
Figure 5-4   CROSSRANGE REDESIGNATION DURING P64
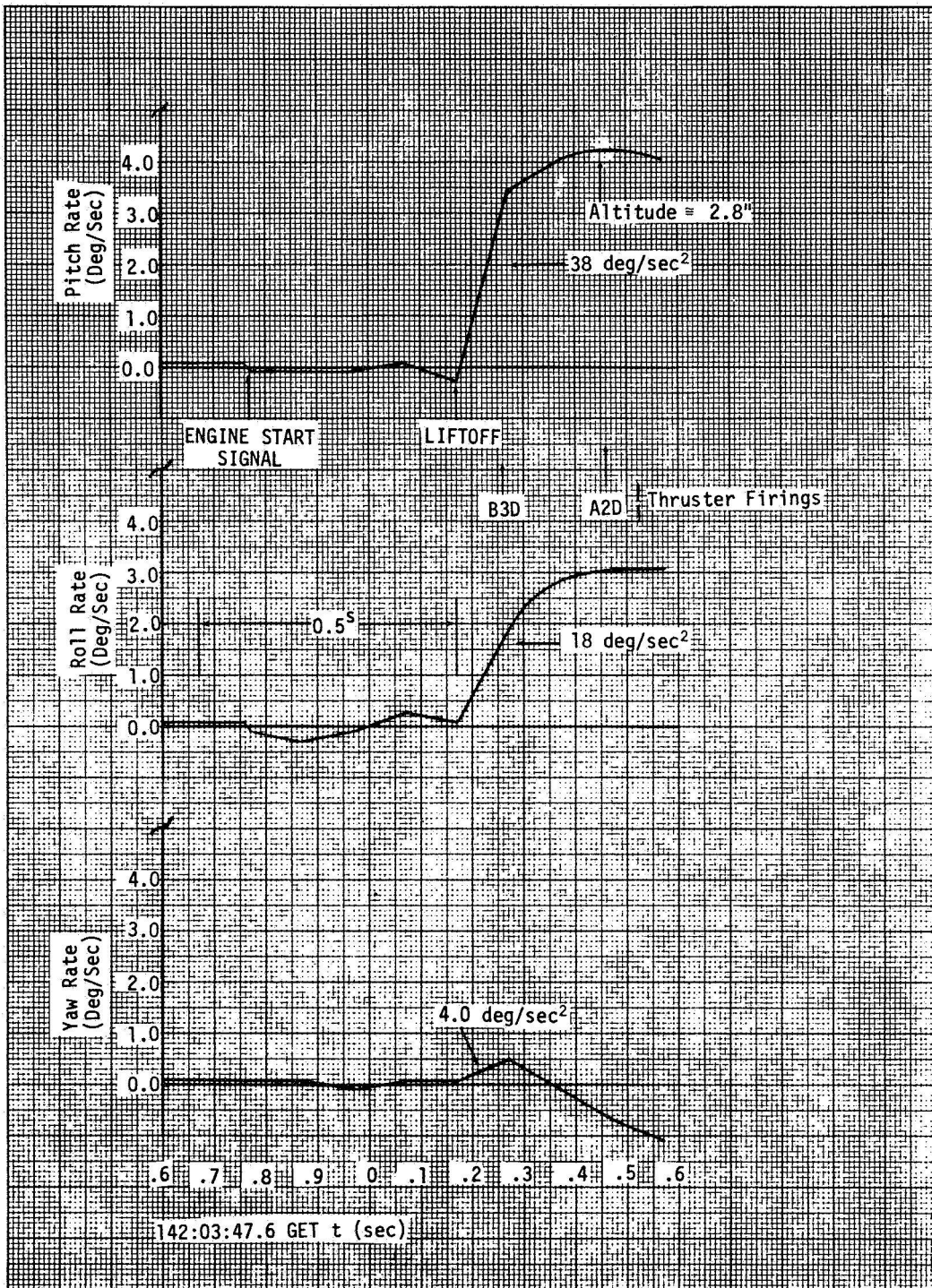
Figure 5-5   ANGULAR RATES AND ACCELERATIONS
AT LIFTOFF FROM THE MOON
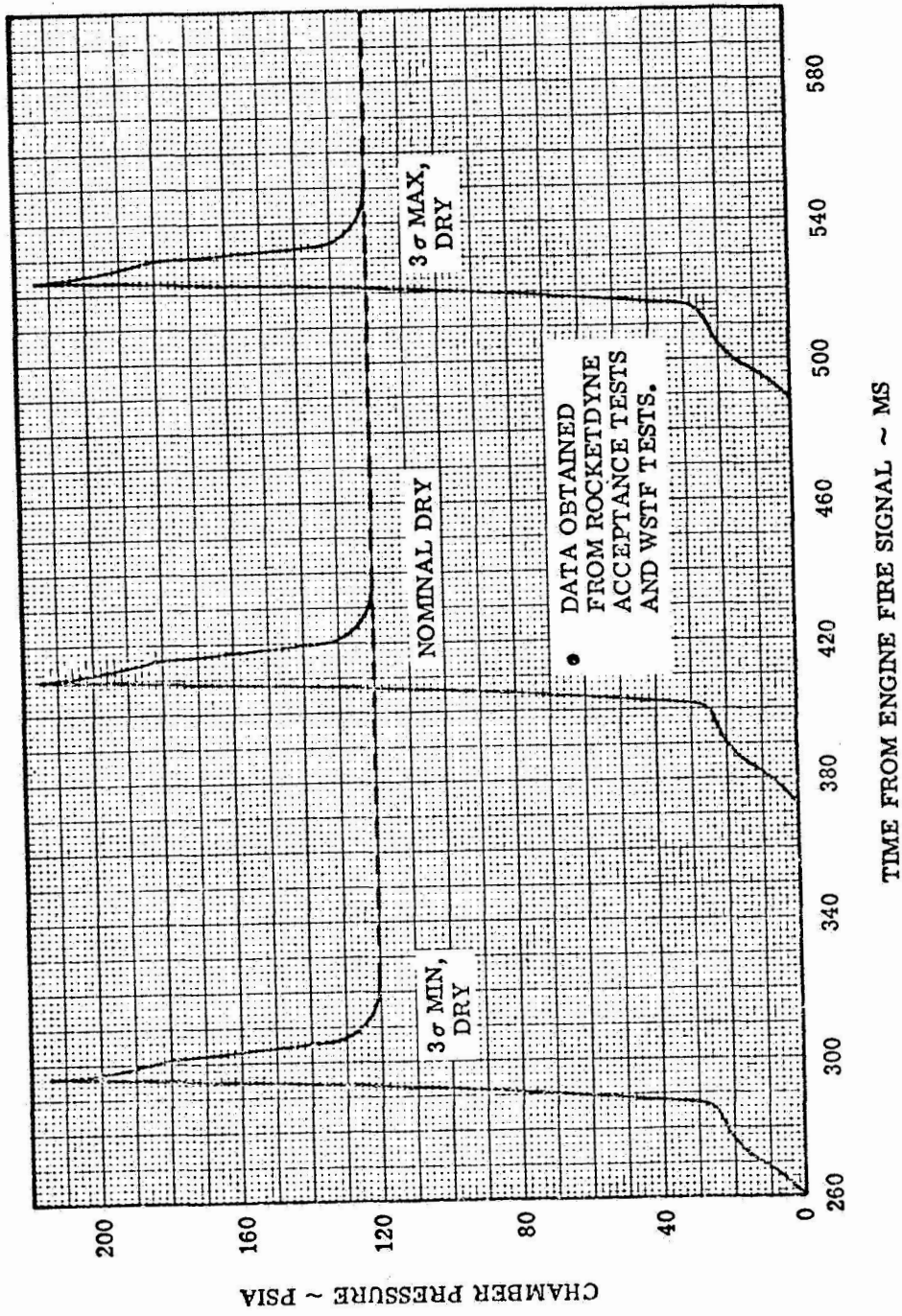
Figure 5-6   APS TRANSIENT DRY START CHAMBER PRESSURE VERSUS TIME

Figure 5-7   PITCHOVER MANEUVER

5-23
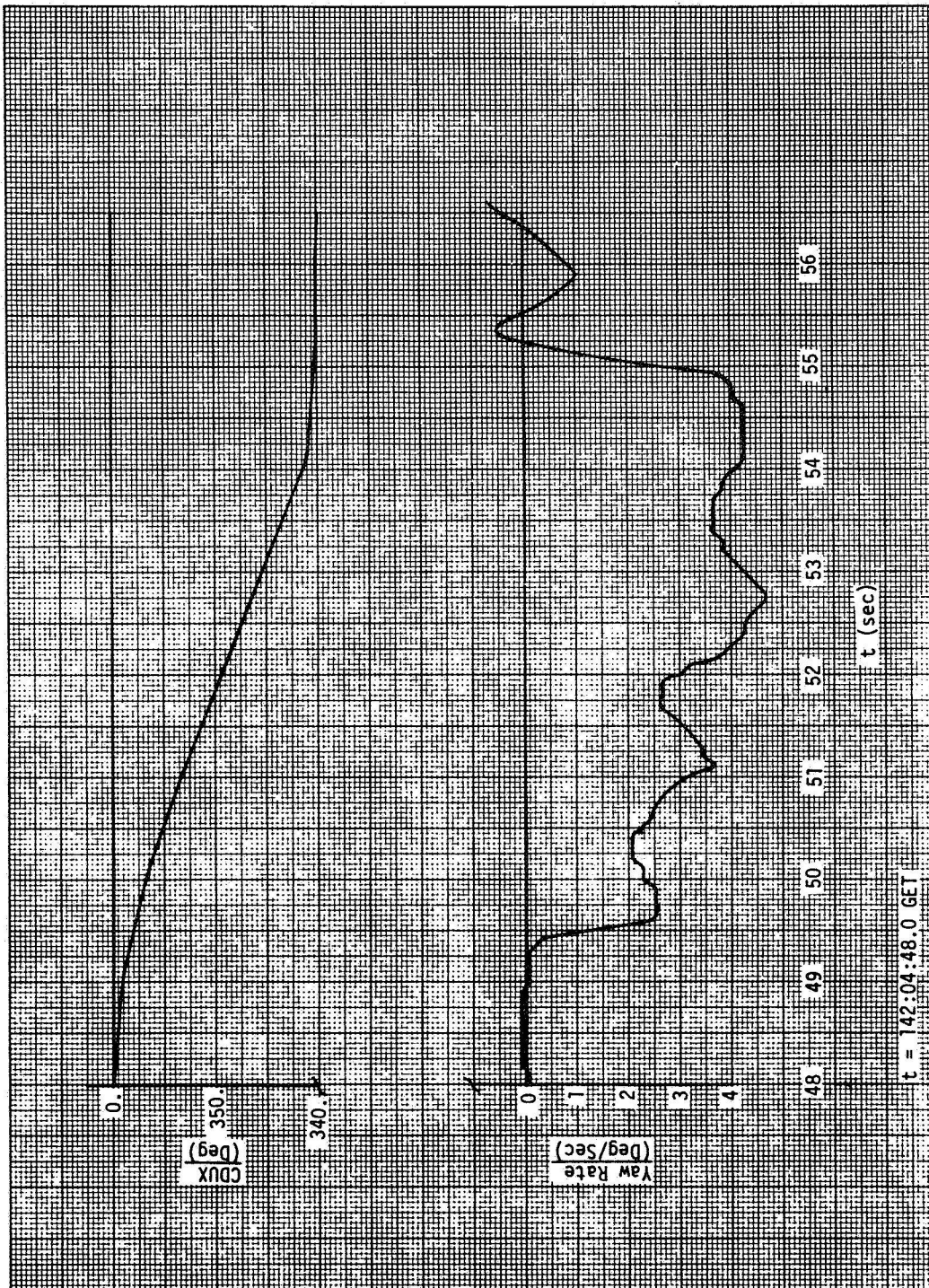
Figure 5-8   MANUAL X-AXIS MANEUVER
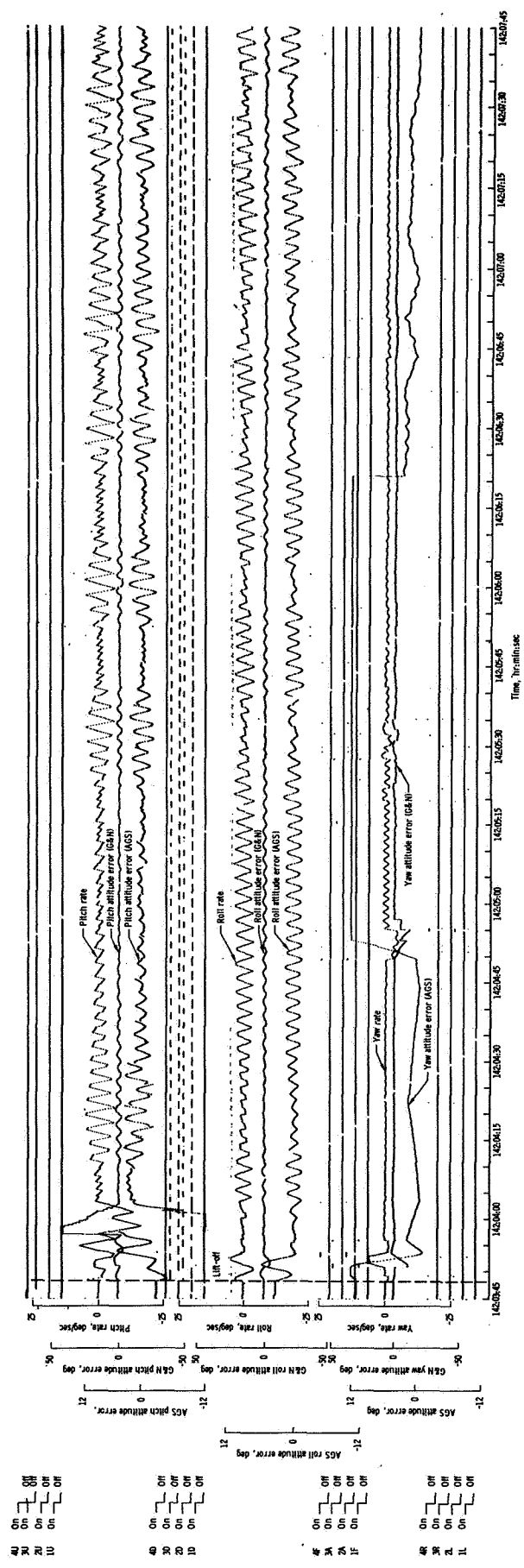
Figure 5-9a SPACECRAFT DYNAMICS DURING APS LUNAR ASCENT

5-25
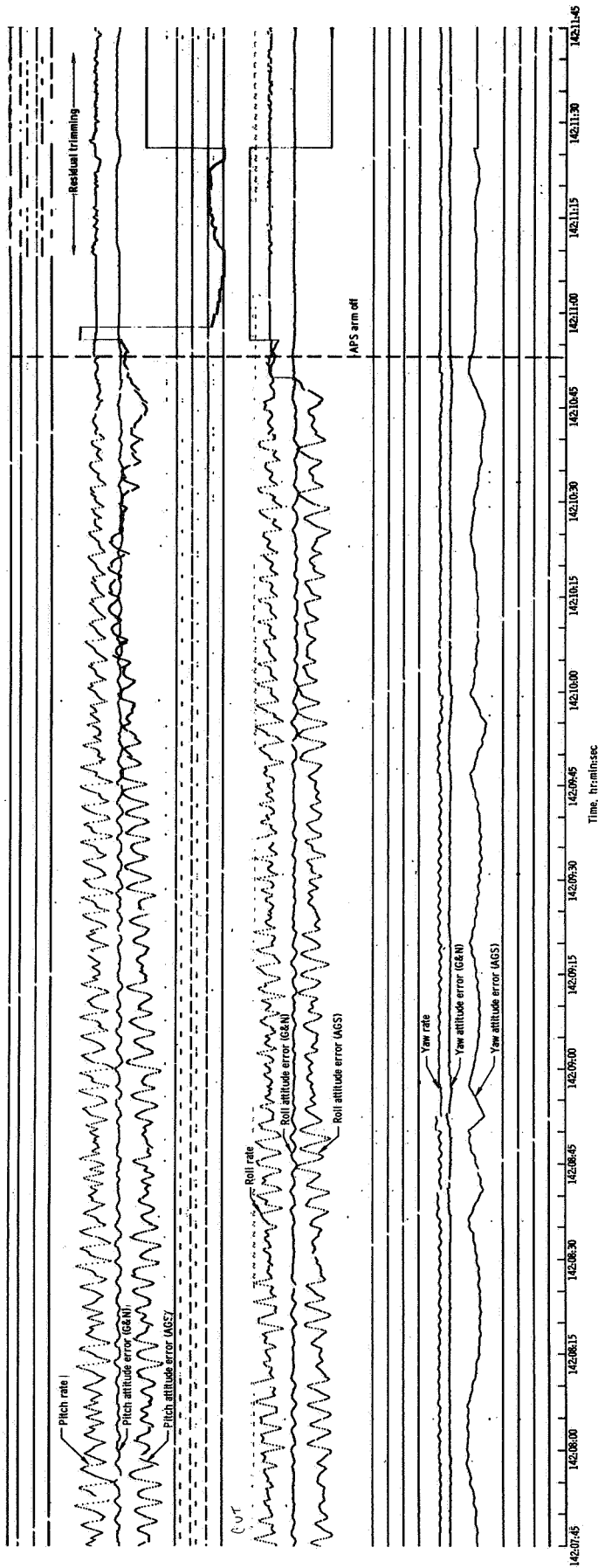
Figure 5-9b SPACECRAFT DYNAMICS DURING
APS LUNAR ASCENT

5-27
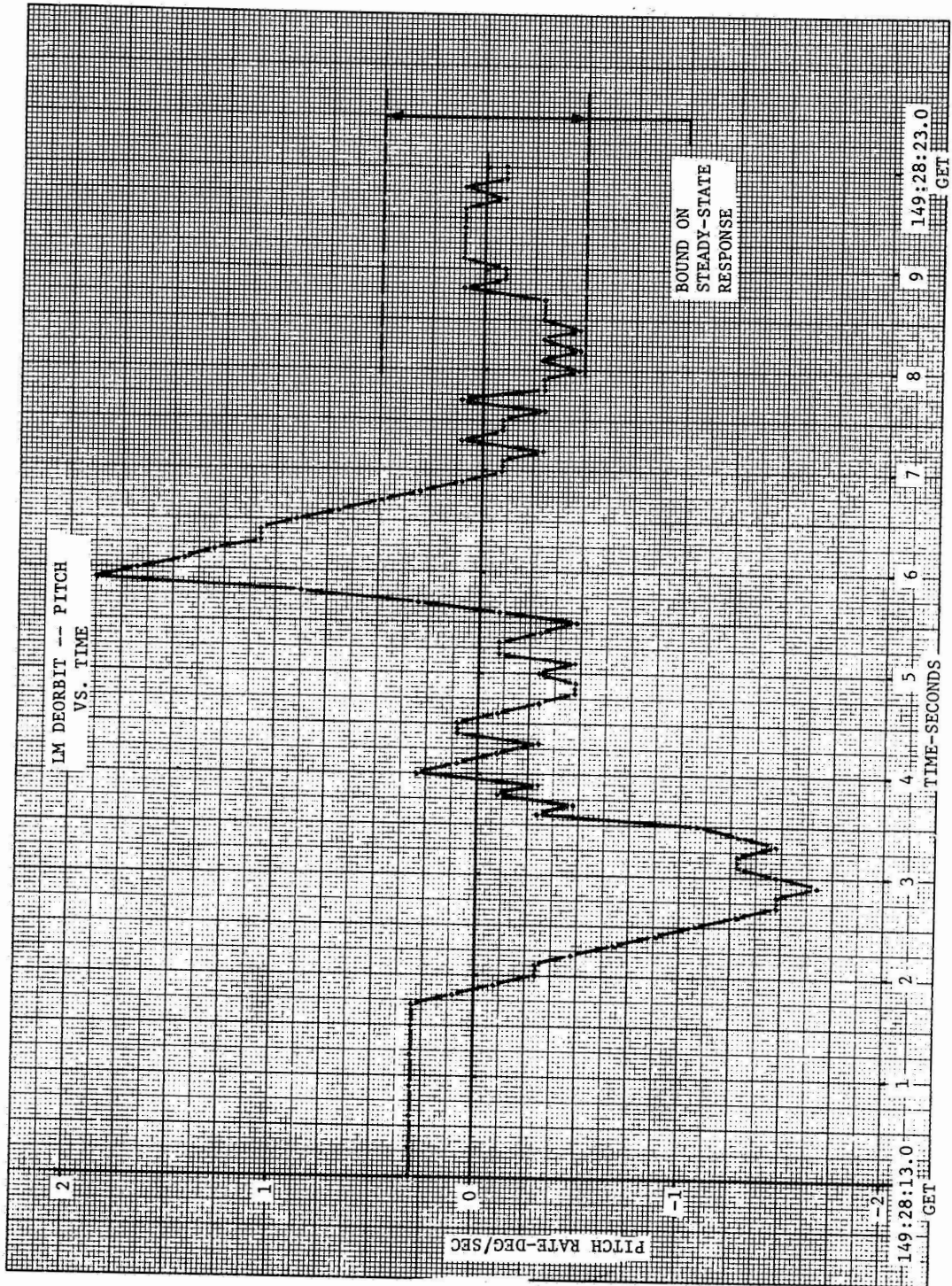
Figure 5-10   LM DEORBIT PITCH RATES

5-29
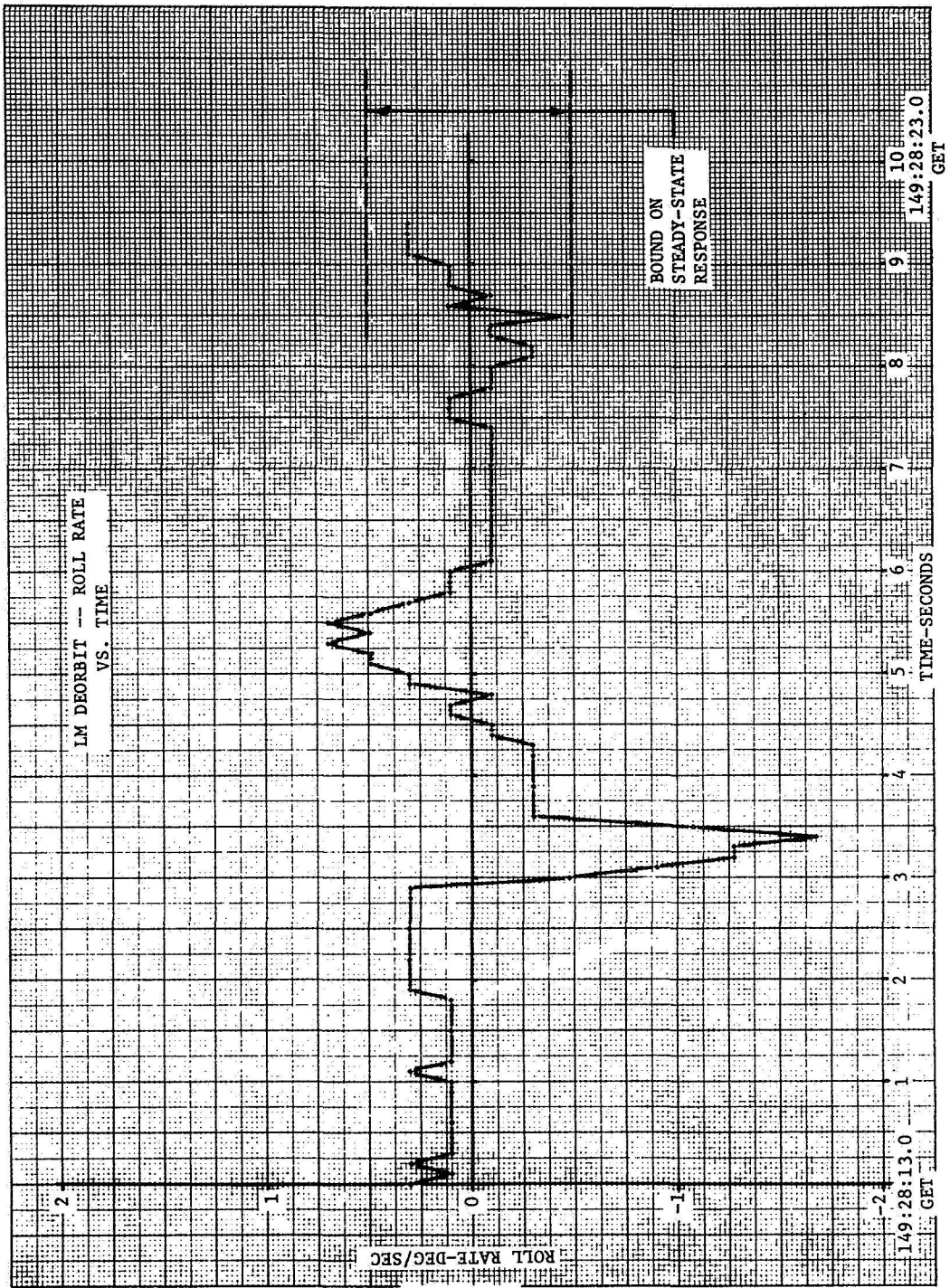
Figure 5-11   LM DEORBIT ROLL RATES
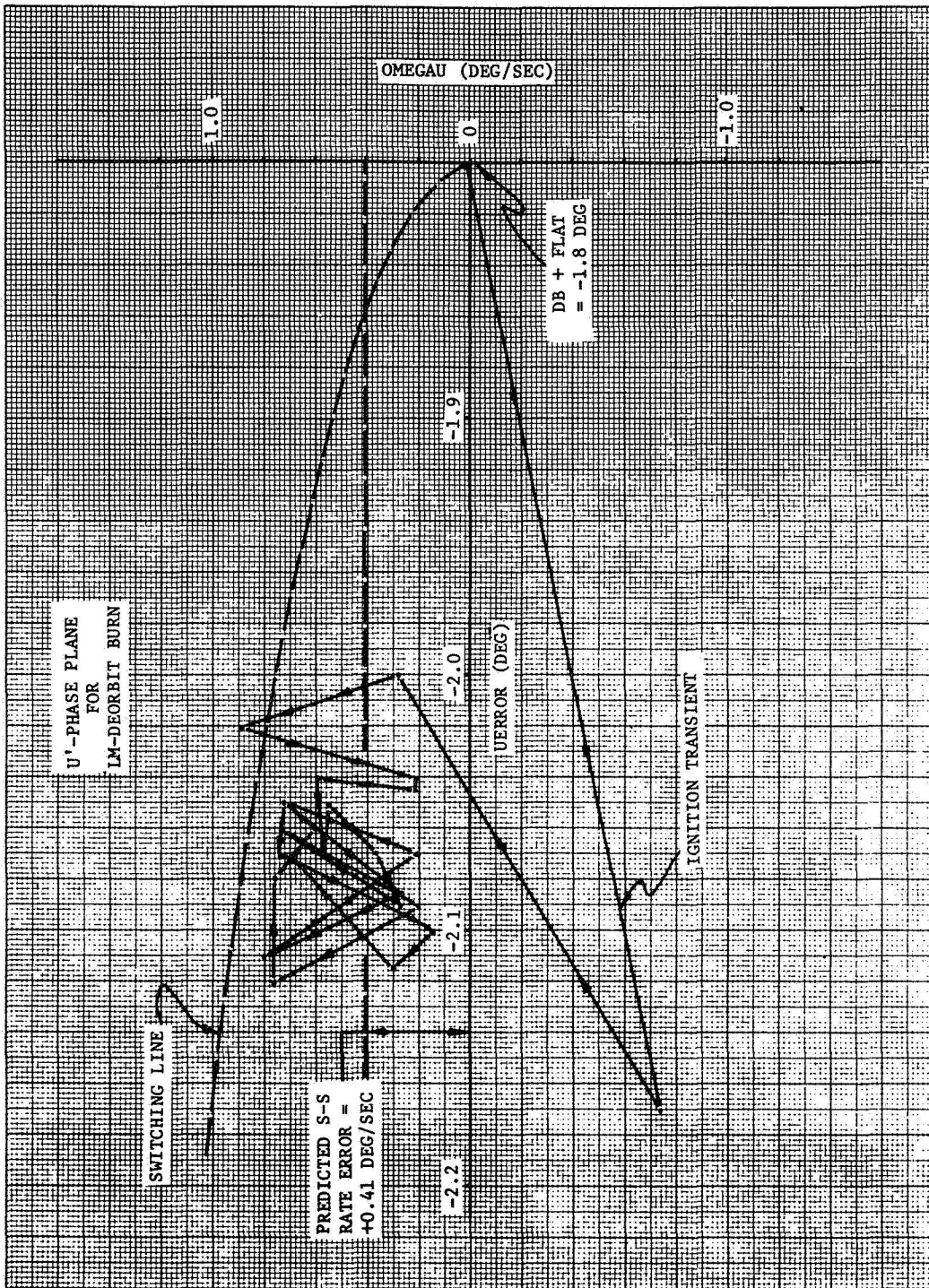
Figure 5-12   LM DEORBIT U' PHASE PLANE

5-31
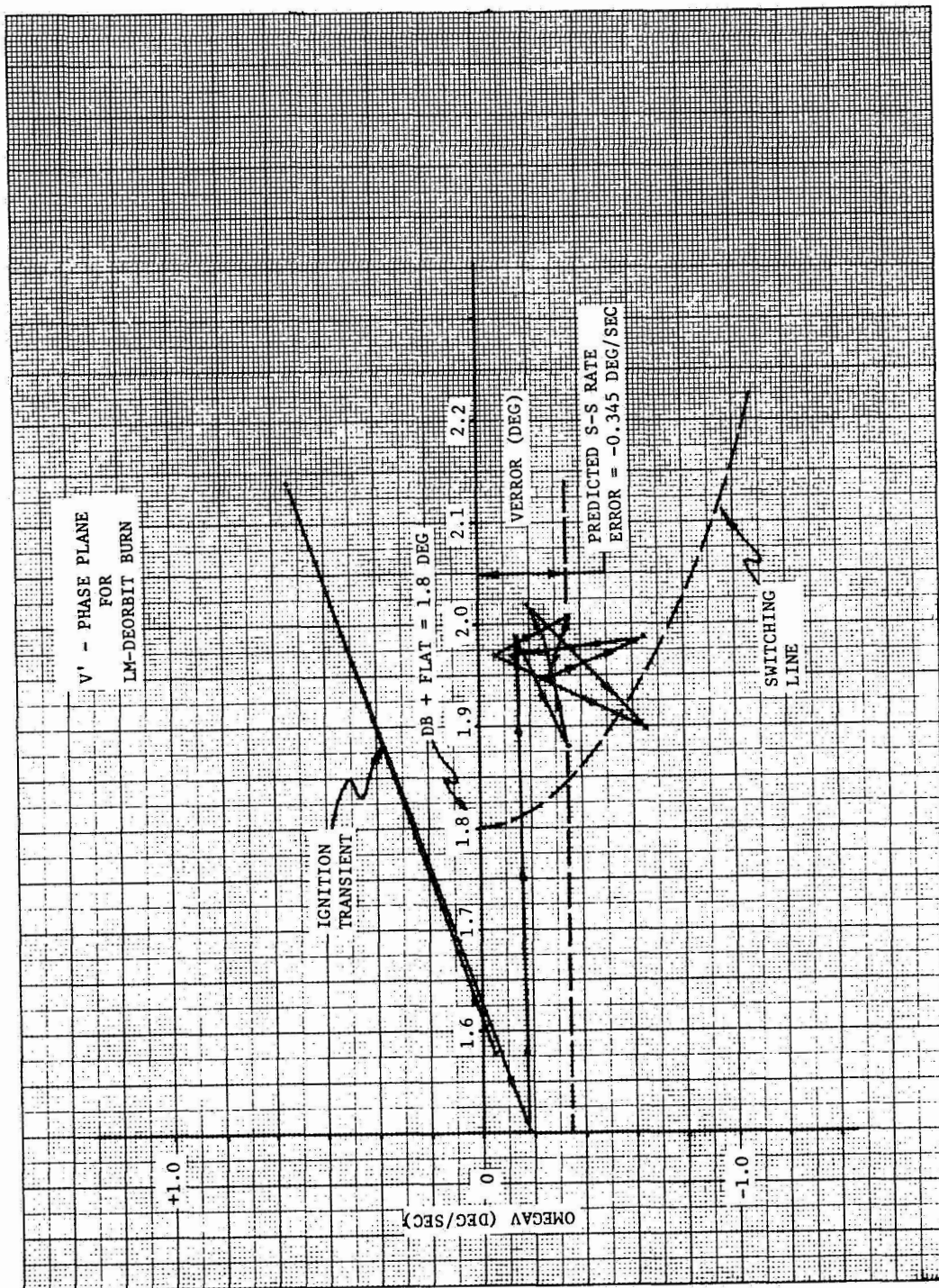
Figure 5-13   LM DEORBIT V' PHASE PLANE

6.0   AGS

During the Apollo 12 flight the AGS performance as a mission monitor was excellent. During all phases of powered flight favorable comparisons were obtained between AGS and PGNCS. During coasting flight state vector updates, sensor calibrations and attitude reference alignments were made without apparent difficulty. On the lunar surface, gyro calibrations and attitude reference lunar alignments were successfully accomplished. In general, Abort Sensor Assembly performance was in agreement with current capability estimates.

6.1   FUNCTIONAL ANALYSIS

6.1.1   State Vector Updates

PGNCS/AGS Transfers

Eight known state vector transfers from the primary system were performed. Five were performed prior to lunar touchdown and the others were performed on the lunar surface. The resulting position and velocity differences after completion of the transfer are presented in Table 6.1. The average magnitude of the position and velocity errors after a transfer were 1294 ft and 0.99 ft/sec. These are reasonable values when considering the onboard quantization errors (512 ft and .5 fps in each axis) and the error in the postflight analysis technique.

Altitude Updates

Three AGS altitude updates via DEDA entry were performed during descent. The first occurred approximately 5.5 minutes after start of PDI at 30,976 ft, the second at 24,000 ft and the third at 6,000 ft. Because of these updates, good agreement between the AGS and PGNCS indicated altitude was obtained through most of the descent phase. Although no altitude rate update capability exists, these data also compared favorably with PGNCS throughout descent. Plots of AGS and PGNCS altitude are shown in Figure 6-1. Due to the absence of AGS altitude updating during the last 3.5 minutes of powered descent and

no AGS altitude rate updating for the duration of powered descent, the AGS altitude diverged from PGNCS altitude and was in error by approximately -1000 ft at touchdown. For example an average rate error of -1.4 ft/sec would cause the observed -1000 altitude error.

Rendezvous Radar Updates

Based on pilot reports, rendezvous radar updating of the AGS LM state vector was successfully accomplished during most of the rendezvous. Since most of the updating operations were accomplished on the back side of the moon limited data are available. A procedural error prior to the CSI maneuver degraded the state vector and as a result the AGS was externally targeted for the CSI burn. The problem is discussed in detail in the Mission Report (Reference 1).

6.1.2 Attitude Reference Alignments

PGNCS/AGS Alignments

The AGS was aligned to the PGNCS inertial reference ten times during the mission. Six of the alignments were made in free flight and four on the lunar surface. Comparisons of the PGNCS gimbal angles and corresponding AEA direction cosine euler angles after each alignment are shown in the Reference 1 report. All comparisons for inflight alignments were within the 0.067 degree specification and all lunar surface alignments were within the 0.12 degree specification.

Lunar Surface Alignments

Immediately after touchdown the crew set the lunar surface flag which stored the touchdown azimuth. At approximately two minutes after touchdown the first lunar alignment was entered. Comparisons of the PGNCS gimbal angles and AGS Direction cosine euler angles following lunar align are shown below:

	PGNCS	AGS	Δ ANGLE	AGS 3σ SPEC*
CDUX	350.497	350.501	-0.004	N/A
CDUY	3.098	3.012	0.086	0.12°
CDUZ	356.243	356.311	-0.068	0.12°

*AGS Performance and interface specification

6-2

The AGS was put into the lunar align mode the second time at approximately 30 minutes prior to liftoff and left in this mode until two minutes before APS ignition. Since the AGS reference is holding a local vertical attitude until liftoff and the PGNCS IMU is not equivalent to local vertical until the time of liftoff, an AGS to PGNCS comparison is not valid until liftoff time. A comparison shortly before ignition is shown below:

	PGNCS	AGS	Δ ANGLE	AGS 3σ SPEC*
CDUX	349.640	349.634	0.006	N/A
CDUY	2.878	2.886	-0.006	0.12°
CDUZ	356.210	356.217	-0.007	0.12°

6.1.3 ASA Calibrations

During the mission one inflight calibration (IFC) and three lunar surface calibrations (LSC) were successfully accomplished. Data from the calibrations along with free flight data, lunar surface data, and preflight data were grouped together to indicate the degree of stability of the instruments. Results of the calibrations are included in the Sensor Performance Section 6.2.

6.1.4 Post Burn Residuals

AGS monitoring accuracy for short burns (AGS and PGNCS target vectors approximately equal) is evidenced in the comparison of velocity remaining to-be-gained after engine cutoff with PGNCS indicated velocity-to-be-gained. Burn residuals for DOI, CSI, CDH, and TPI are shown in Table 6.2. The only significant differences are in the CSI ΔV_Z and TPI ΔV_X. The TPI X component is explainable in that the AGS TPI target vector was 3 ft/sec greater than PGNCS vector. The CSI Z component is explainable in that the AGS target vector had a 0.8 ft/sec Z component but the PGNCS Z component was zero.

---

*AGS performance and interface specification.

6.2 SENSOR PERFORMANCE

6.2.1 Powered Descent

Start of powered descent (PDI) occurred at approximately 11:20:38 GET. Touchdown was at 110:32:36 GET. Average thrust acceleration during the burn was 9.5 ft/sec^2 and the total accumulated velocity was approximately 7000 ft/sec. PGNCS sensed velocity data in body axes were subtracted from the AGS sensed velocity and the resulting differences, subsequently referred to as Case I uncompensated velocity differences, are shown in Figures 6-2 through 6-4. Estimates of AGS accelerometer bias errors and scale factor errors were obtained from these graphs by assuming the PGNCS data are correct. Case 1 velocity differences are independent of AGS gyro performance. A second set of differences were derived in which the AGS sensed velocity was corrected by the AGS accelerometer errors deduced from the Case I differences. In addition, the AGS direction cosine matrix was used in place of the PGNCS gimbal angle direction cosine matrix in the reconstruction of the PGNCS sensed velocity in body axes. These differences subsequently referred to as Case II differences, contain the effects of AGS gyro drift and attitude reference initial misalignments and are presented in Figures 6-5 through 6-7.

The Z velocity errors, (Figures 6-4 and 6-7) show a 1.0 ft/sec step change at 110:29:10.83 when the PGNCS entered the Approach Phase Program (P64). At the entrance into P64 PGNCS commanded a pitchover maneuver of 32 degrees to permit pilot visibility of the landing site. The most significant acceleration on the IMU and ASA in the Z body direction during this maneuver is that due to angular rotation and the fact that both systems are offset from the body center of rotation. Figure 6-8 is a reconstruction of this acceleration using the PGNCS and AGS telemetry data. The AGS reconstruction agrees closely with the calculated values based on offset and body rate data. However, the PGNCS reconstruction differs significantly and at the end of the transient

6-4

a net positive acceleration is observed which when integrated amounts to
1.0 ft/sec more velocity than AGS. When forming the AGS minus PGNCS
comparison, the result is a 1.0 ft/sec step in the Z velocity error
plots. The cause of the problem is difficult to isolate due to the low
sample rate of the downlink data and the relatively high frequency of
the body acceleration across this period. The accumulated PIPA count
(2 second interval) must be expressed as acceleration and then rotated
into body coordinates. These steps require significant interpolations
and are probably the major error sources. A comparison of change of
velocity across the 10 second period in which the 32 degree maneuver
occurred was made using the AGS state vector velocity and a PGNCS
reconstructed state vector that does not contain LR updating. This

comparison shows a difference of $\begin{bmatrix} .26 \\ .01 \\ .44 \end{bmatrix}$ ft/sec between AGS and PGNCS

indicated change of velocity in the platform inertial coordinate system.
Other 10 second time intervals in the vicinity of the maneuver were
examined and the change of velocity as seen by AGS differs from that
seen by PGNCS up to .3 ft/sec. Over a longer time period the differences
appear to get smaller, indicating a significant part of these differences
must be due to downlink sample rates and interpolations.

It is therefore concluded that the effects noted in the Case I and
Case II Z component comparisons are partially due to some actual dif-
ferences in onboard data, partially due to downlink sample rates, and
partially due to methods used to reconstruct accelerations and attitudes
from the telemetry data.

6.2.2 Powered Ascent

Powered ascent started at approximately 142:03:48 GET and lasted
until orbit insertion at 142:10:56. Average thrust acceleration during
the burn was 14 ft/sec^2 and the total accumulated velocity was approxi-
mately 6000 ft/sec. PGNCS sensed velocity outputs during ascent were
differenced from the AGS data to form Case I and Case II differences in
the same manner described in the above section. The Case I and Case II
differences are presented in Figures 6-9 through 6-14.

6.2.3 Accelerometer Errors

Since the Case I uncompensated comparisons for both descent and ascent were based on gimbal angles which define spacecraft axes relative to the PGNCS platform, the velocity differences are independent of the AGS attitude reference and no AGS gyro errors appear in the comparison. The comparison is, however, AGS relative to PGNCS and thus contains PGNCS accelerometer scale factor, CDU and quantization errors as well as the AGS accelerometer errors. The AGS accelerometer errors sufficient to null the Case I velocity differences are listed in Table 6.3. The accelerometer biases were divided into two parts; dynamic bias which represents the difference between the total biases used to null the residuals during the burn and the static biases determined from coasting flight data. Reasonably consistent results were obtained for all accelerometer errors except the dynamic biases. For all three instruments a considerable increase in dynamic bias was detected for the ascent burn.

6.2.4 Attitude Reference Misalignment and Gyro Drift

The Case II velocity differences include all gyro errors and initial misalignment of AGS attitude reference relative to PGNCS. The initial misalignment is due to AGS/PGNCS alignment computational errors, PGNCS gimbal angle quantization and accumulated AGS/PGNCS relative drift since the time of the last alignment. Misalignments are solved for by determining the difference between two sets of body coordinates; one formed from gimbal angles, the other formed from AGS euler angles. PGNCS is assumed perfect. Gyro static errors for descent and ascent were based on the AGS/PGNCS angular differences calculated over coasting flight intervals prior to descent and after insertion, respectively. The gyro dynamic errors selected which fit the velocity error after compensation for misalignment errors and gyro static bias are shown in Table 6.3. Gyro errors were comparable to previous mission results and were small. Like

6-6

the accelerometers, the Z gyro dynamic error exhibited a marked variation in value between descent and ascent. The difference is possibly due to non-symmetric gyro scale factor which would be most significant during ascent where high frequency body limit-cycling exists. The Z gyro asymmetry error was small, however, during preflight testing.

Compensating the descent and ascent velocity error profiles for the error values listed in Table 6.3 yields the compensated velocity differences presented in Figures 6-15 through 6-20. The clustering of the residuals about zero indicates the chosen error sources provided a reasonable fit to the velocity error profiles.

The error uncertainties in Table 6.3 are due to velocity and CDU quantization, AEA computational error, and sampling and processing errors. Comparisons of the values in Table 6.3 with the ASA 010 Error Model and the Capability Estimate Error Budget are presented in Tables 6.5 and 6.6 for Descent and Tables 6.8 and 6.9 for Ascent. A discussion of the errors is presented in Section 6.2.5.

6.2.5 Comparison of Sensor Analysis Results to AGS Error Models

6.2.5.1 Total and Dynamic Errors

Descent Burn

Based on the AGS Capability Estimate, the estimates of the dynamic and total sensor errors are all within the expected 3σ ranges. Table 6.4 lists the ratio of the parameter values minus their expected means to their expected 1σ values. The expected values were determined from the ASA 010 Performance Estimate. Excellent corroboration of the a priori system modeling is obtained. It is concluded that ASA 010 performed well within mission requirements during the descent burn.

Tables 6.5 and 6.6 present the inflight error estimates in the form of the model used in the AGS Capability Estimate (Reference 3).

Two comparison models are used. The first is an estimate of system performance based on the ASA 010 Monte Carlo error models of data from

6-7

KSC, HSSC, and GAC tests. The second is the Error Budget from the AGS Capability Estimate.

Ascent Burn

Table 6.7 lists the ratio of the parameter values minus their expected mean to their expected 1σ value. The expected values were determined from the ASA 010 Performance Estimate. Except for the X-accelerometer, all the estimated dynamic and total sensor errors were within the Performance Estimate 3σ ranges; causes of the large X-accelerometer dynamic bias are unknown. None of the sensor errors exceeded the capability Estimate Error budget. Table 6.8 and 6.9 present a comparison of the inflight error estimates with the ASA 010 Monte Carlo error model and the Error Budget from the AGS Capability Estimate.

It must be noted here that the Ascent ASA 010 preflight performance estimates were developed assuming that AGS was guiding the LM. Actually, PGNCS guided the LM and determined the limit-cycle environment resulting in a more severe environment, higher rates and frequency than is expected under AGS guidance. Since the major AGS error sources (Aysmmetry and HVSIR) are highly rate dependent it may be expected that higher rates will cause larger errors. Postflight analysis indicated that the Z gyro was most sensitive to the limit-cycle environment. Consequently, rate data were used to reproduce the actual Z axis environment profile that existed during Ascent. This environment was used to develop the Z gyro preflight estimate of Table 6.9. Under AGS guidance Asymmetry and HVSIR will produce a mean drift of -0.03 deg/hr. Under PGNCS guidance Asymmetry and HVSIR will produce a mean drift of -.28 deg/hr.

6.2.5.2 Bias Performance

Based on the Capability Estimate, the bias time stabilities for both gyros and accelerometers were well within their 3σ ranges. The gyros also exhibited excellent bias repeatability with values within their expected 1σ ranges. Table 6.10 presents the ratios of the means

of the stability and repeatability values to their 1σ capability estimate values.

Gyro static drift is measured directly by the IFC and the ,lunar surface calibrations (LSC). One IFC and three LSC's were accomplished and the gyro drift measurements are presented in Table 6.11.

Accelerometer bias measurements are presented in Table 6.12. Table 6.13 presents accelerometer 64-day time stability comparisons with the Error Budget and Capability Estimate models. A measure of short term accelerometer bias stability is apparent from the comparison of the IFC value prior to descent with the post-ascent accelerometer bias. Table 6.14 compares the total shift across that period with the Capability Estimate 3σ values. The 3σ values are the RSS of all the 3σ values of the error sources during ascent and descent from the Capability Estimate. Clearly, the accelerometer bias shifts were well with the 3σ value which implies that performance was good.

TABLE 6.1   AGS NAVIGATION INITIALIZATION

Initialization Complete GET (Hr:Min:Sec)	ΔẊ (ft/sec)	ΔẎ (ft/sec)	ΔŻ (ft/sec)	Vector Magnitude	ΔX (ft)	ΔY (ft)	ΔZ (ft)	Vector Magnitude
106:10:55	0.60	0	-2.3	2.38	-3118	- 35	- 2035	3723
106:14:21	-1.00	-0.29	0.40	1.11	458	-123	- 53	477
108:37:40	1.80	0.05	0.40	1.85	1172	- 50	42	1174
108:44:06	1.2	0.10	-0.20	1.22	509	226	176	584
110:14:14	-0.10	-0.18	-0.30	0.36	223	-138	352	439
140:07:35	-0.28	-0.23	-0.08	0.37	1123	804	2214	2609
140:15:11	0.24	-0.23	-0.08	0.34	999	-204	70	1022
141:46:47	-0.04	-0.22	+0.17	0.28	26	295	128	322

Average 0.99 ft/sec   Average 1294 ft

Table 6-2   AGS/PGNCS RESIDUAL COMPARISONS
(LM ACTIVE RENDEZVOUS)

	AGS	PGNCS
DOI		
ΔV_X (fps)	0.3	0
ΔV_Y (fps)	0.1	0.2
ΔV_Z (fps)	-0.6	-0.6
CSI		
ΔV_X	-0.4	+0.1
ΔV_Y	+0.4	-0.1
ΔV_Z	+0.6	-0.3
CDH		
ΔV_X	0	-0.1
ΔV_Y	-0.2	0
ΔV_Z	-0.1	-0.2
TPI		
ΔV_X	+2.9	-0.1
ΔV_Y	-0.3	-0.1
ΔV_Z	-0.2	0

Table 6.3   ASA DETERMINED ERRORS

Error Source	Descent Value (1)	Ascent Value (1)
Accelerometer Errors		
X accelerometer bias (μg)		
Static	- 29.6 + 16	- 52.6 + 19
Dynamic	- 25.1 $\mp$ 30	-165.4 $\mp$ 32
Y accelerometer bias (μg)		
Static	- 9.9 + 16	- 19.7 + 19
Dynamic	0 $\mp$ 30	91.3 $\mp$ 32
Z accelerometer bias (μg)		
Static	- 29.6 + 16	- 59.1 + 19
Dynamic	- 98.4 $\mp$ 30	-104.9 $\mp$ 32
X accelerometer scale factor (ppm)	- 60.0 + 85	- 60.0 + 53
Y accelerometer misalign toward X (sec)	- 15.1 + 18	10.0 + 12
Z accelerometer scale factor (sec)	- 45.0 + 18	- 55.0 + 12
Gyro Error & Initial Misalignment		
Initial misalign about X (sec)	- 27.0 + 35	100.0 + 35
Initial misalign about Y (sec)	- 8.0 + 35	6.0 + 35
Initial misalign about Z (sec)	- 9.0 + 35	62.0 + 35
X Gyro bias (deg/hr)		
Static	0.05 + 0.18	0.05 + 0.19
Dynamic	0.05 $\mp$ 0.25	- 0.30 $\mp$ 0.27
Y Gyro bias (deg/hr)		
Static	- 0.07 + 0.18	0 + 0.19
Dynamic	- 0.17 $\mp$ 0.22	- 0.40 $\mp$ 0.25
Z Gyro bias (deg/hr)		
Static	- 0.03 + 0.18	- 0.14 + 0.19
Dynamic	0.08 $\mp$ 0.23	- 0.46 $\mp$ 0.32
Y Gyro scale factor	-215.0 + 119	-215.0 + 102.0

(1) Comparisons of these values with the ASA 010 Error Model and the Capability EStimate Error Budget are presented in Tables 6.5 and 6.6 for Descent and Tables 6.8 and 6.9 for Ascent.

TABLE 6.4   PERFORMANCE SUMMARY

Descent

Ratios of Parameter Values Minus Expected Means to the Expected 1σ Values*

	X	Y	Z
Accelerometer Dynamic Error	-1.1	1.6	-2.5
Total Accelerometer Powered Flight Error	1.3	1.3	-2.6
Gyro Dynamic Error	.7	.3	1.2
Total Gyro Powered Flight Error	.6	-.2	.3

* From the ASA 010 Performance Estimates.

TABLE 6.5   EQUIVALENT ACCELEROMETER BIAS ERROR, μg

Descent

		ASA 010 Inflight Estimate	ASA 010 Preflight Estimate Performance Mean	ASA 010 Preflight Estimate Performance 3σ	Error Budget from AGS P&I Specification Mean	Error Budget from AGS P&I Specification Gaussian 3σ
Accelerometer Bias and Nonlinearity (1)	X	- 30	0	106	0	246
	Y	- 10	0	93	0	240
	Z	- 30	0	93	0	240
X-Scale Factor and Dynamic Errors (2)	X	- 25	0	66	0	100
Y and Z Dynamic Errors, ASA Accelerometer Internal Misalignment and ASA to IMU Mounting Points Misalignment (2)	Y	0	-96	183	0	392
	Z	- 98	+51	180	0	392
TOTAL (μg)	X	- 55	0	125	0	266
	Y	- 10	-96	205	0	459
	Z	-128	+51	203	0	459

NOTES: (1) Inflight Estimate: Last Free-Flight Data Period **before descent.**
  (2) Inflight Estimate: Difference between measured total error and measured fixed bias.
  The alignment and scale factor error in this table appear dissimilar to the capability estimate tables because they have been converted to equivalent bias errors in μg's.

TABLE 6.6 EQUIVALENT GYRO BIAS ERROR, DEG/HR

Descent

		ASA 010 Inflight Estimate	ASA 010 Preflight Estimate Performance		Error Budget from AGS P&I Specification Gaussian 3σ
			Mean	3σ	
Gyro Fixed Drift (1)	X	-.05	0	.56	.59
	Y	-.07	0	.58	.60
	Z	-.03	0	.58	.60
X-Gyro Dynamic Drift (2)	X		-.05	.35	.52
		+.05			
X-Gyro Spin Axis Mass Unbalance (2)	X		0	.22	.52
Y and Z Gyro Dynamic Drift (2)	Y	-.17	-.20	.30	.58
	Z	+.08	-.04	.30	.58
TOTAL (deg/hr)	X	+.10	-.05	.70	.94
	Y	-.24	-.20	.65	.83
	Z	+.05	-.04	.65	.83

NOTES: (1) Inflight Estimate: Last Free-Flight Data Period before descent.
(2) Inflight Estimate: Difference between measured total error and measured fixed bias.

TABLE 6.7 PERFORMANCE SUMMARY

Ascent

	Ratios of Parameter Values Minus Expected Means to the Expected 1σ Values*		
	X	Y	Z
Accelerometer Dynamic Error	-5.4	2.5	.3
Total Accelerometer Powered Flight Error	-4.3	2.3	- .4
Gyro Dynamic Error	1.7	-1.6	-1.3
Total Gyro Powered Flight Error	- .8	-1.0	-1.6

* From the ASA 010 Performance Estimates.

TABLE 6.8 EQUIVALENT ACCELEROMETER BIAS ERRORS, µg

Ascent

		ASA 010 Inflight Estimate	ASA 010 Preflight Estimate Performance		Error Budget from AGS P&I Specification	
			Mean	3σ	Mean	Gaussian 3σ
Accelerometer Bias and Nonlinearity (1)	X	− 53	0	112	0	280
	Y	− 20	0	3	0	276
	Z	−59	0	2	0	276
X-Scale Factor and Dynamic Errors (2)	X	−165	+ 7	96	0	122
Y and Z Dynamic Errors, ASA Accelerometer Internal Misalignment and ASA to IMU Mounting Points Misalignment (2)	Y	+ 91	−133	265	0	565
	Z	+105	+ 76	261	0	565
TOTAL (µg)	X	−218	+ 7	148	0	306
	Y	+ 71	−133	265	0	628
	Z	+ 46	+ 76	261	0	628

NOTES: (1) Inflight Estimate: Free-Flight Data Period after Orbit Insertion.
(2) Inflight Estimate: Difference between measured total error and measured fixed bias.

The alignment and scale factor error in this table appear dissimilar to the capability estimate tables because they have been converted to equivalent bias errors in µg's.

TABLE 6.9   EQUIVALENT GYRO BIAS ERRORS, deg/hr

Ascent

		ASA 010 Inflight Estimate	ASA 010 Preflight Estimate Performance		Error Budget from AGS P&I Specification
			Mean	3σ	Gaussian 3σ
Gyro Fixed Drift (1)	X	.05	0	.49	.50
	Y	.00	0	.46	.49
	Z	-.14	0	.46	.49
X-Gyro Dynamic Drift (2)	X	⎫	-.07	.26	.51
		⎬ -.30			
X-Gyro Spin Axis Mass Unbalance (2)	X	⎭	0	.32	.52
Y and Z Gyro Dynamic Drift (2)(3)	Y	-.40	-.22	.32	.56
	Z	-.46	-.28	.38	.60
TOTAL (deg/hr)	X	.25	-.07	.64	.88
	Y	-.40	-.22	.56	.74
	Z	-.60	-.28	.60	.77

NOTES: (1) Inflight Estimate: Free-Flight Data Period after Orbit Insertion.
        (2) Inflight Estimate: Difference between measured total error and measured fixed bias.
        (3) Z gyro preflight estimate dynamic drift is based on the actual Apollo 12 limit-cycle rate environment.

TABLE 6.10   ACCELEROMETER & GYRO BIAS PERFORMANCE

	Ratios of Parameter Value to the Expected 1σ Values*		
	X	Y	Z
Accelerometer Bias Time Stability (60 days)	0.8	0.6	0.9
Gyro Bias Repeatability	-0.9	-0.9	+ 0.7
Gyro Bias Time Stability (30 days)	1.2	0.6	0.0

* From the AGS Capability Estimate

Table 6.11 LM 6 ASA 010 GYRO DRIFT (DEG/HR)

	X	Y	Z
Pre-installation calibration (PIC) 9/15/69	+.06	-.16	-.07
Final earth pre-launch calibration (EPC) 10/23/69	-.27	-.31	-.06
Inflight calibration (IFC) 11/18/69	-.04	-.19	.00
1st lunar surface calibration* (LSC #1) 11/19/69	-.19	-.25	-.01
2nd lunar surface calibration* (LSC #2) 11/20/69	-.20	-.26	-.07
3rd lunar surface calibration* (LSC #3) 11/20/69	-.20	-.27	-.06
1σ of bias shifts**	-.07	-.03	-.02
Mean of bias shifts**	-.05	-.03	-.02

*Y and Z gyro calibration values have been corrected to account for the known Calibration Error. Calibration Software assumes Y input axis is along moon rotation vector, but actual direction was 15 degrees from north.

**Evaluated for data from IFC to LSC #3.

Table 6.12   LM 6 ASA 010 ACCELEROMETER BIAS (µg)

Biases	X	Y	Z
Pre-installation calibration (PIC) 9/15/69	462	119	- 79
Free flight data Pre-IFC (106:10 - 106:48 GET)	394	68	-155
Inflight Calibration (IFC)	405	93	-124
Free flight - Post-IFC, pre-descent 11/18/69 (107:57 - 108:19 GET)	375	84	-153
Free flight, Post-IFC, post-ascent 11/20/69 (143:23 - 143:35 GET)	363	71	-169

TABLE 6.13 ACCELEROMETER BIAS TIME STABILITY

Channel	Δ-Time (Days)	Δ-Bias	Ensemble Cap. Est (3σ) (60 days)	Error Budget (3σ) (60 days)
X	64	-58	263	430
Y	64	-51	263	430
Z	64	-82	263	430

TABLE 6.14 ASA 010 ACCELEROMETER BIAS PERFORMANCE
FROM IFC TO POST-ASCENT FREEFLIGHT
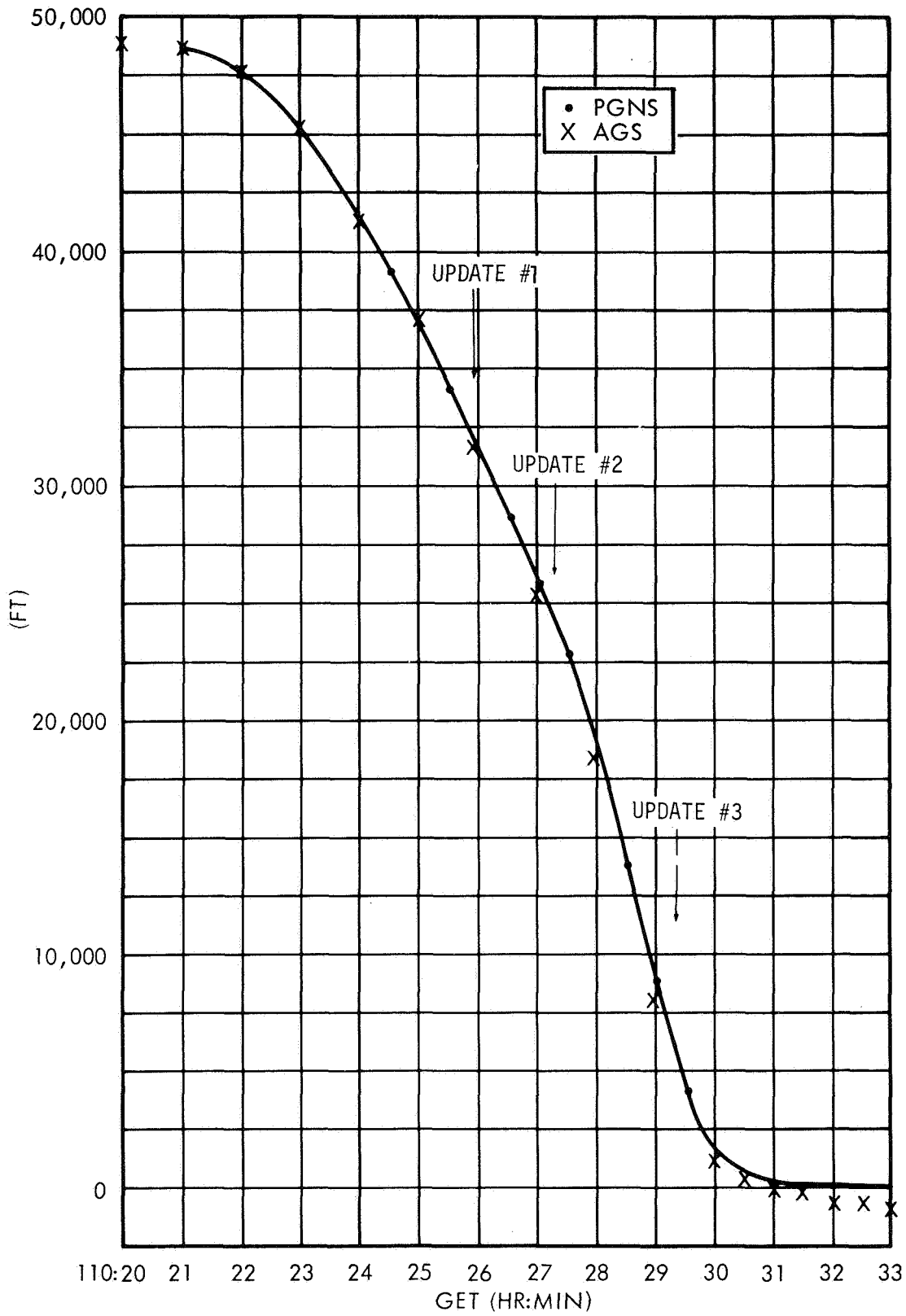
Actual Bias Shift		Capability Estimate (3σ)
X	-42	47
Y	-22	47
Z	-45	47

Figure 6-1   ALTITUDE DURING DESCENT

Figure 6-2   CASE 1 UNCOMPENSATED VELOCITY
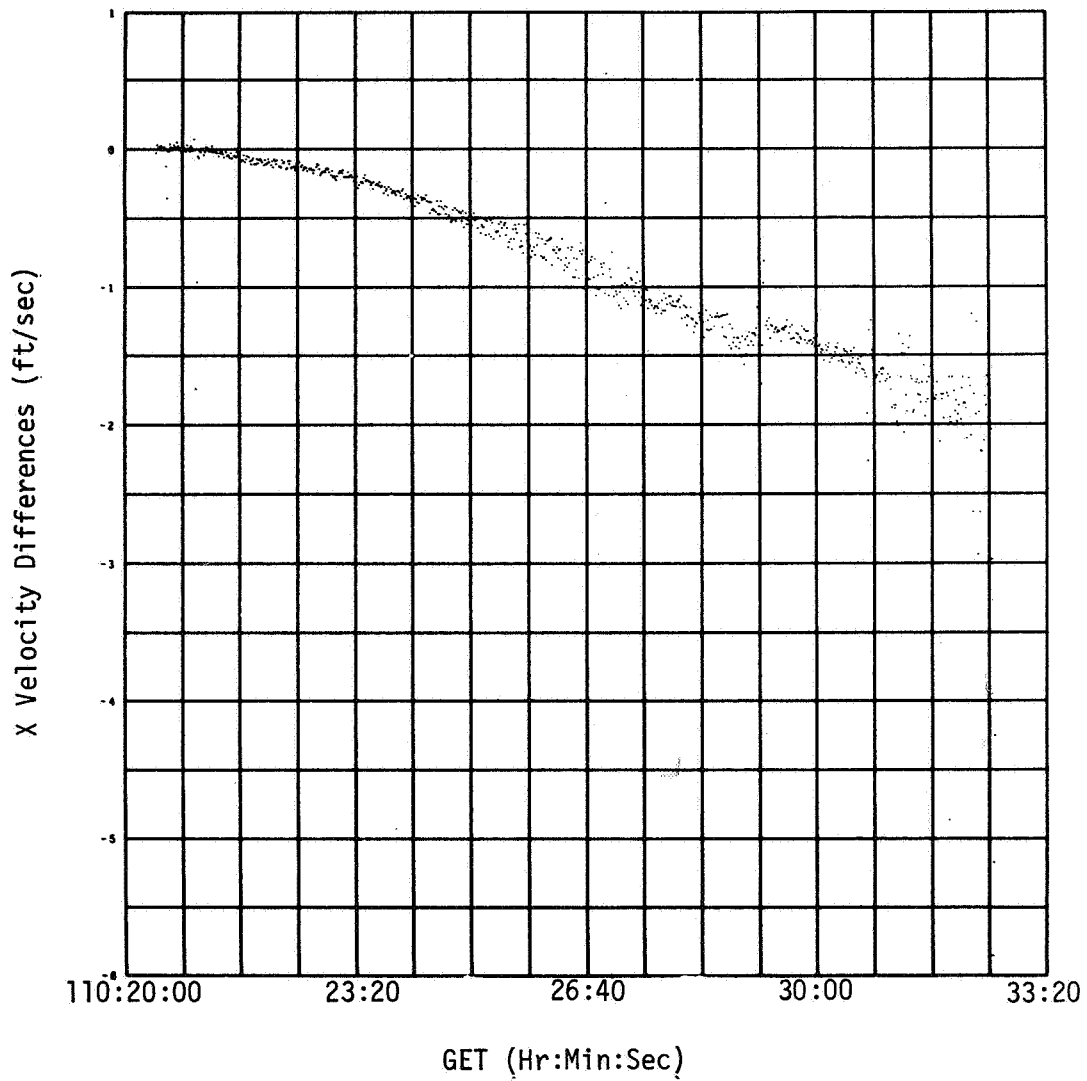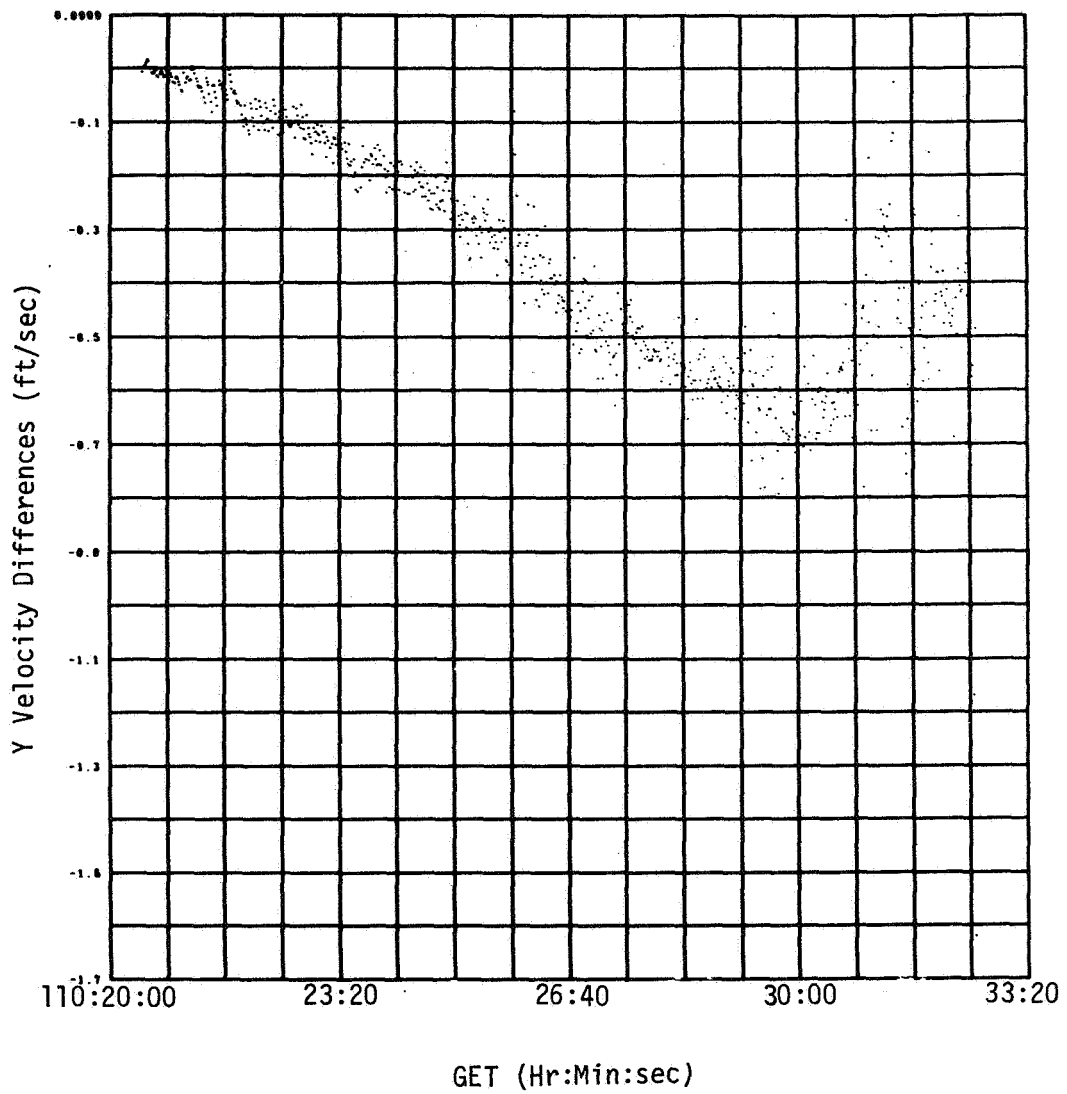DIFFERENCES FOR DESCENT (X AXIS)

6-21

Figure 6-3   CASE 1 UNCOMPENSATED VELOCITY
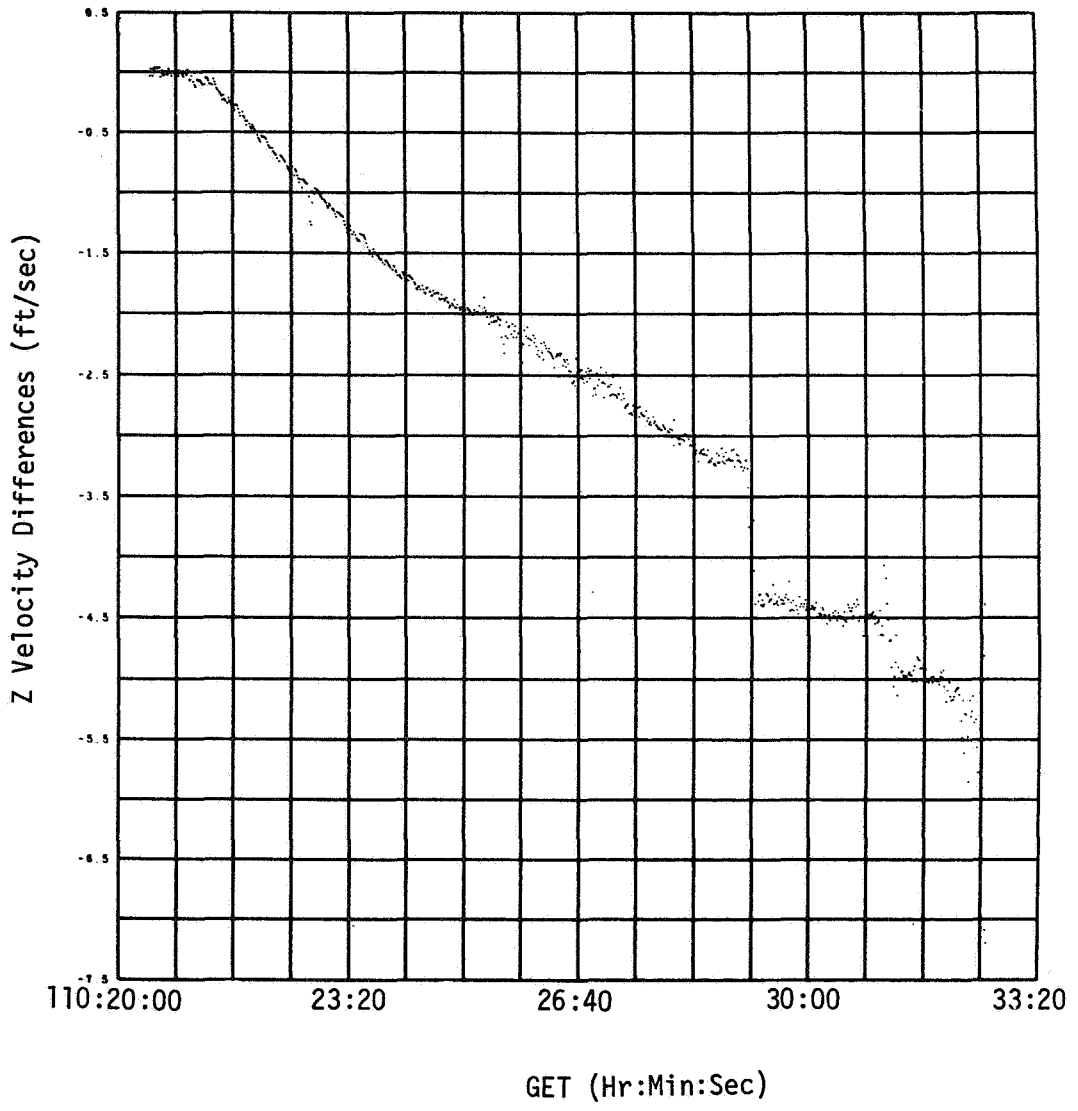   DIFFERENCES FOR DESCENT (Y AXIS)

Figure 6-4 CASE 1 UNCOMPENSATED VELOCITY
DIFFERENCES FOR DESCENT (Z AXIS)
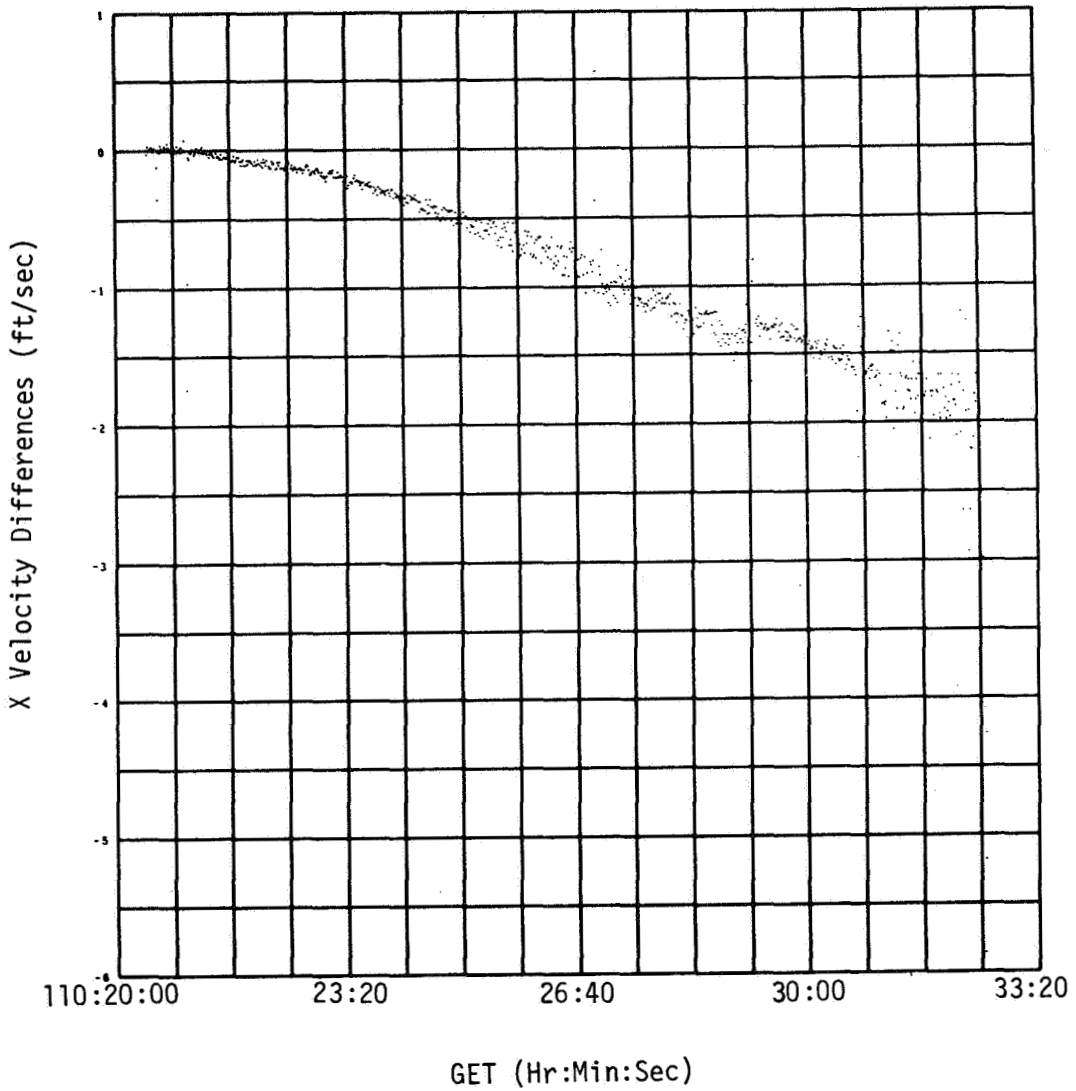
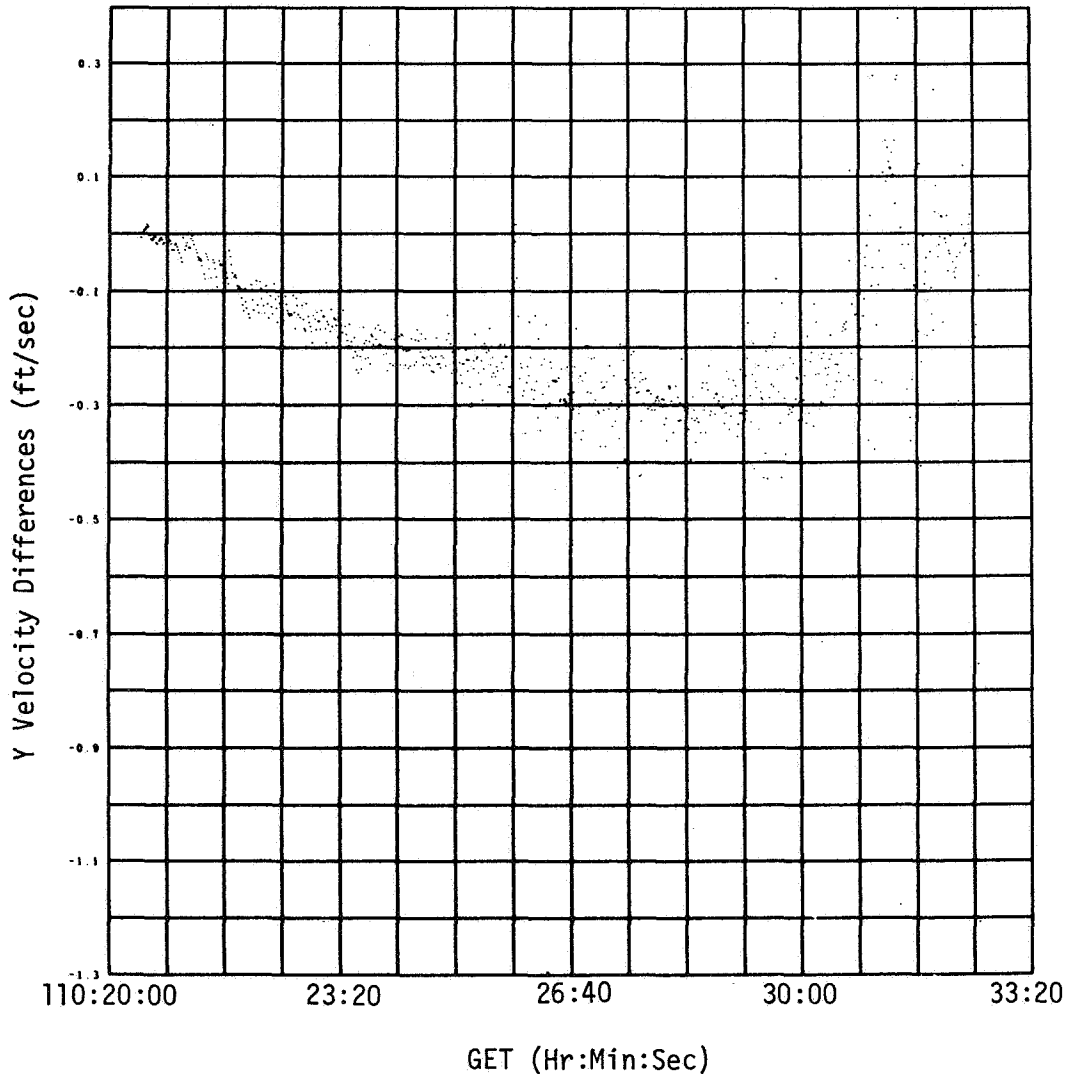Figure 6-5   CASE 2 UNCOMPENSATED VELOCITY
DIFFERENCES FOR DESCENT (X AXIS)

Figure 6-6   CASE 2 UNCOMPENSATED VELOCITY
              DIFFERENCES FOR DESCENT (Y AXIS)
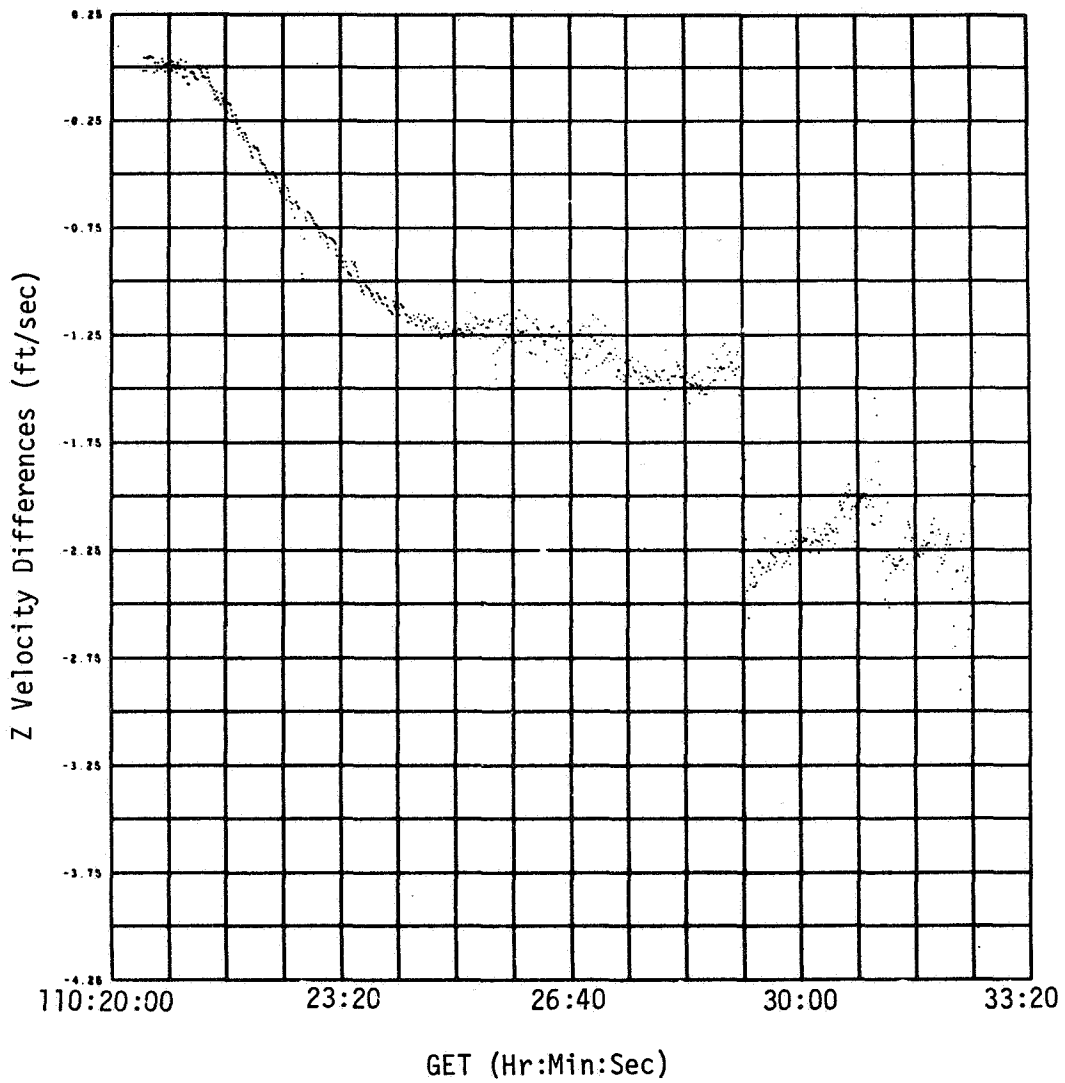
6-25

Figure 6-7   CASE 2 UNCOMPENSATED VELOCITY
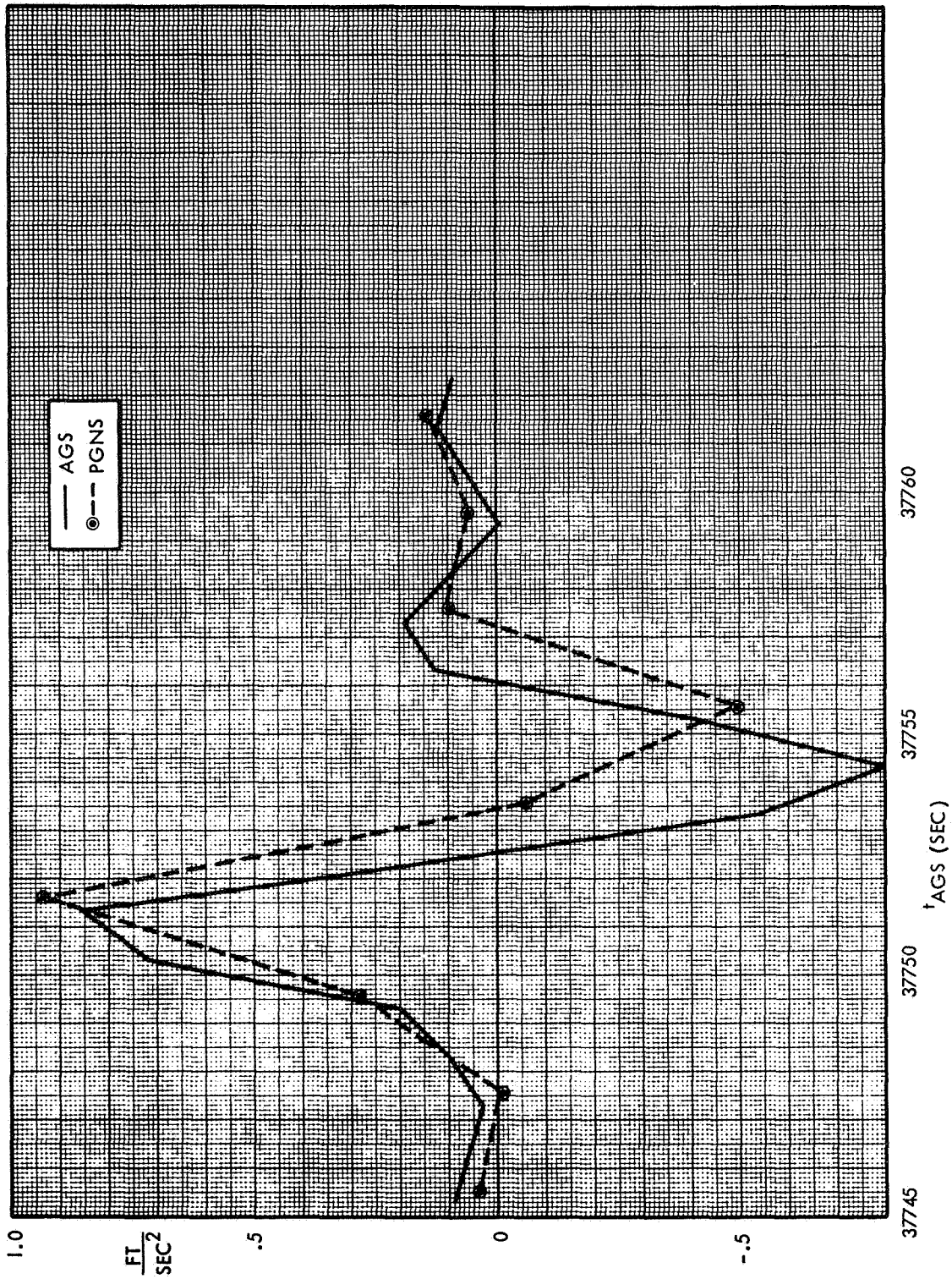   DIFFERENCES FOR DESCENT (Z AXIS)

Figure 6-8   AGS & PGNCS SENSED ACCELERATION RECONSTRUCTION
DURING 32 DEGREE PITCHOVER MANEUVER (Z AXIS)

Figure 6-9   CASE 1 UNCOMPENSATED VELOCITY
DIFFERENCES FOR ASCENT (X AXIS)

6-28

Figure 6-10   CASE 1 UNCOMPENSATED VELOCITY
              DIFFERENCES FOR ASCENT (Y AXIS)

6-29

Figure 6-11   CASE 1 UNCOMPENSATED VELOCITY
              DIFFERENCES FOR ASCENT (Z AXIS)
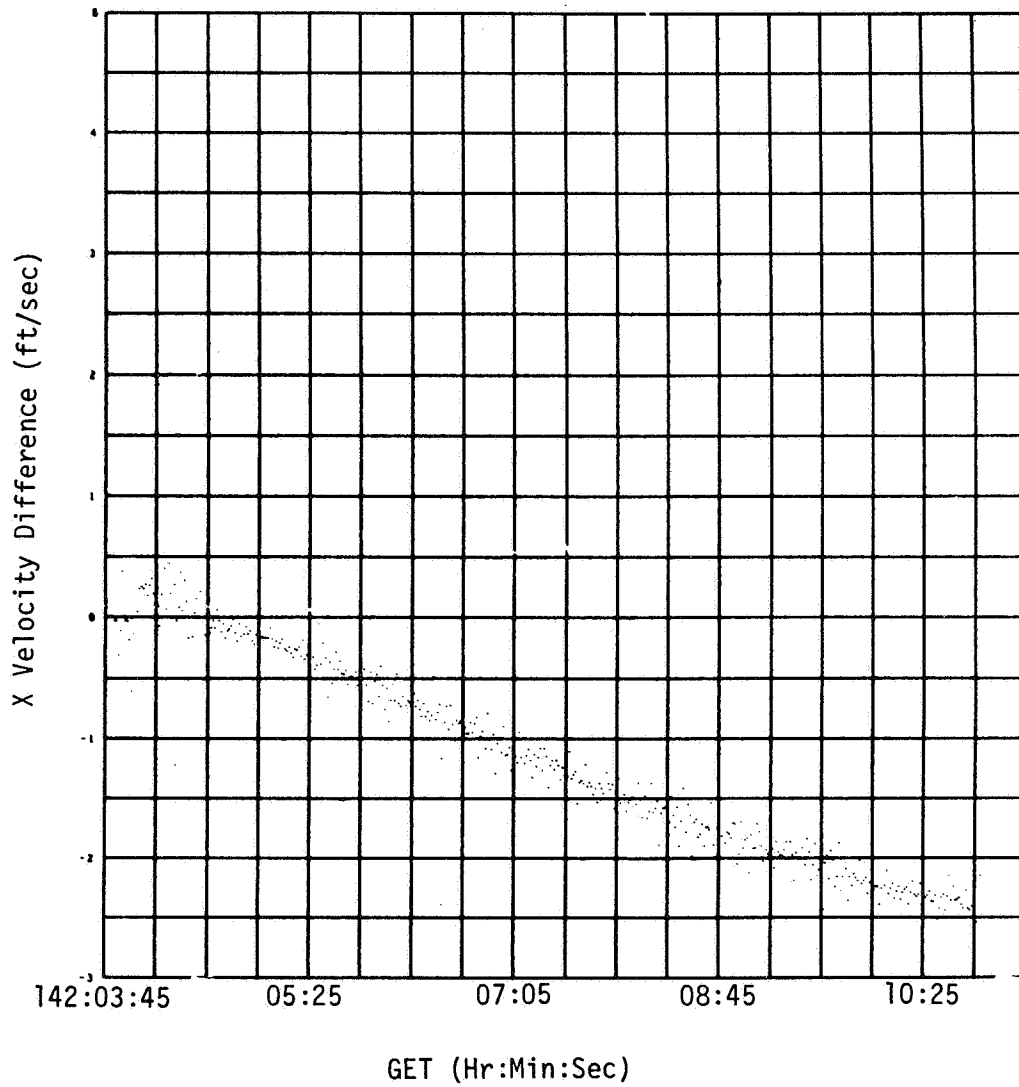
Figure 6-12   CASE 2 UNCOMPENSATED VELOCITY
DIFFERENCES FOR ASCENT (X AXIS)
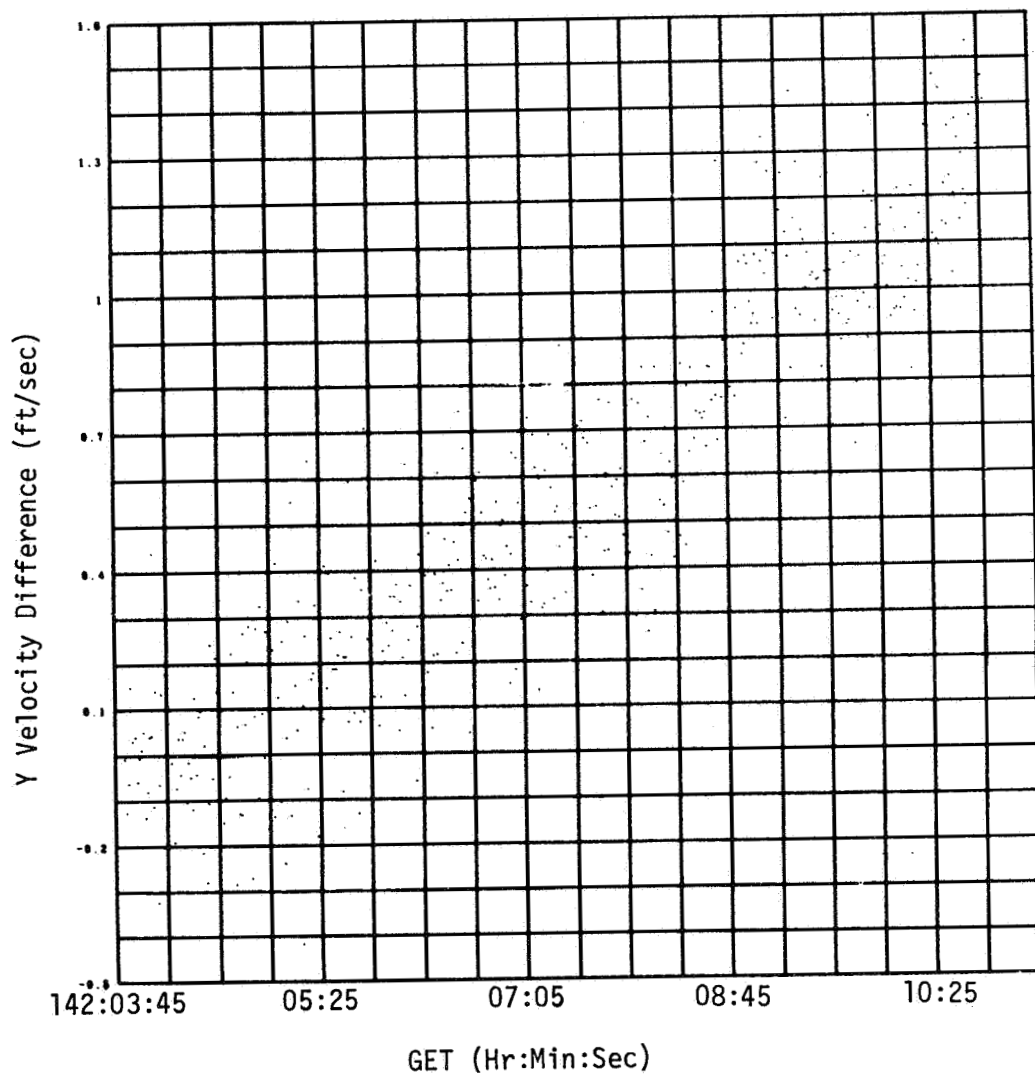
Figure 6-13   CASE 2 UNCOMPENSATED VELOCITY
              DIFFERENCES FOR ASCENT (Y AXIS)

Figure 6-14   CASE 2 UNCOMPENSATED VELOCITY
DIFFERENCES FOR ASCENT (Z AXIS)

6-33

Figure 6-15   COMPENSATED VELOCITY DIFFERENCE
FOR DESCENT (X AXIS)

Figure 6-16   COMPENSATED VELOCITY DIFFERENCE
FOR DESCENT (Y AXIS)

6-35

Figure 6-17   COMPENSATED VELOCITY DIFFERENCE
FOR DESCENT (Z AXIS)

6-36

Figure 6-18   COMPENSATED VELOCITY DIFFERENCES
FOR ASCENT (X AXIS)

6-37
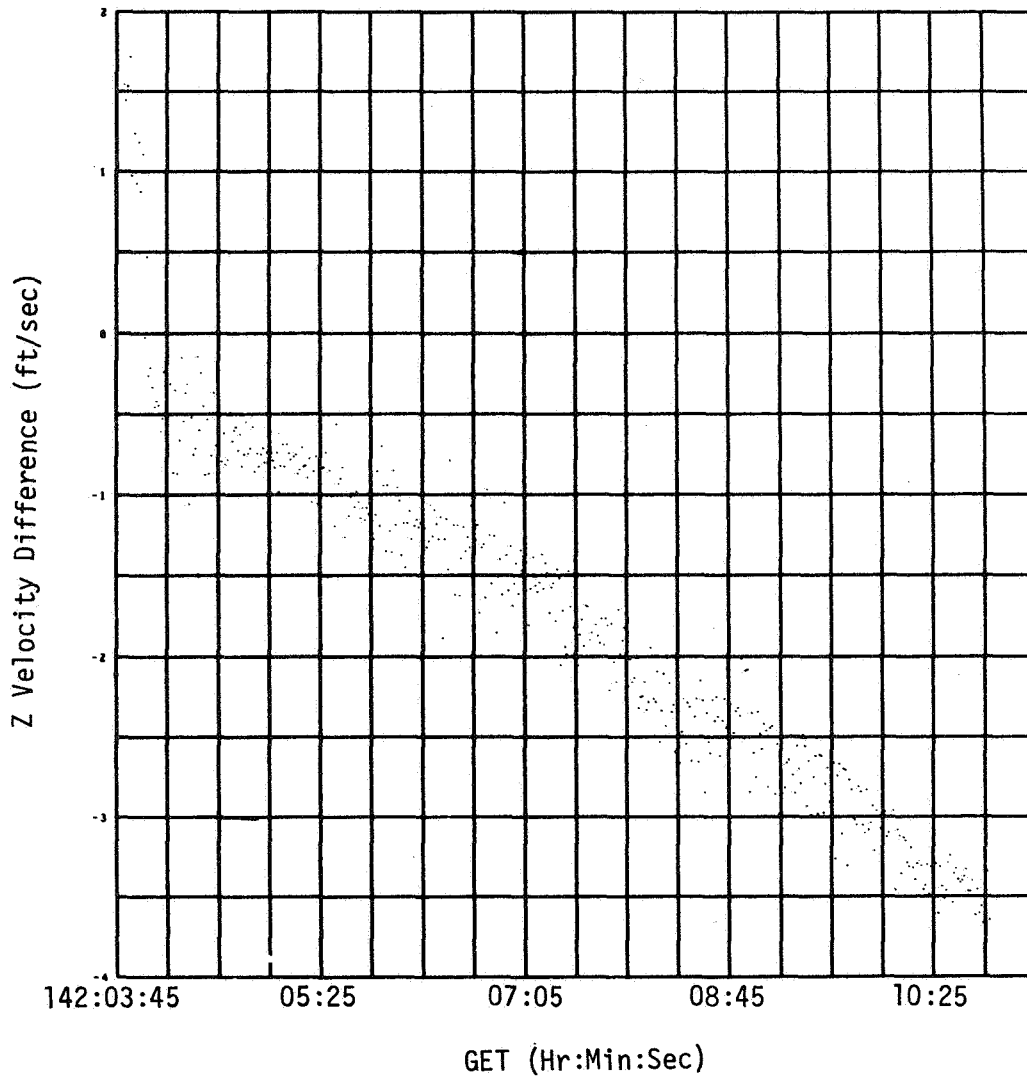
Figure 6-19   COMPENSATED VELOCITY DIFFERENCES
FOR ASCENT (Y AXIS)

Figure 6-20   COMPENSATED VELOCITY DIFFERENCES
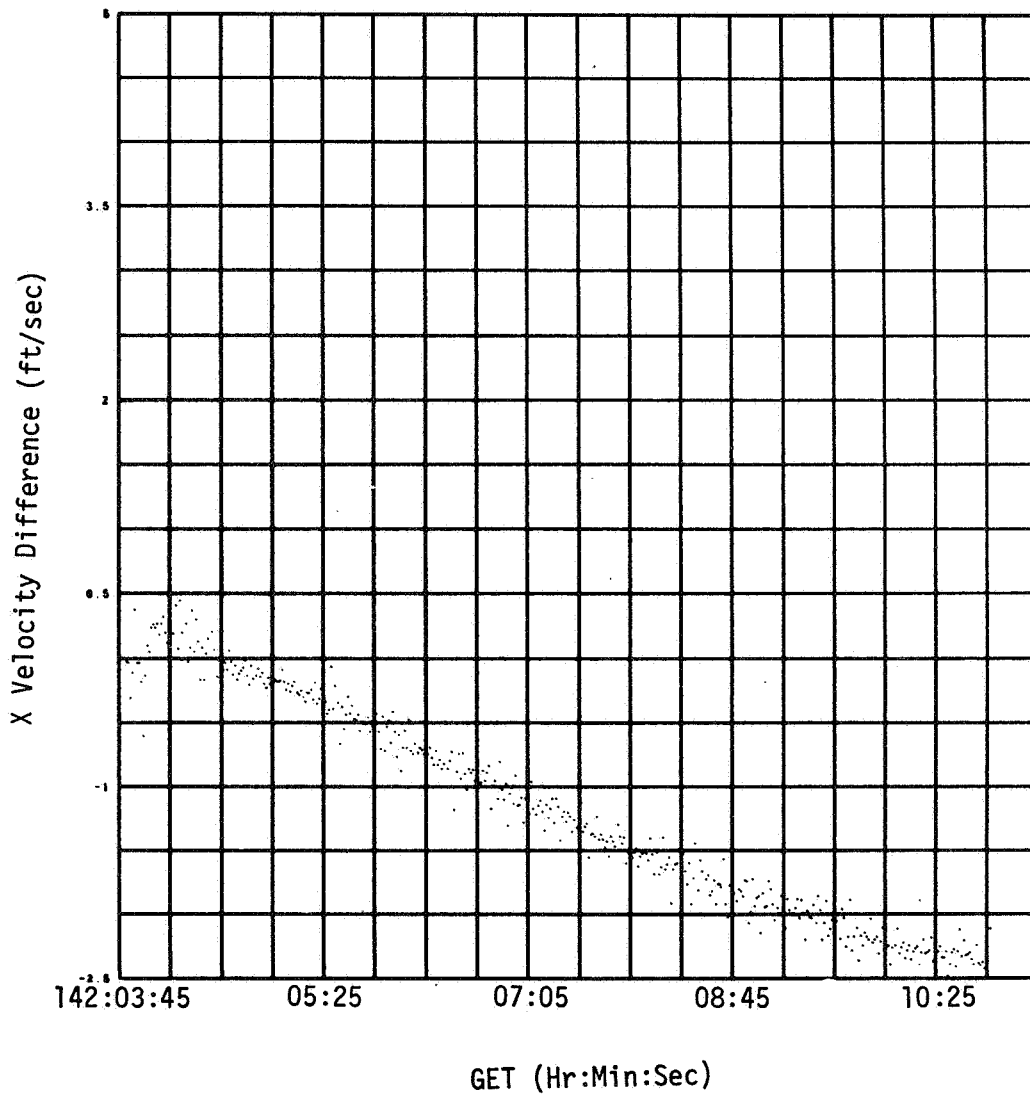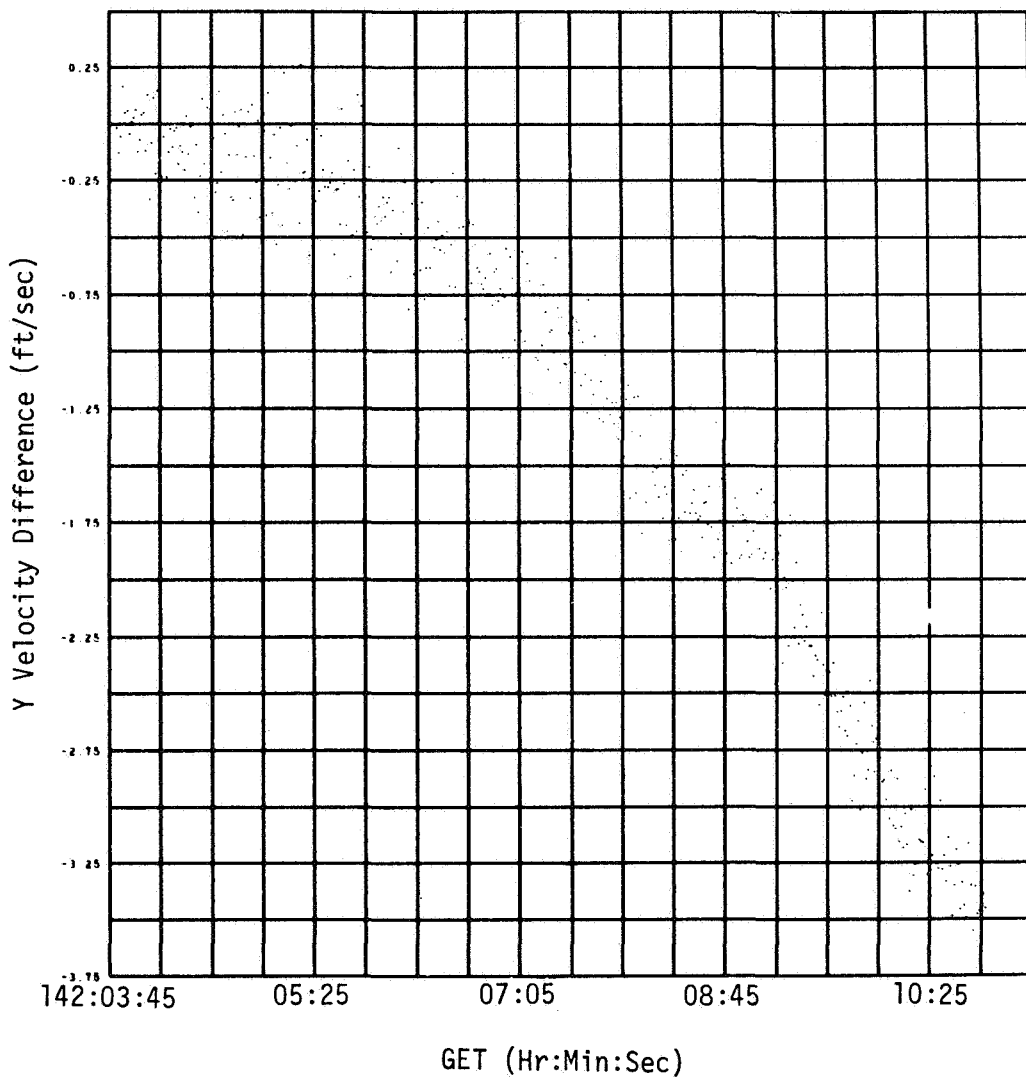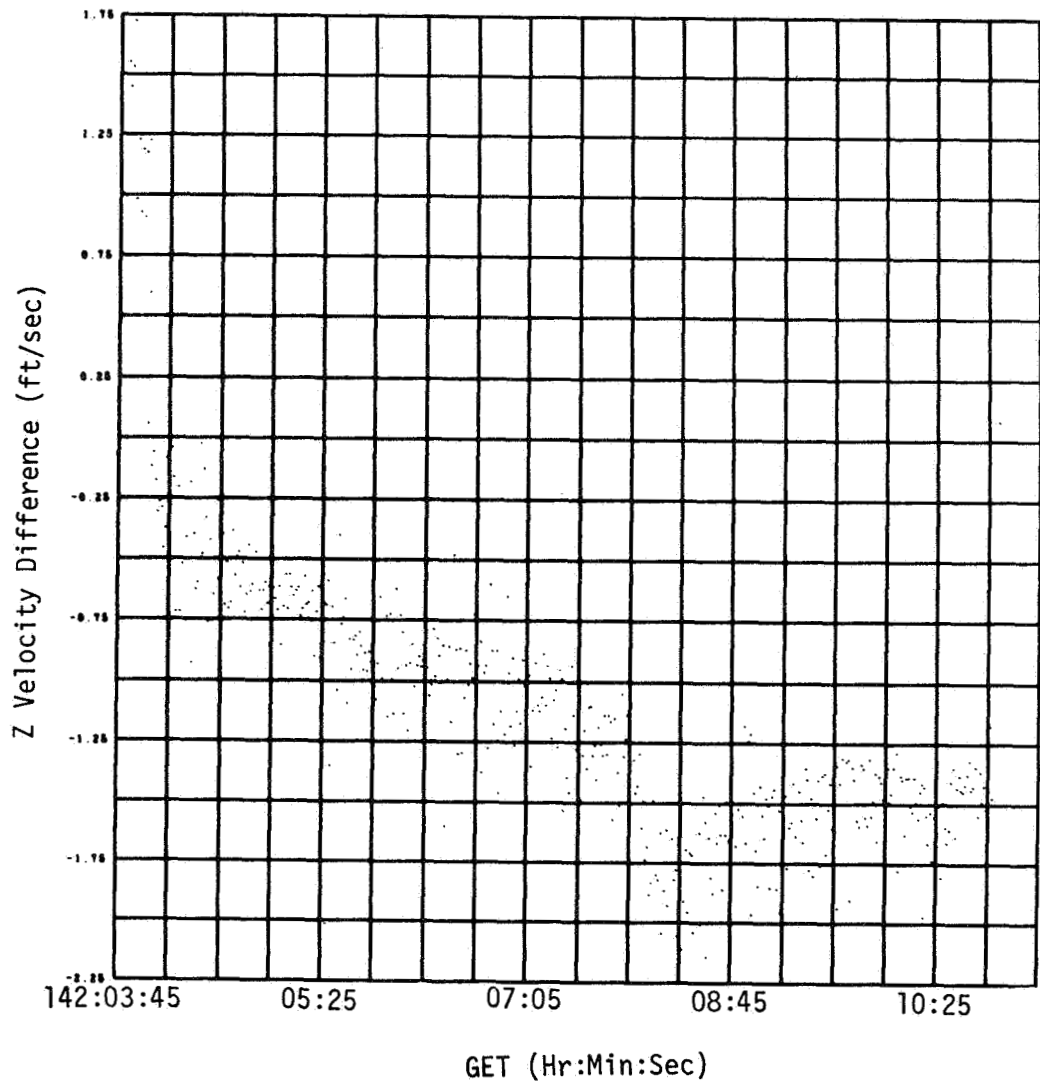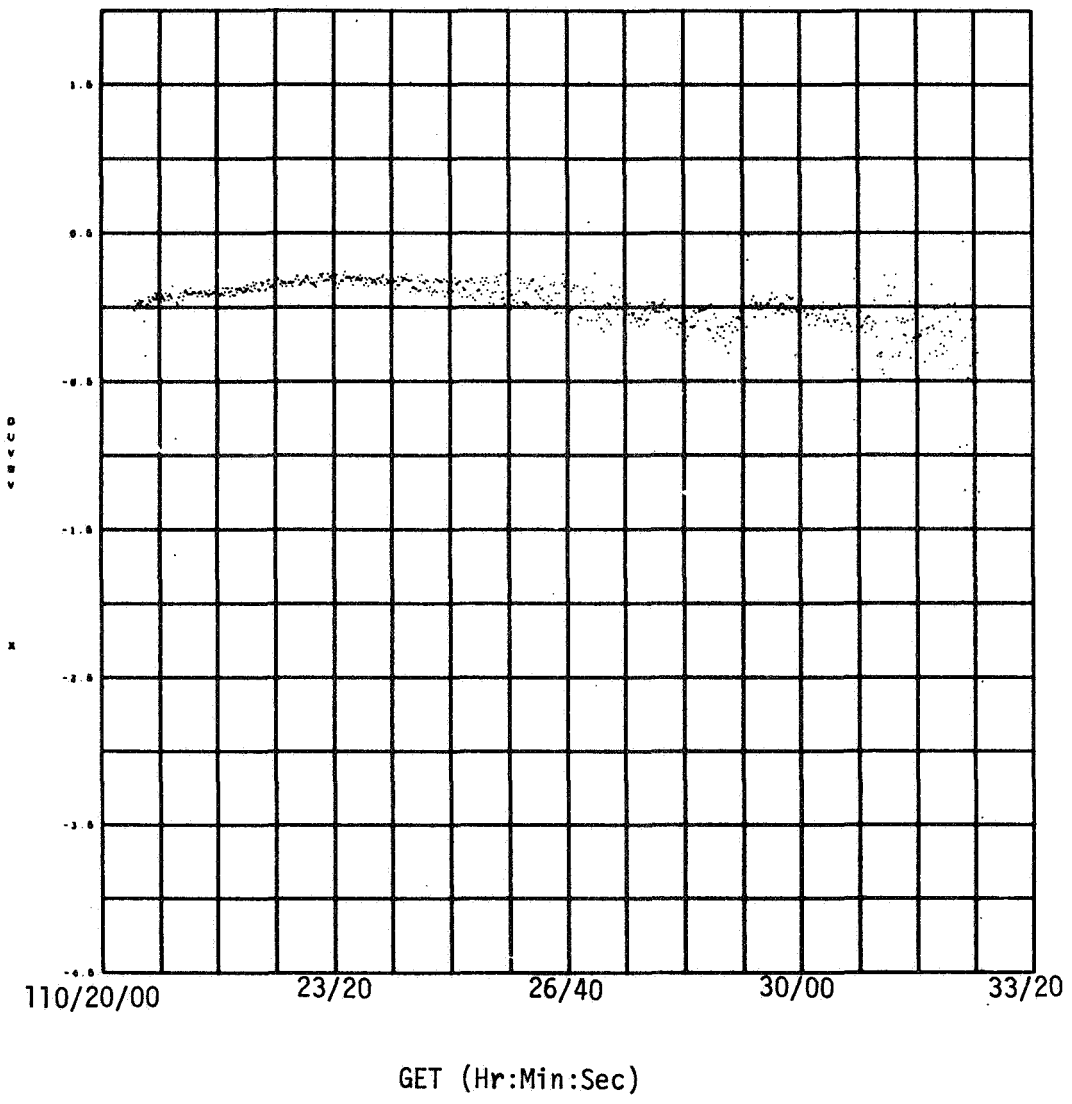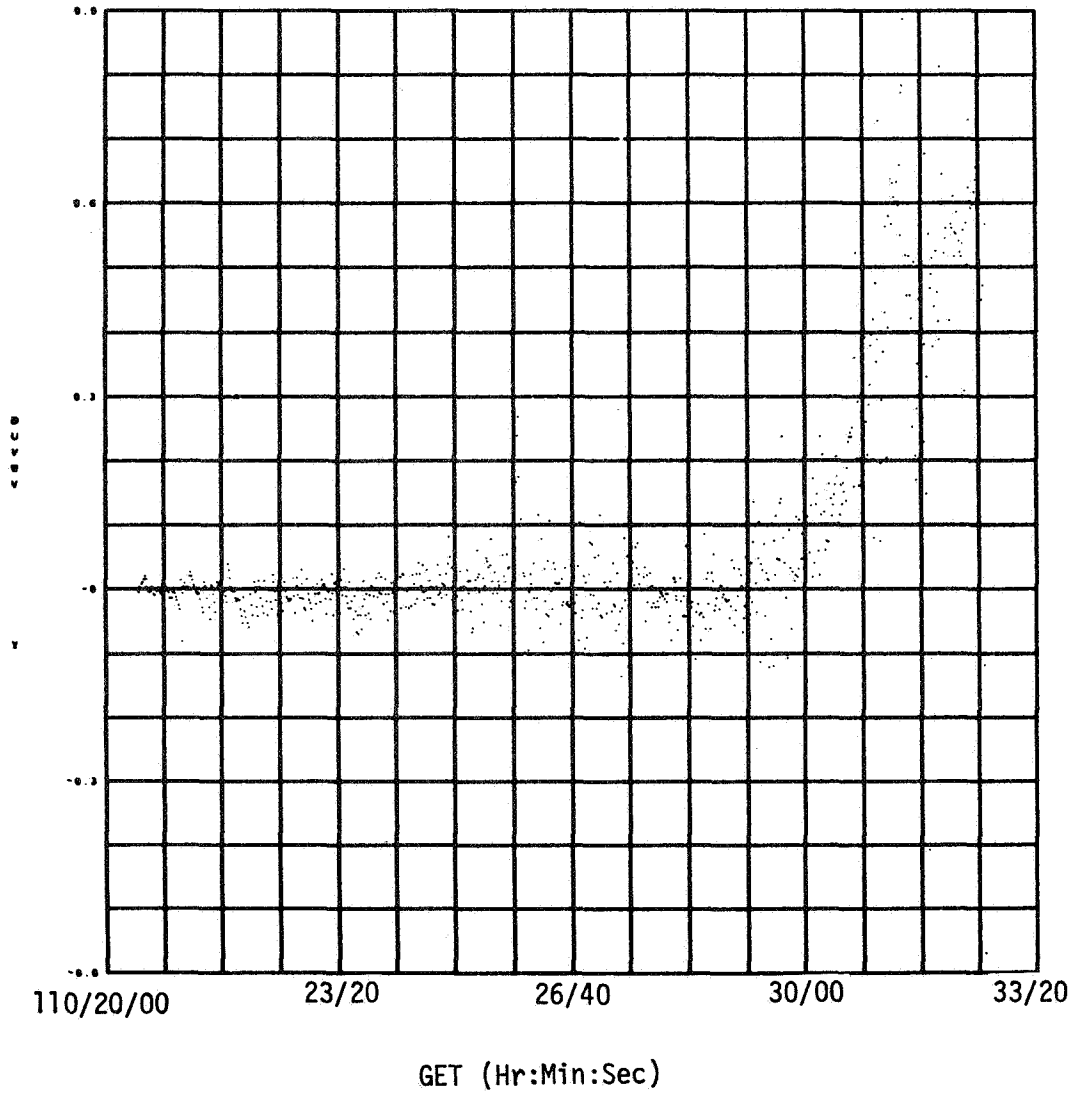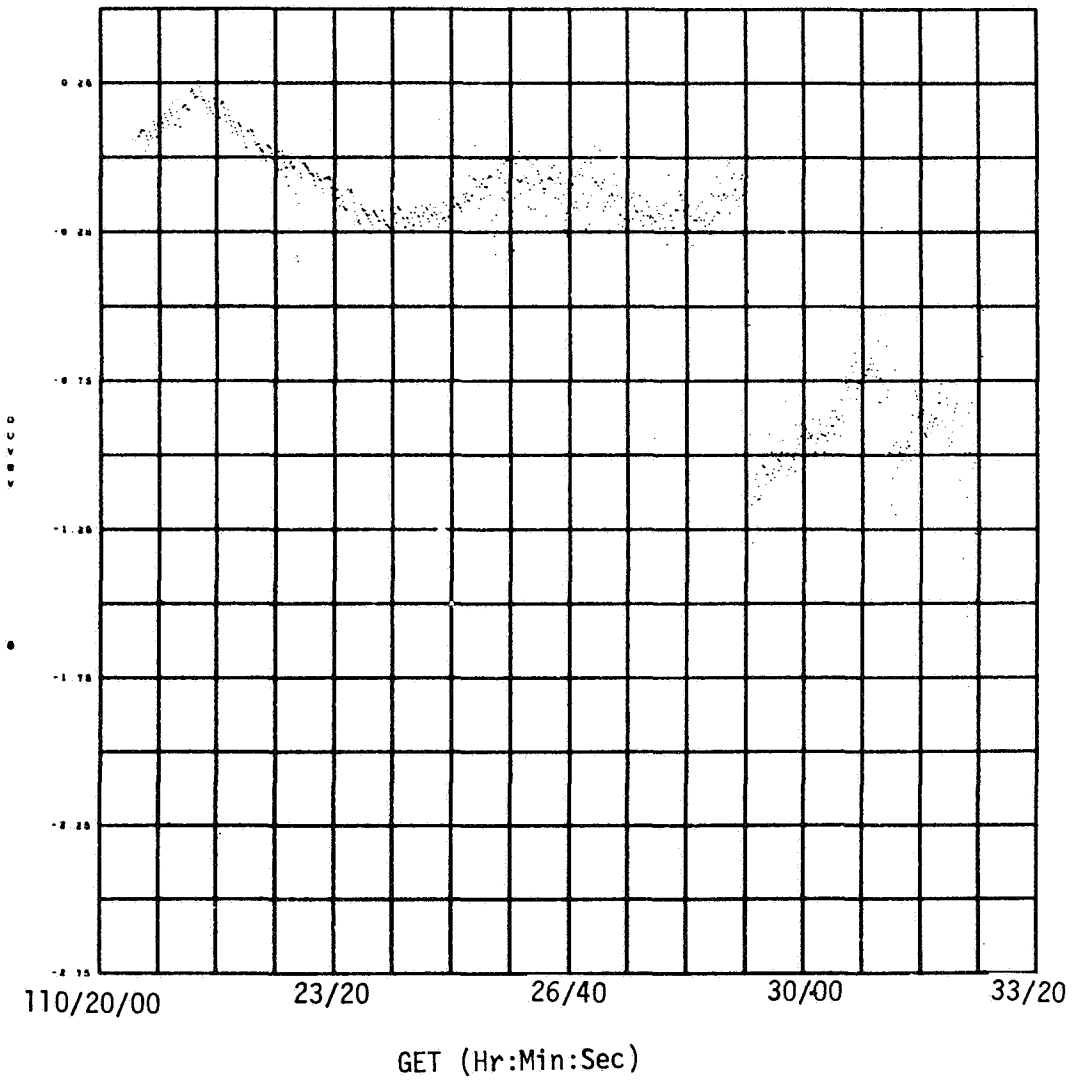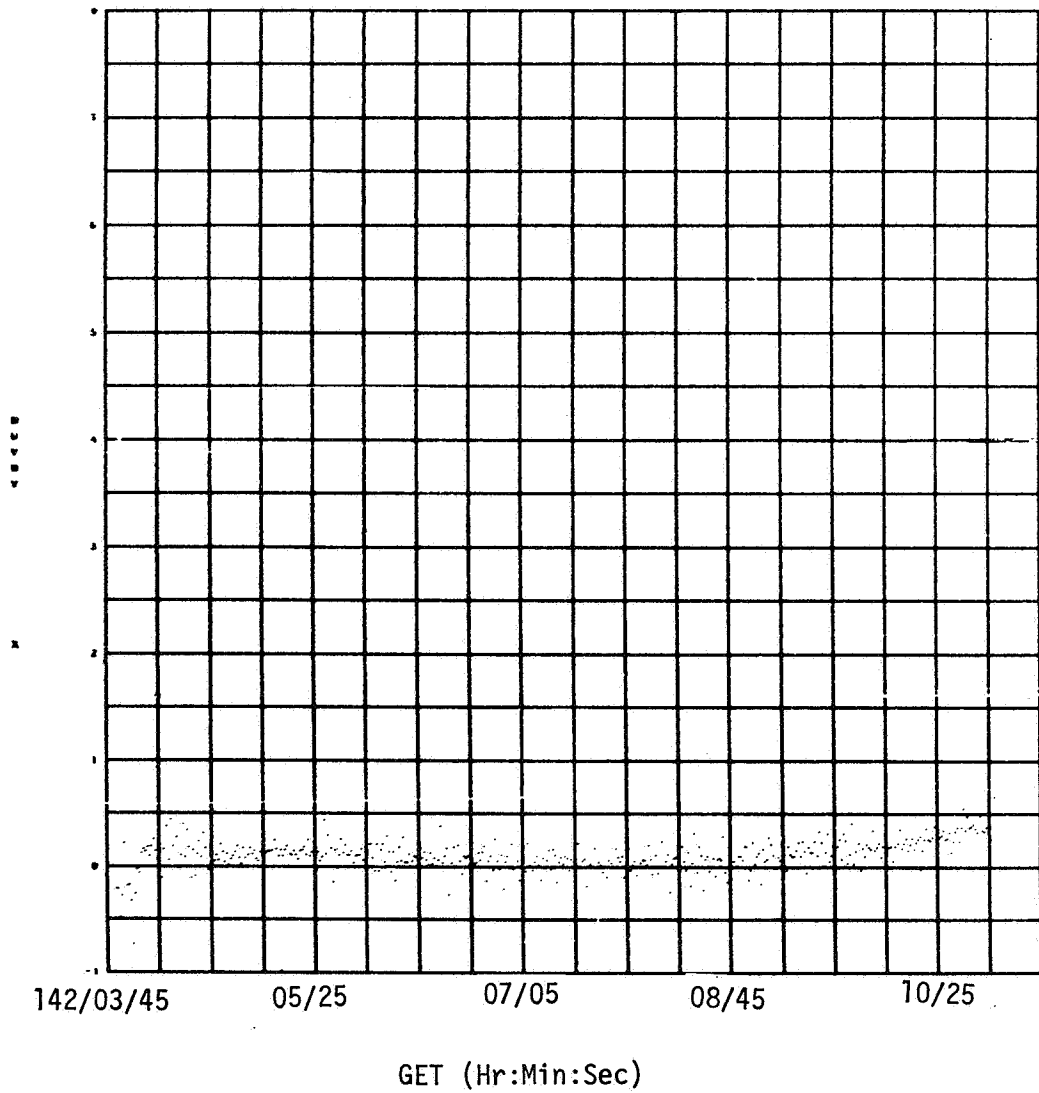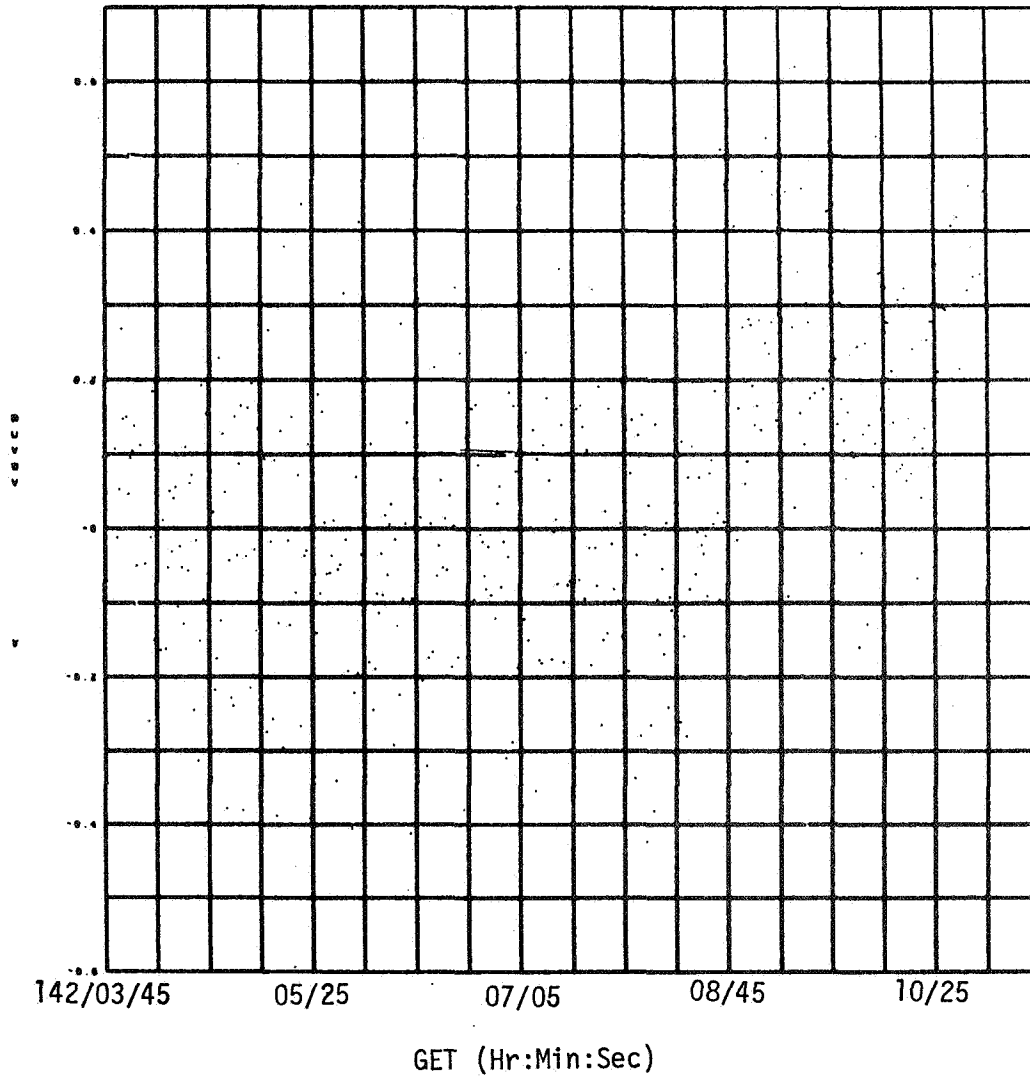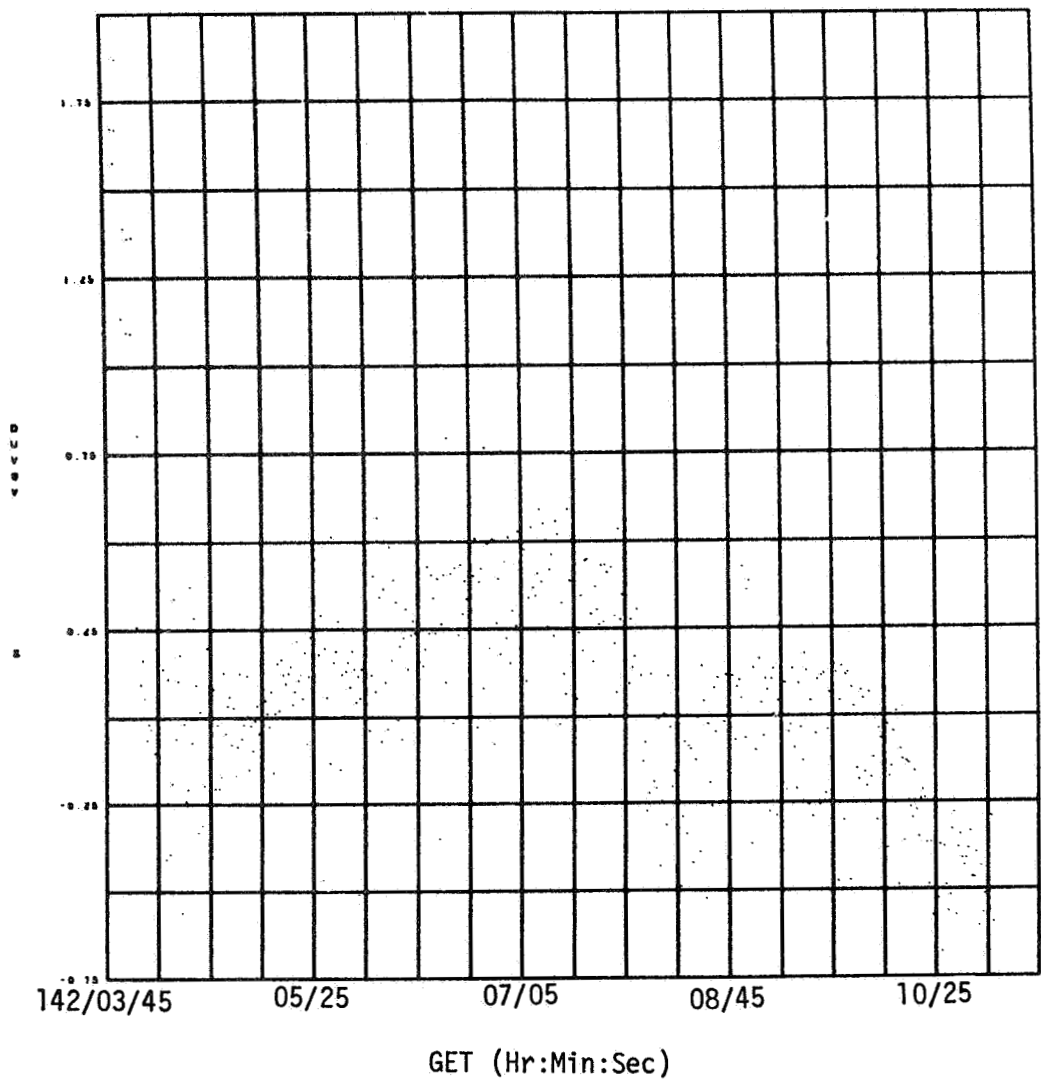   FOR ASCENT (Z AXIS)

6-39

7.0   STAR HORIZON MEASUREMENTS

Star-horizon (P23) data were processed using the inflight measured trunnion bias. Reasonably consistent values were obtained for the earth-horizon bias and trunnion noise. The value of computed earth-horizon bias ranged from 16,700 ft to 82,300 ft with an average value of 51,300 ft (15.6 km), excluding Batch 1. The computed sigma for the trunnion errors was .003 degree ($\hat{10}$ seconds) and is within specifications for the sextant.

The trunnion bias and horizon bias were solved for simultaneously, however, the results were somewhat questionable. Consequently, the inflight measured trunnion bias was used as a constant and all errors were then forced into the solution for horizon bias. The trunnion bias was determined by an RMS of all inflight measured values. Eight (8) measurements gave -.003 degree and six (6) measurements gave -.006 degree. The resulting value used was -.0045 degree. Table 7.1 contains the results for all marks taken. Batch number 1 shows a large horizon bias, but according to transcripts of the voice communications, the horizon used for marking during Batch 1 was recognized as being higher than the one used for the remainder of the marks. The residuals listed are the differences between theoretical and measured trunnion angles and are taken in the sense of measured angle minus computed angle. Sigma's were computed for each star in each batch of data and are a measure of the consistency of the marks on each star. For all cases the scatter was within the three sigma limits for trunnion noise (0.009 degree) and in most cases was less than 0.003 degree. Jupiter consistently exhibited a negative bias of .006 degree, however, the sigma computed each time it was used indicates that the Jupiter marks were very consistent. The three dimmest stars (112, 113, and 118) were used once each and evaluated as a batch, indicate the most inconsistency in marking. Star 118 taken seperately gave nominal results whereas star 113 gave the worst results. It should be noted that the substellar point

for star 113 was nearer the terminator than for the other stars, and probably contributed most of the error, however, that represents only one data point and cannot be concluded as the cause with any degree of confidence.

A second analysis approach was tried for the Apollo 12 midcourse sightings which consisted of processing two batches of data together. The HOPE program was modified to accept two initialization times, without having to integrate over the interval between the times, and then to solve for trunnion bias and horizon bias using all the observations taken near each of the initial times. This improves the geometry and allows a better separation of the effects of trunnion bias and horizon bias.

All possible pairs of Batches 2 through 6 were processed. The computed trunnion bias ranged from -.002 degree to -.006 degree with the average value of -.004 degree. The computed value of horizon bias ranged from 22,440 feet to 77,660 feet with an average value of 43,600 feet (13.3 km). These values of horizon bias are smaller and show less scatter than ones obtained by using the fixed trunnion bias of -.0045 degree.

TABLE 7.1   STAR-HORIZON MEASUREMENT ERRORS

Table 7.1   STAR-HORIZON MEASUREMENT ERRORS

Star	Residual	Mean	Sigma	Magnitude
Batch 1 – Horizon Bias 158,320 Ft Trunnion Bias -.0045 Deg				
19 Near Horizon	-.008, -.009, -.002	-.006	.003	2.2
13 Far Horizon	-.004, .001, .004	+.003	.001	-1.6
20 Near Horizon	-.001, .006, -.001, -.004, .002, -.001	+.002	.003	2.8
14 Far Horizon	-.003, -.003, -.010	-.005	.003	0.5
Batch 2 – Horizon Bias 42,000 Ft Trunnion Bias -.0045 Deg				
20 Near Horizon	.007, .000, .004	+.004	.003	2.8
14 Far Horizon	.003, -.003, .007	+.002	.004	0.5
22 Near Horizon	-.003, .009, .002	+.003	.005	1.2
17 Far Horizon	.000, .001, .003	+.001	.002	2.2
19 Near Horizon	-.002, -.004, -.003	-.003	.001	2.2
Batch 3 – Horizon Bias 82,289 Ft Trunnion Bias -.0045 Deg				
VENUS Near Horizon	-.005, .000, .001	-.001	.003	-4.1
20 Far Horizon	.004, -.001, -.001	.001	.002	2.8
22 Far Horizon	-.002, -.001, -.001	-.001	.000	1.2
112 Far Horizon	-.006, -.002, -.005	-.005	.002	2.9
117 Near Horizon	-.001, -.003, -.003	-.003	.001	2.6
25 Far Horizon	.001, .001, .003	+.002	.001	0.2
Batch 4 – Horizon Bias 48,520 Ft Trunnion Bias -.0045 Deg				
124 Near Horizon	.004, .012, -.005	+.004	.007	2.7
20 Far Horizon	.006, .009, .008	+.007	.001	2.8
22 Far Horizon	.001, .005, .005	+.004	.002	1.2
JUPITER Far Horizon	-.007, -.008, -.007	-.007	.001	-2.4
25 Far Horizon	.002, .001, .001	+.001	.000	0.2
118 Near Horizon	.004, -.003, .004	+.001	.003	2.9
Batch 5 – Horizon Bias 16,700 Ft Trunnion Bias -.0045 Deg				
113 Far Horizon	-.022, -.003, .013	-.013	.008	2.9
124 Near Horizon	.004, -.003, -.008	-.002	.005	2.7
22 Far Horizon	.005, .006, .007	+.006	.001	1.2
25 Far Horizon	-.002, -.004, -.004	+.002	.003	0.2
JUPITER Far Horizon	-.005, -.006, -.004	-.005	.001	-2.4
20 Far Horizon	.010, .007, .004	+.007	.002	2.8
Batch 6 – Horizon 66,760 Ft Trunnion Bias -.0045 Deg				
22 Far Horizon	.003, .003, .007	+.004	.002	1.2
JUPITER Far Horizon	-.006, -.005, -.006	-.006	.001	2.4
20 Far Horizon	-.004, .005, .004	+.002	.004	2.8
25 Far Horizon	.003, -.004, .000	.000	.003	0.2

8.0   LM IMU PERFORMANCE

8.1   LM IMU ERRORS

Performance of the LM IMU was based on the corrections required to satisfy desired end conditions for the descent and ascent trajectories. Based on the results obtained IMU performance was satisfactory, however, unexpecedly large bias shifts were encountered across the IMU power down while on the lunar surface. For the descent trajectory the desired end condition was;   minimal moon relative velocity at the known touchdown time. The approach used was to reconstruct a trajectory initialized with the best known pre-PDI state vector and shaped thereafter using PIPA count data. That trajectory was then altered using the IMU error model and selected error coefficients to meet the desired end point conditions. A set of errors which fit the desired end conditions was:

Error	Magnitude	Sigma
ϕX (Platform misalignment about X)	157.2 sec	0.79
ϕY (Platform misalignment about Y)	-110.0 sec	0.55
XZMSL (X PIPA misalignment toward Z)	- 53.8 sec	2.69
ZXMSL (Z PIPA misalignment toward X)	- 59.5 sec	2.97

Using the corrected trajectory the landing point coordinates agree well with the "Best Estimate" landing site. The best estimate was derived from Rev. 15 Rendezvous Radar tracking of the CSM and Rev. 16 SXT sightings on the LM. The landing site comparison is shown below:

Source	Latitude	Longitude	Altitude
Reconstructed	-3.027°	-23.426°	-6354 ft
Best Estimate	-3.043°	-23.416°	-6861 ft

For ascent, the desired end conditions were; match the free flight trajectory conditions near insertion. Free flight trajectory conditions were determined from MSFN doppler data, SXT sighting data, VHF ranging data and RR data. Again the ascent trajectory was reconstructed from PIPA count data and subsequently altered using the IMU error model with selected error coefficients until the desired end conditions were achieved. A set of errors which fit the desired end conditions was:

Error	Magnitude	Sigma
BX (X accelerometer bias)	0.15 cm/sec	0.75
BY (Y accelerometer bias)	0.20 cm/sec	1.00
BZ (Z accelerometer bias)	-0.29 cm/sec	1.45
φY (platform misalignment about Y)	-21.6 sec	0.11
φZ (platform misalignment about Z)	-43.2 sec	0.22

The PIPA bias errors were predicted errors based on preliminary free flight data before PDI and after insertion. An improved estimate of the free flight biases indicate the shifts while on the lunar surface were slightly larger than indicated here. The bias change is believed to be a result of removing power to the IMU and is further discussed in Section 8.2.

Confidence in the platform misalignment values is enhanced based on the results from the postflight IMU attitude determination program discussed in Section 10.0. The table below indicates good agreement with results well within the one sigma uncertainty of the attitude determination processor.

	Attitude Processor Misalignment Angles	Best Fit Misalignment Angles
ϕX	-47 ± 90 sec	None
ϕY	-36 ± 90 sec	-21.6 sec
ϕZ	-25 ± 90 sec	-43.2 sec

Using the above error set, the following trajectory match is obtained at insertion.

Time	Powered Flight Coordinates	Powered Flight Reconstruction	Best Estimate Free Flight Trajectory	Error
142:11:51.77	X	5604697.1	5604377.1	320
	Y	736.1	- 293.3	1029
	Z	1317309.3	1316757.5	552
	V_X	- 1227.86	- 1227.99	0.13
	V_Y	- 1.05	- 0.88	- 0.17
	V_Z	5401.84	5403.27	- 1.43

8.2 ACCELEROMETER BIAS SHIFTS DETERMINED BY P57 G MEASUREMENT DATA

Real time computations for PIPA biases during free fall before lunar landing, and then after orbit insertion show significant bias shifts in all channels. The values obtain just before PDI and soon after orbit insertion were:

$$\text{Bias before PDI} = \begin{pmatrix} -.349 \\ 0 \\ +.677 \end{pmatrix} \text{ cm/sec}^2$$

$$\text{Bias after orbit insertion} = \begin{pmatrix} -.154 \\ +.200 \\ +.265 \end{pmatrix} \text{ cm/sec}^2$$

Let

$$\Delta B_F = (\text{Bias before PDI}) - (\text{Bias after orbit insertion})$$

8-3

then

$$\Delta B_F = \begin{pmatrix} -.195 \\ -.200 \\ +.412 \end{pmatrix} \text{ cm/sec}^2.$$

An analysis to determine the accelerometer bias while on the lunar surface was made. Data generated during the unit g measurements while in the IMU alignment program (P57) were used. The basic data used were the CDU values and the DELV (X, Y, Z) scaled PIPA counts. The computations were made for GET = 110:43 (before power shutdown), and for GET = 141:18 (after power back on). The values found were:

$$b_1 = \text{bias before power shutdown} = \begin{pmatrix} -.360 \\ +.020 \\ +.708 \end{pmatrix} \text{ cm/sec}^2$$

and

$$b_2 = \text{bias after power back on} = \begin{pmatrix} -.192 \\ +.258 \\ +.330 \end{pmatrix} \text{ cm/sec}^2$$

Let

$$\Delta b = b_1 - b_2$$

then

$$\Delta b = \begin{pmatrix} -.168 \\ -.238 \\ +.378 \end{pmatrix} \text{ cm/sec}^2$$

The change in bias computed from the P57 data compares favorably with the change in free fall bias:

$$\Delta B_F - \Delta b = \begin{pmatrix} -.195 \\ -.200 \\ +.412 \end{pmatrix} - \begin{pmatrix} -.168 \\ -.238 \\ +.378 \end{pmatrix} = \begin{pmatrix} -.027 \\ +.038 \\ +.034 \end{pmatrix} \text{ cm/sec}^2.$$

8-4

The differences in the individual comparisons are somewhat larger:

$$\text{(Free fall before PDI)} - b_1 = \begin{pmatrix} +.011 \\ -.020 \\ -.031 \end{pmatrix} \quad \text{cm/sec}$$

$$\text{(Free fall after insertion)} - b_2 = \begin{pmatrix} +.038 \\ -.058 \\ -.065 \end{pmatrix} \quad \text{cm/sec}$$

This particular case (Apollo 12) therefore, implies that the better prediction of true bias for ascent is obtained by forming Δb and subtracting this from the last free fall value; as opposed to using b_2 as the prediction of bias during ascent.

9.0   LM LUNAR SURFACE ALIGNMENTS

9.1   LEAST SQUARES ATTITUDE PROCESSOR

The P57 Alignment Technique 2 (AT-2) star sighting data for Apollo 12 has been processed in the iterated weighted least squares program. IMU misalignment at touchdown and liftoff and the LGC P57 computed gyro torquing angles for each lunar surface alignment as compared with those calculated by the postflight IMU attitude determination program are presented. Using the attitude results from this program and the lunar gravity measured onboard during P57 Alignment Technique 2, LM Landing site can be obtained. These results are compared with other available landing site data in Section 10.2.

To determine the GTA's for the AT-3 alignments and the liftoff misalignment, it was necessary to assume that the LM body shift with respect to the lunar surface was accurately measured by the PGNCS gravity vectors. If a shift about the gravity vector occurs, a resulting attitude error approximately about the LM X-axis will be introduced in the estimate of platform orientation in the attitude program.

9.1.1   Touchdown and Liftoff Misalignments

Misalignments about the X, Y, and Z platform axes are presented below. The misalignments are defined as the small Euler angle rotations about the X, Y, and Z platform axes, respectively, which would be required to rotate the platform to the desired orientation.

Event	Time (GET)	Misalignment (deg)		
		X	Y	Z
Touchdown	110:32:37	+.019	+.017	-.018
Liftoff	142:03:47	-.013	-.010	-.007

Considering that the attitude processor has an uncertainty of 0.025 degree (1σ), the above results indicate that the platform was aligned prior to PDI and prior to liftoff within the one-sigma AOT accuracy (.06 degree).

9.1.2 Comparison of P57 Gyro Torquing Angles With Results of Attitude Processor

The attitude processor was used to generate estimates of the gyro torquing angles just prior to the time of torquing for the four P57 lunar surface star alignments. The results are compared below with the LGC computed values for the gyro torquing angles:

Alignment	Time of Torque (GET)	LGC Computed GTA's (Degrees)			Attitude Processors GTA's (Degrees)		
		X	Y	Z	X	Y	Z
AT-2 (1)	111:18:57	+.027	+.017	-.045	+.046	+.028	-.029
AT-2 (2)	111:30:39	+.034	+.036	+.019	+.011	+.017	+.012
AT-3 (1)	139:34:32	+.001	+.057	+.033	-.019	+.048	+.037
AT-3 (2)	141:29:01	-.023	+.004	+.015	-.011	0	+.004

The above results indicate that all alignments were performed within the one-sigma accuracy of the AOT.

9.2 LM LANDING SITE

Following the calculation of the body attitude in inertial space (determined using platform orientation and gimbal angles), the LM landing site was determined from the first two lunar gravity vectors measured in the P57 Alignment Technique 1. The results are given below:

1)   Using first AT-1 gravity vector:

$$\phi = -3.040 \text{ deg}$$
$$\lambda = -23.406 \text{ deg}$$

2)   Using second AT-1 gravity vector:

$$\phi = -3.047 \text{ deg}$$
$$\lambda = -23.422 \text{ deg}$$

where ϕ is latitude

λ is longitude.

The average of the above results ($\phi_{AVE} = -3.044$ deg, $\lambda_{AVE} = -23.414$ deg) compares very closely with the current postflight estimate for the LM landing site:

$$\phi_{BEST} = -3.036 \text{ deg}$$
$$\lambda_{BEST} = -23.418 \text{ deg}$$

REFERENCES

1. "Apollo 12 Mission Report," MSC Report 01855, April 1970.

2. "Apollo 11 Guidance, Navigation and Control Performance Analysis Report," TRW Report 11176-H433-R0-00, 31 December 1969.

3. "LM AGS Capability Estimate, Rev. 4," TRW Report 03358-6134-R000, 31 December 1969.